Railway Transition Zones

MSc Thesis
T.J. van Gent

ŤUDelft

Condition monitoring of railway transition zones through axle box accelerations using multi body simulation software

by

T.J. van Gent

to obtain the degree of

Master of Science
in Civil Engineering

at the Delft University of Technology,
to be defended publicly on the 2nd of April 2024.

Student number: 4342070
Thesis committee: Dr. V. L. Markine, TU Delft, supervisor (CiTG, Railway Engineering)
Dr. Z. Yang, TU Delft (CiTG, Railway Engineering)
Dr. A. Kumar, TU Delft (CiTG, Pavement Engineering)

An electronic version of this thesis is available at http://repository.tudelft.nl/.

TUDelft

Contents

Abstract

Transition zones in railway tracks are locations with an abrupt change in stiffness in the vertical rail supporting structure. These locations are typically located as approaches near engineering structures where there is a sudden change in track substructure. Due to these abrupt changes the dynamic forces of the wheel-rail interaction on the railway track are significantly amplified resulting in the deterioration of track geometry. With higher operational velocities, the degradation process of the track is accelerated.

The goal of this research is the investigation of the relationship between vertical acceleration from the axle box of the vehicle bogie (axle box accelerations - ABA) and track geometry changes at transition zones. While most studies investigate the behavior of railway transition zones making use of finite element models, this study focuses on the use of a more computational efficient multi body simulation (MBS) software (VI-Rail flextrack).

After the software is tested and the results validated, different stages of the service life of a transition zone (new - used - heavily used) are simulated. From the results two main conclusion can be drawn. First, the vertical acceleration is able to show the changes in differential settlement and stiffness that are occurring at transition zones. The indicators for these changes are the frequency responses with a wavelength between $1.2 < \lambda < 5$ meters. This shows that ABA is a powerful non-invasive monitoring technique for long wavelength track irregularities. Second, the multi body simulation software is able to model complex railway tracks. The software shows the same characteristic frequencies as the measurement data does.

The results of this investigation could especially be of interest for asset owners and contractors. By showing that ABA measurements tends to be an effective way of monitoring transition zones, predictive maintenance could be implemented which saves time and high costs.

1

Introduction

This research will focus on the condition assessment of transition zones with the use of axle box accelerations and multi body simulation software. In this chapter an introduction to railway transition zones is given together with the main problems that arise at these locations, arguing the need of this research. After the motivation, the research questions are formulated and the outline of the thesis is presented in the methodology.

1.1. Transition zones

During the service life of a railway track, monitoring and maintenance are the most important factors to keep the track reliable and available. Some parts of the track like transition zones however, need more attention than others. A transition zone is an area with abrupt stiffness changes in the vertical rail supporting structure. These locations are typically located as approaches near engineering structures where there is a change in track substructure. Think of ballast track to slab track, or vice versa, which have different foundations and material properties. Examples of these locations can be found near bridges, tunnels, culverts, and level crossings (figure 1.1).

(a) Tunnel transition zone   (b) Bridge transition zone   (c) Transition zone side view (from ballast to slab track)

Figure 1.1: Examples of transition zones (TU Delft, 2020a)

Due to these abrupt changes in the vertical rail supporting structure the dynamic forces of the wheel-rail interaction on the railway track are significantly amplified resulting in the deterioration of track geometry. With higher operational velocities, the degradation process of the track is accelerated (Wang & Markine, 2018b). Figure 1.2 shows a transition zone in the Netherlands with clear visible settlements ('dips') on the embankments (approaching zones) of the bridge. These displacements are the result of the deterioration of the track geometry leading to large settlements.
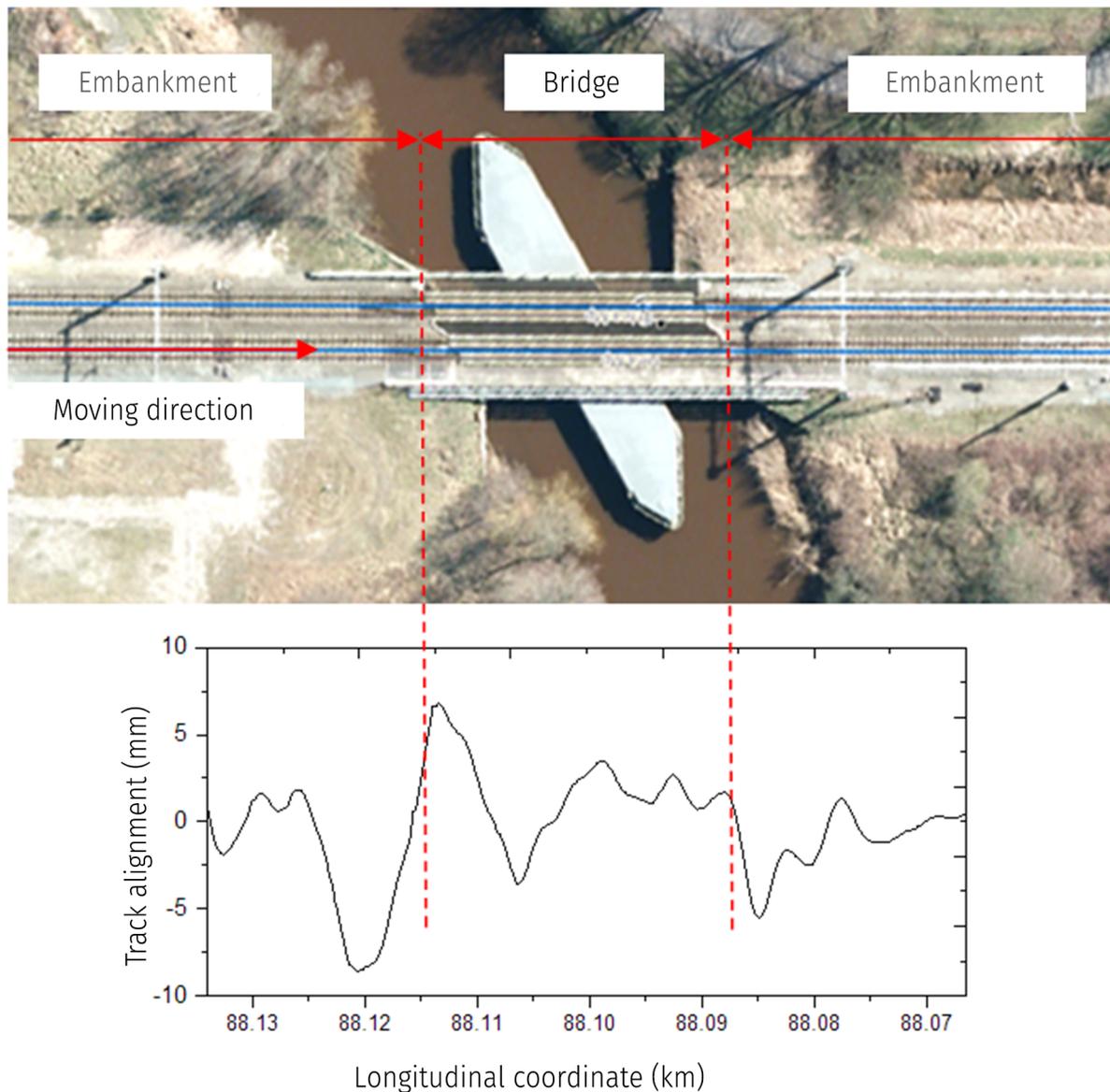
Figure 1.2: Track vertical geometry (Wang, H., & Markine, V., 2018)

As a result of the fast deterioration, hanging sleepers, decrease in passenger's comfort, vibrations, cracking of sleepers, breakage of ballast (leading to poor drainage) all occur at transition zones increasing the maintenance costs significantly (Ramos et al., 2022) (Wang & Markine, 2018b). In the worst case, even derailment is possible without proper maintenance. In the Netherlands transition zones need 4 – 8 times more maintenance compared to open tracks (Wang, Markine, & Liu, 2018). This maintenance can be split up into short- and long-wave irregularities, rail profile and track irregularities respectively. With maintenance for rail irregularities mostly consisting of grinding, milling, and planning of the rails. Whereas the maintenance of track irregularities consists of (but not limited to) tamping, stone blowing or (quite newly introduced) adjustable fastening.

According to a research by Sañudo et al. (2016) and Wang and Markine (2018b), there are three main factors causing track degradation at transition zones. These factors are highlighted

together with the reasons why they cause fast track deterioration.

- Vertical stiffness variation: Rail deflection during loading cycles (i.e. train passages) is a direct result of the vertical stiffness of the track. With a variation in stiffness, the vertical acceleration of a train is fluctuating which can lead to higher wheel forces and thus higher ballast stresses.

- Differential settlement: Appears due to the different material properties of the ballast and engineering structure. The ballast experience compaction over time (rapid compaction of the particles after construction and a normal settlement rate during train passages due to the frictional sliding of the ballast particles), while the engineering structure remains in place due to the stiff layers. A difference in settlement will occur. Figure 1.3 shows the settlement process of the ballast.

- Geo-technical/construction/maintenance issue: Can occur due to poor quality of the embankment/soil, bad compaction of the ballast, poor drainage conditions. Also, high moisture content in the ballast increases the dynamic wheel forces.
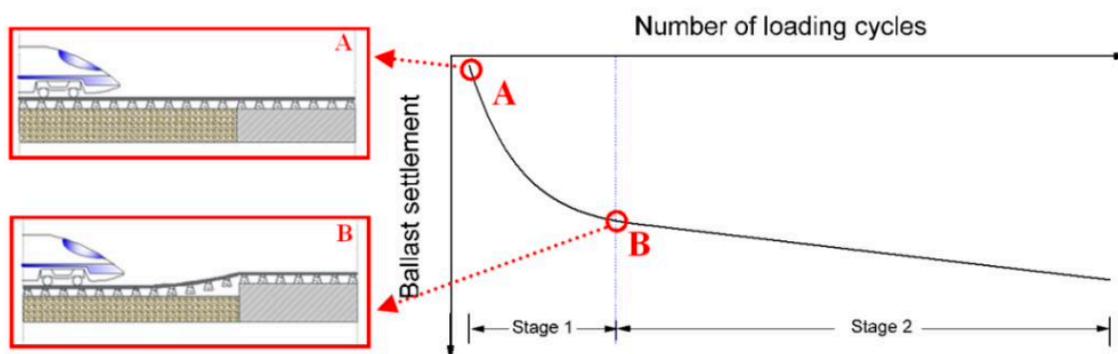

Figure 1.3: Permanent settlement process of the ballast during loading cycles (Wang, 2018)

With the research done so far it is shown that differential settlement is the main contributor for amplification of the wheel force and therefore of the track degradation at transition zones (Wang, 2018). Differential settlement results in voids underneath the sleepers. Due to the bending resistance of the track the sleepers will lose contact with the ballast bed and hang underneath the rails, hence the name hanging sleepers. These sleepers are responsible for the high dynamic wheel forces on the track (causing short-wave damage such as corrugation) and uneven load distribution of these forces to the ballast bed causing voids underneath adjacent sleepers as well. Resulting in the fast deterioration rate at transition zones (Wang et al., 2016) (Lundqvist & Dahlberg, 2005). Due to this principle, most countermeasures are aimed at preventing or correcting the abrupt stiffness change and/or differential settlement to avoid the occurrence of hanging sleepers (Wang & Markine, 2018a) (Coelho et al., 2010) (Paixão, Fortunato, et al., 2015).

1.1.1. Problem statement

During the service life of a railway track, transition zones are prone to degradation resulting in a high maintenance rate. The combination of the complexity of the degradation process and the accompanying high costs and unavailability of the track during maintenance, makes this element of the railway track an important part to investigate. To gain more insight in the degradation process of transition zones and to enhance predictive instead of reactive/corrective maintenance, more research on transition zones should be conducted.

1.2. Motivation

To better understand the degradation process of a transition zone, a more comprehensive understanding of the current behavior of transition zones through measurements and model simulations should be obtained (condition assessment based on data). However, current measurements at transition zones are still insufficient compared to open tracks (Wang, Markine, & Liu, 2018). Besides, most of the numerical models made have to deal with high computational times.

Different measurement techniques have been used at transition zones. Digital image correlation (DIC) (Wang, Markine, & Liu, 2018) (Le Pen et al., 2014), optical level instruments (D. Li et al., 2005), linear variable differential transformers (LVDT) and strain gauges (Stark & Wilk, 2016), geophones and accelerometers within the soil (Coelho et al., 2010), and position sensitive detectors (PSD) (Paixão et al., 2014) (Chapter 2 gives a more elaborate overview of these different techniques). In the research of Wang, Markine, and Liu (2018), DIC is used to obtain the vertical displacement of the rails to capture the dynamic profile in order to make an assessment of the health condition, showing large settlements near the bridge due to higher dynamic wheel forces. Also Stark and Wilk (2016) shows that by using LVDT's and strain gauges large wheel forces are responsible for the larger settlements and hanging sleepers near the engineering structure. In Coelho et al. (2010), geophones and accelerometers showed that extra settlement and poor performance of the transition zone are strengthened by an approaching slab, in contrary of it's principle. In the research of Paixão et al. (2014) a transition zone with backfill is investigated using PSD's, LVDT's, strain gauges and accelerometers on the sleepers. Results show a decreasing settlement near the bridge, and no indication of hanging sleepers. This implies that a gradual increase of stiffness is an effective solution to the transition zone problem.

Most of the before mentioned techniques rely on complex methods, non-continuous data acquisition and wayside monitoring, obstructing the availability of the track. Onboard sensing however, like axle box accelerations (ABA), is a technique already widely available, inexpensive to use and easy to implement on running vehicles (Molodova et al., 2011). Making this a more sustainable monitoring technique. By using axle box accelerations (ABA) as the onboard sensing technique, transition zones can be continuously monitored to acquire the health condition of the track. In the research of Unsiwilai et al. (2023) multi-ABA measurements have been used to monitor different transition zones. Results show that on the assumption of more track degradation larger ABA energy will arise. Hence, a condition monitoring through axle box accelerations could be made.

1.3. Objective and research questions

To investigate the problem stated above, a research goal is presented. From this goal a research question (and sub-questions) is (are) stated together with the methodology.

1.3.1. Goal

Before differential settlements occur, a variation of stiffness already exists between the ballast track and engineering structure (stage A in figure 1.3). In other words, a change in vertical (and longitudinal) acceleration during train passes already exists before the transient settlements occur and contributes to the amplification of the dynamic forces. After compaction of the ballast layer (stage B), a certain settlement rate is present and a slowly development of differential settlement will continue (eventually creating hanging sleepers).

The goal of this research will be to investigate the relationship between vertical acceleration from the axle of the vehicle bogie and track geometry changes at transition zones using a computational efficient multi body simulation (MBS) software. Which can be considered as a novelty. Especially the effect of the abrupt stiffness change (between track and structure) and differential settlement on the acceleration of the wheelset will be of key interest in this research as this will be the main parameter for trying to make a condition assessment of a transition zone using MBS software. By finding the characteristics of these accelerations using measurement data and creating a simulation model of a transition zone, the hypothesis if vertical acceleration can assess long wave track irregularities is tested. The results of this investigation could especially be of interest for asset owners and contractors. If ABA tends to be an effective way of monitoring transition zones, maintenance can be done premature which saves time and high costs.

1.3.2. Research questions

The problem definition leads to the following research question.

"How can ABA-data serve the condition assessment of transition zones?"

In order to answer the question stated above, several sub questions are formulated.

1. What is the current state of the art regarding ABA implementation and monitoring of transition zones?

2. From the acceleration data, is it possible to indicate characteristics of the transition zones?

3. Is it possible to simulate the behavior of a transition zone using a multi body simulation (MBS) software?

4. How do the measurement ABA-data and simulation data relate to each other?

5. What does the vertical acceleration tell about the condition of a transition zone using MBS software?

1.4. Research Methodology

To answer the research question stated above a research methodology has been set up. The corresponding sub-questions for each part of the research are shown schematically in figure 1.4. Below this methodology is described more elaborate.

The essence of the research will be the investigation of the feasibility of condition monitoring through vertical (axle box) accelerations at transition zones using a computational efficient simulation model. First, a literature study is performed as a basis for this thesis (chapter 2). Here, the question of why this research is conducted is answered more elaborately with background information regarding current condition monitoring techniques for transition zones, axle box accelerations, data processing techniques and existing simulation models. This would also serve as the answer to the first sub-question.

In chapter 3 ABA measurement data is analyzed and processed using Python. The measurement data, both vertical as longitudinal acceleration, comes from different transition zones located between the corridor between Lage Zwaluwe and Dordrecht. The characteristics and dominant frequencies of the signal are investigated and a trend is tried to be derived between the different transition zones in the data sets through statistical analysis. A relationship between the characteristics of the transition zone and axle box acceleration is discussed (sub-question two).

With the use of a multi body simulation software, a model is made of a transition zone in chapter 4. One of the key aspects of this model is the relative simplicity of the model relative to other finite elements models in terms of computational effort. After the model is validated, changes in vertical stiffness are applied to simulate differential settlements and thus the behavior of a transition zone. Together this answers the third sub-question.

Next, in chapter 5 the simulation data is compared with the measurement data from chapter 3. Here it is investigated if the same characteristics can be distinguished (sub-question four).

After acquiring the relationship between vertical accelerations and the characteristics of the transition zone (from chapter 3 and 5), the feasibility of acceleration based condition monitoring is presented (sub-question five) in chapter 6 using different models made with the multi body simulation software. The different models will represent different stages in the service life of a transition zone.

At last, chapter 7 gives a conclusion and answers to the main research question. This is followed by a discussion and suggestion for future work.
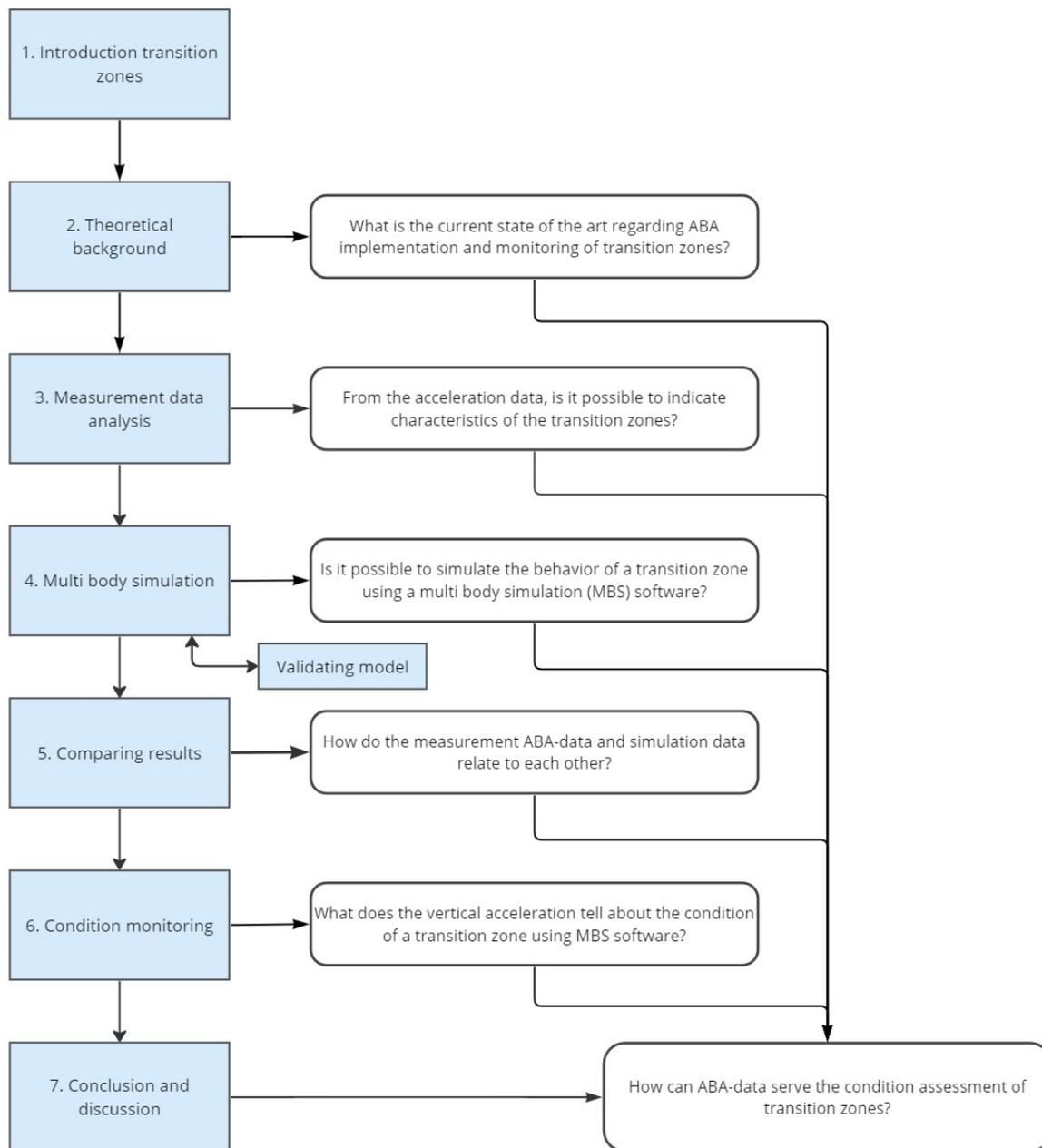
Figure 1.4: Report structure including research questions

2

Context

In this chapter relevant background information is gathered and discussed. The goal of this chapter is to find an answer to the second sub-question, 'What is the current state of the art regarding ABA implementation and monitoring of transition zones?'. First, the monitoring techniques of transition zones are summed up and briefly discussed. Second, the use of axle box accelerations and its implementations are mentioned. Also different data process techniques are explained. At last, the use of multi body simulation software and its capabilities are discussed.
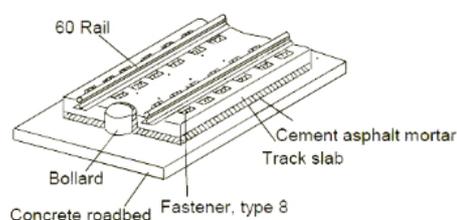
2.1. Railway track

The standard railway track, also called classical track or conventional track, has been around since the beginning of railways. Only changes (e.g. concrete sleepers, heavier rail profiles, et cetera) has been implemented, the principle however, has never changed substantially (Esveld, 2001). The elements of this conventional ballasted railway track are shown in figure 2.1a. Each element of the track structure has it's own functions and requirements. Due to the available data at the trajectory between Lage Zwaluwe and Dordrecht consisting mostly of ballast track, this study will mainly focus on the principle of a ballast railway track. The slab track principle will be briefly discussed.

The track structure can be divided into a sub- and superstructure. Where the substructure consists of the sub grade (the soil underneath the ballast bed), the superstructure consists of the actual track structures, like rails, sleepers and the ballast bed. Both structures are divided by a thin layer called the sub ballast. Below the main functions of every element are listed (table 2.1).
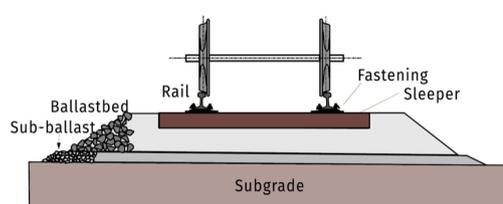
(a) Ballast railway track (TU Delft, 2020b)   (b) Slab track (TU Delft, 2020b)

The particularity of a transition zone however, is that most of the time the ballast track consists of a countermeasure as well. These countermeasures can be for example adjustable

Substructure elements	Main functions
Subgrade	- Sufficient strength to transfer and bear loads from the superstructure - Reasonable settlement behavior - Drainage ability of rain water from the ballast
In between layer	
Sub ballast	- Prevent particles from mixing between the layers - Load transfer and distribution to the subgrade - Frost protection
Superstructure elements	
Ballast bed	- Supporting the rails and sleepers (vertical, lateral and longitudinal resistance) - Transfer and equally distribute load to subgrade - Drainage ability of rain water - Providing resilience and damping of dynamic contact forces from the wheel-rail contact
Sleeper	- Supporting the rails - Preserve track gauge, rail inclination and track geometry - Sustain and distribute rail forces (vertical, lateral and longitudinal) to the ballast bed
Fasteners	- Transfer rail forces to the sleepers - Preserve track gauge, rail inclination and track geometry
Rail pads*	- Load transfer to sleepers while filtering out high frequency force components
Rails	- Bear forces vertically, laterally for wheel guidance - Provide smooth running surface and adhesion for acceleration and braking of the railway vehicles - Transfer and distribute forces from the wheel-rail contact to the sleepers - Return conductor for electrical traction power (electrified railway) and signalling currents for train detection

Table 2.1: Railway track elements (TU Delft, 2020b), *the rail pads are located between the rail, fasteners and sleepers

fasteners, approaching slabs, additional rails, different sleeper dimensions, reinforcement of the ballast layer, et cetera (C. Shi & Chen, 2021). In general, these countermeasures try to achieve the goal of obtaining a gradual stiffness change from the transition zone to the engineering structure and vice versa.

For high speed railway lines mostly, the conventional ballast track is replaced by a slab track (figure 2.1b). A slab track is a railway type that replaces the ballast bed by a concrete slab, making it more rigid. The rails are directly fastened on the concrete slab without the need for any ballast particles or sleepers. The initial construction costs are higher but many advantages arise. These advantages are lower maintenance costs, easier implementation, no deterioration of ballast is possible, less likely to settle or rails to buckle, lower profile (good for tunnels) and lower weight. This latter advantage is particular interesting for bridges as a lower weight of the railway track also means less bearing capacity of the bridge structure is needed, making it cheaper. Figure 2.2 shows how a slab track and ballast track together would look like. Over
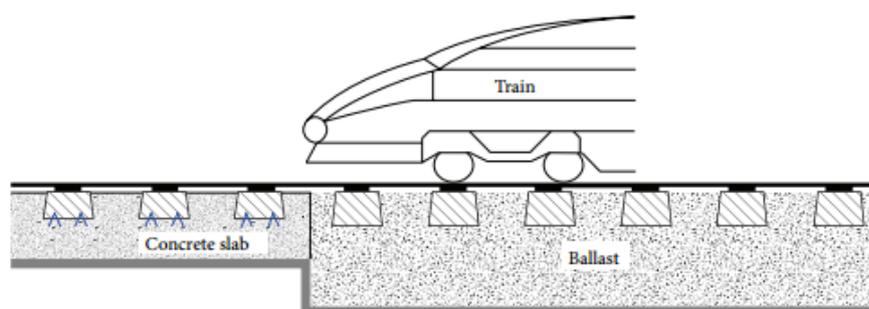
Figure 2.2: Ballast and slab track (Basirat, R., et al., 2017)

time the ballast would settle creating a transition zone in front of the slab track section.

2.2. Measurement techniques

Different railway track measurement methods have been used to monitor the condition of transition zones. In table 2.2 these methods are gathered and their properties are highlighted. The working principles of the methods are briefly described and can be found in attachment A.

Measurement equipment	Type	Placement	Output	Sources
VGS/DIC	Optical method	Wayside	Displacement: Transient settlement	(Le Pen et al., 2014) (Bowness et al., 2007) (Wang, Markine, & Liu, 2018)
Optical level	Optical method	Wayside	Displacement: Permanent settlement	(D. Li et al., 2005)
Geophones	Electromechanical sensor	Wayside	Velocities: Transient and permanent settlement (integration), accelerations (integration)	(Le Pen et al., 2014) (Coelho et al., 2010) (Iskander, 2018) (Kouroussis et al., 2015)
Accelerometers	Electromechanical sensor	Wayside	Accelerations: Settlements (integration)	(Coelho et al., 2010) (Iskander, 2018) (Yoder & Adams, 2014)
LVDT (MDD)	Electromechanical sensor	Wayside	Displacement: Transient and permanent settlement	(Stark & Wilk, 2016) (Yoder & Adams, 2014)
Strain gauge	Electromechanical sensor	Wayside	Strain: Stress, dynamic forces, displacements	(Omega, n.d.) (Kouroussis et al., 2015)
PSD	Optical sensor	Wayside	Displacement: Transient settlement	(Paixão et al., 2014) (Pinto et al., 2015) (Paixão, Alves Ribeiro, et al., 2015)
InSAR	Satellite	Not applicable	Displacement: Transient and permanent settlement	(Wang, Chang, et al., 2018) (D'Amico et al., 2020)
GPR	Radar based	Onboard	Thickness railway structure layers, layer settlements, moisture content	(D'Amico et al., 2020) (Wang et al., 2017)
Smartphones	Micro-electromechanical sensor	Onboard	Acceleration: Settlements (integration)	(Rodríguez et al., 2021)

Table 2.2: Measurement methods used at transition zones

From the literature the measurement equipment can be divided into two groups considering their position relative to the track. The first option is called wayside monitoring (WTMS - wayside train monitoring system). This consists of monitoring systems / sensors placed on or near the track itself (Trackopedia, n.d.). While the second option, appointed as onboard monitoring, describes the placement of sensors on the train (monitoring while moving).

Table 2.2 shows that most measuring equipment is used to obtain the transient and/or permanent settlements that occur at the transition zones. With permanent displacement described as the absolute static rail displacement (i.e. unloaded condition) relative to the original position after construction and transient settlement described as the displacement relative to the unloaded position of the rails while a train passes.

2.3. ABA

From table 2.2 it becomes clear that there is a deficient number of non-intrusive onboard measuring techniques being used for the monitoring of transition zones. Next to that, most of the monitoring techniques used are based upon acquiring settlement behavior. Research on transition zones is somewhat more focused on displacements than accelerations. One of the reasons for this could be the demand for double integration to obtain displacement from acceleration data. For dynamic displacements this is rather difficult taking into account the errors that emerge in low and high frequencies, e.g. temperature effects, hysteresis of the sensor and the presence of noise (Coelho et al., 2011). For that reason, this research will investigate the accelerations as the condition monitoring parameter of transition zones. By early detection of track degradation, maintenance can be planned as preventive instead of corrective, which saves time and costs. Measuring the differential settlements of transition zones means that corrective maintenance is inevitable. However, by measuring the acceleration and derive where hanging sleepers most likely would occur, preventive maintenance can be deployed. For this reason the use of axle box accelerations is investigated.

Axle box accelerations, in short ABA, is a data acquiring method through accelerometers mounted on the axle boxes of the operating vehicle. The system consists of accelerometers both in longitudinal as vertical direction together with a GPS receiver in combination with either a tacho- or speed-sensor (Nunez et al., 2018). ABA could be described as a measure of vibrations of the wheel during the wheel-rail interaction to give an indication of track irregularities at the wheel–rail interface (Molodova et al., 2011) (see figure 2.3a). The ABA-method has been developed to ease the process of local track detection.

Unlike most other monitoring systems, ABA does not rely on complex methods for continuous data acquisition. In fact, many other advantages can be associated to this method (TU Delft, 2014).

- Simple and Durable: The system is easy to install and easy to maintain. Next to that, the use of accelerometers is relative cheap.

- Continuous and non-intrusive: During monitoring the track availability is not compromised and the system is ready to use on different trains with varying operational speeds (Z. Li et al., 2015), (Nunez et al., 2018).

- Automatic detection and diagnosis of visible and invisible damage: With the use of multiple accelerometers signal noise is reduced and the hit rate of defects is increased (e.g. corrugation, squats, joints, switch & crossing damage, anomalies, et cetera).
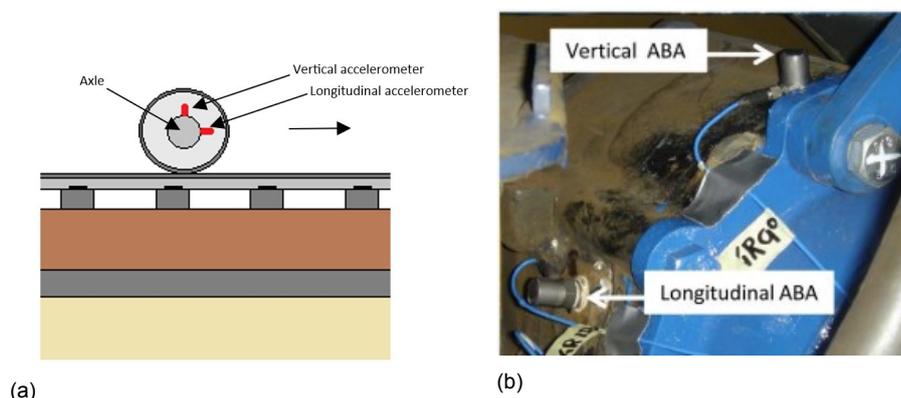
Figure 2.3: ABA setup. (a) schematic view of accelerometers of the axle. (b) in practise (Z. Li et al., 2015)

2.3.1. Research

From previous research it's proven that ABA is a reliable method for the detection of high frequency defects and condition monitoring of the track structure. Most of the implementation of ABA consists of the detection of local defects (e.g. squats, corrugation, insulated joints, welds, et cetera) and is often used with the goal of assessing the track condition and stimulate the principle of predictive instead of corrective maintenance.

An early mention of the use of axle box accelerations for condition monitoring of railway tracks through the use of in-service trains is found in the research of Mori et al. (2010).
In Molodova et al. (2011) the ABA-method is used for the detection of short track defects. An initial detection procedure is established based upon a quantitative relationship between the characteristics of the ABA-data and defects simulated in a finite element model. Overall, results showed that this relationship exists in both magnitude as frequency range. In Molodova, Li, Nunez, et al. (2014) the ABA measurements are used for an automatic squat detection method based upon the enhancement of the characteristic squat frequencies (wavelet analysis). Similarly in Molodova, Li, Núñez, et al. (2014) a suitable FE-model is developed for the simulation of axle box accelerations at squats. The model is validated with real ABA-data of squats, with both light as severe damage. Later on this model is used for a parametric analysis investigating which parameters influence the ABA measurements the most. Results show that this is the train velocity (Molodova et al., 2015). Which is in agreement with later performed and discussed research by Unsiwilai et al. (2023).
Molodova et al. (2016) investigates the health condition of insulated rail joints (IRJ's). Here, the damage assessment is obtained through indicators based on frequency characteristics of the ABA power spectrum with IRJ's in different conditions. In the research of Miao et al. (2023) voids in mortar layers in ballastless tracks are detected using vertical ABA-data combined with a high-order statistical analysis. The use of axle box acceleration show a high recognition accuracy. Whereas in Pieringer and Kropp (2022) the ABA-data is used to estimate the rail roughness through analysing the data in the time-domain. With the advantage that in the time-domain localized defects can be detected through the spatial variations of roughness. Again, in Carrigan and Talbot (2023) the rail roughness is derived from ABA. However, now also taking into account the stiffness variation of the track and wheel-to-wheel coupling while using a transfer function in the frequency domain to estimate the rail roughness. In Liu et al. (2023) a FE-model is made to study the dynamic responses of weld irregularities at high-speed lines. From the model the axle box accelerations are acquired at different velocities

and a safety limit for the running speed as a function of the defect size is proposed. Another research about condition monitoring of local track defects has been done by Nunez et al. (2018). Here, different severity levels of squats were detected using ABA measurements to prove the capabilities of the ABA system in multiple countries. In Wei, Núñez, et al. (2017) the degradation of railway crossings is investigated using ABA measurements. After an algorithm was proposed to determine the characteristics of the ABA-data related to the degradation of level crossings, a damage assessment method has been set up. Again, the ABA system proves to be an effective way to monitor the condition of these track structures. This research continues in Wei, Shen, et al. (2017) where wear and plastic deformation at crossings of the wheel-rail impact is investigated using a FE-model. After verification with ABA-measurements, the model can be used as a tool for damage analysis and structure optimization.

Next, in Oregui et al. (2017) rail joints are investigated upon their bolt tightness with the use of ABA measurements at different bolt tightness conditions. After the verification of the method, it has been shown that ABA can indeed monitor the condition of the IRJ.

Furthermore, with the research of Salvador et al. (2016) data acquisition and processing techniques are discussed to enhance the use of onboard measuring. Optimal sampling, filtering frequencies and the location of the accelerometers are determined.

In the research of Unsiwilai et al. (2023) however, axle box acceleration has been used to set up a methodology for monitoring transition zones. Here, four KPI's (key performance indidcators) were proposed based upon the ABA energy differences at different transition zones, their entrance and exit sides, inner and outer rails. Results showed that ABA responses differ at transition zones, meaning a health condition could potentially be estimated. Yet, no use is made of a finite element model to validate the behavior of acceleration data over time at transition zones.

In conclusion, with the implementation of axle box accelerations a variety of topics have been investigated. With the focus mainly on the detection of damage of high frequency irregularities, an argument can be made to use the ABA to monitor the condition of transition zones with the aid of a multi body simulation software.

2.4. Data processing

From the literature it is concluded that both magnitude and frequency spectrum are sufficient tools for analysing the condition of a railway track using axle box acceleration (Molodova et al., 2015), (Molodova, Li, Núñez, et al., 2014), (Nunez et al., 2018), (Molodova et al., 2011) and (Unsiwilai et al., 2023). As for the scope of this research, the data analysis will remain at these methods. Within the time-frequency transform, two mathematical tools can be used, the fast Fourier transform and the continuous wavelet transform. Both have their advantages and disadvantages. Below these two signal-processing tools are explained.

2.4.1. Fourier

The Fourier Transform principle consists of converting a time-domain signal into a frequency-domain signal. The principle of the method consists of breaking down a complex signal into a summation of simpler sinusoidal waves, each having its own frequency. In figure 2.4 this principle is visualised.

Different Fourier Transforms (FT) exists, but all belong to either the Continuous Fourier Transform (CFT) or the Discrete Fourier Transform (DFT). Latter can be computationally demanding,
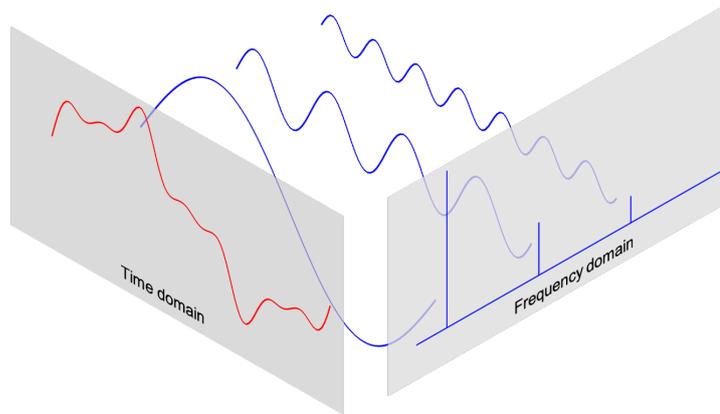
Figure 2.4: Fourier Transform visualisation (Kong, Q., et al., 2020)

a more commonly tool is the Fast Fourier Transform (FFT) which can be used instead. Each of these mathematical tools convert a signal into the frequency domain, however, with different frequency representations. With the data as the main distinction, either discrete of continuous, time measurements can appear to be both. As a continuously measurement, time-data is acquired as continuous data. In practical applications however, time-data can also be obtained at specific time intervals making it a discrete measurement (Kong et al., 2020) (Torrence & Compo, 1998).

The DFT is based upon the following function:

$$x_k = \frac{1}{N} \sum_{n=0}^{N-1} x_n \, e^{-\frac{2\pi k n}{N} i} \tag{2.1}$$

With X_k as the DFT with both amplitude and phase information, N as the total number of samples, n the current sample, x_n the sine value at n and k as the current frequency ($k \in$ [0,N-1]).

While as the CFT is denoted as:

$$X(\omega) = \int_{-\infty}^{\infty} x(t) \, e^{-i\omega t} \, dt \tag{2.2}$$

With $X(\omega)$ as the CFT with both amplitude and phase information, $x(t)$ the function to transform and ω as the frequency. Please note that the DFT is always 2π periodic, while the CFT is not.

By making use of the symmetries within the function of the DFT and breaking down the function into smaller functions, the FFT can be formed. The FFT's complexity and therefore computational effort is much smaller than of the DFT ($N * log N$ instead of N^2 as the output

values). For a mathematical explanation a reference is made to the work of Cooley and Tukey (1965) and Kong et al. (2020). Using only the real part ($Re(X_k)$) of the complex numbered outcome, gives an one-sided ordinary Fourier Transform. With the frequency spectrum at hand, a drawback of the Fourier Transform is the unknown position in time of the occuring frequencies. The phase and amplitude is known but not the location. With the Short Time Fourier Transform (STFT) the time localization of the frequency components can be obtained through windowing the signal, addressing the non-stationarity of the signal (for both continuous or discrete transforms). In this method each output signal X of the Fourier Transform is multiplied by a moving window centered around time t. By using a short window, the outcome of the STFT can be seen as a local spectrum of the signal around a specific time. By taking the squared root of the outcome, a spectrogram (visual representation of the spectrum) can be obtained. The method is based upon the following function:

$$X_m(\omega) = \int_{-\infty}^{\infty} x(t)\, w(t - \tau) e^{-i\omega n}\, dt \tag{2.3}$$

With $w(t - \tau)$ as the window function $\in [0,\text{N-1}]$, and $x(t)$ as the signal.

However, just like the FFT, the STFT encounters a dilemma. The optimal window size has to be chosen with keeping in mind that multiplying the signal with a narrow window, the result will give a good time resolution but poor frequency resolution. The other way around, with a wide window the frequency resolution is good but the time resolution will be poor (Molodova, Li, Núñez, et al., 2014), (Hlawatsch & Boudreaux-Bartels, 1992), (MathWorks, 2019).

2.4.2. CWT

From studies in the past, the Continuous Wavelet Transform (CWT) has proven to be an effective mathematical tool to analyse ABA-data (Molodova, Li, Nunez, et al., 2014). It overcomes the latter mentioned drawbacks of the Fourier Transform and is an effective tool to analyse signals in the frequency domain. It's main principle is based upon multiplying a signal by a shifted and scaled group of wavelet functions. The CWT makes use of a so called Mother wavelet function ψ (e.g. Morlet, Paul, DOG). This wavelet has to be chosen based upon the application and characteristics of the signal. Often the complex Morlet wavelet is used due to its Gaussian characteristics in frequency and time (Greenblatt et al., 2012). Next to the Mother Wavelet a certain scale is defined. The scale is similar to the window size in the STFT, however, still maintains a balance between the time and frequency resolution. Obtaining a high resolution both in frequency as in time domain is a major benefit of the CWT (Torrence & Compo, 1998). Using the following formulas:

$$\psi_0(\eta) = \pi^{-\frac{1}{4}} e^{i\omega_0 \eta} e^{-\frac{\eta^2}{2}} \tag{2.4}$$

$$W_n(s) = \sum_{n'=0}^{N-1} x_{n'} \psi\left(\frac{(n' - n)\delta_t}{s} \right) \tag{2.5}$$

Using equation 2.4 and 2.5 results in the wavelet coefficients of a specific time signal. With

W_n as the wavelet coefficient of the signal $x(n)$ with time step δ_t, ψ as the mother wavelet, s the wavelet scale, n' as the time shift, n as the time index and ω as the non-dimensional frequency.

By varying the wavelet scale and translating the signal along the time index, a scalogram can be constructed showing the amplitude of any features and how this amplitude varies over time (Torrence & Compo, 1998). A scalogram is a visual representation (in the form of a heatmap) of the wavelet spectrum in which the absolute values of the squared CWT's coefficients are plotted (equation 2.6). Unlike the spectogram formed by a STFT which does not show the location in time of the frequency, a scalogram does show the location in time of any occuring frequencies (Molodova, Li, Nunez, et al., 2014), (Greenblatt et al., 2012).

$$\left| W_n^2(s) \right| \tag{2.6}$$

At last, the scalogram can be made easier to interpret by taking the average of a certain location within the scalogram (a slice in the spectrum plot). Through the summation of the obtained wavelet spectrum values the average frequencies can be plotted, called the global wavelet spectrum. Using the formula:

$$\frac{1}{n_a} \sum_{n=n_1}^{n_2} \left| W_n^2(s) \right| \tag{2.7}$$

In which n_a acts as the parameter between which location points the average is taken from (between n_1 and n_2) (Torrence & Compo, 1998). In chapter 3 the results of these method are showed using the programming language Python.

2.5. Numerical models

In the past different studies and models have been made of transition zones mainly using finite element methods (FEM). Through this approach the effect of passing train loads are simulated and dynamic structural analyses conducted. However, as axle box vertical acceleration are generated by the vehicle, the use of multi body simulation (MBS) software could give a fast analysis of transition zones in comparison to FEM in terms of computational effort. Just like the axle box acceleration based research, below an overview is given of the research and corresponding models that have been made. The models are discussed briefly as this research will focus on a model made by using MBS software (see 4 for more information).

2.5.1. FE-models

The main reason for making a 2D model is the ease of the calculation since use can be made of symmetry in the longitudinal direction of the track. Next, vertical behavior only can be considered and less DOF's are present, while still maintaining accurate results (Lei & Mao, 2004) (Fortunato et al., 2013). As for the 3D models, they are more common in the literature

than the 2D models. Although having a greater computational effort and longer calculation times (more DOF's are present), they can give a better representation of the reality in terms of occurring stresses and strains (Fortunato et al., 2013).

The first mention in the literature of a model consisting of a transition zone can be found in Hunt (1997). In this research a 2D model was created using a beam-spring system as track structure (I.e. Euler-Bernoulli beam on an elastic foundation, Winkler foundation). From this model using only one single wheel as load, the rail deflection, wheel forces and track settlement were derived. These 2D models have also been made by Z. G. Li and Wu (2008), Lei and Mao (2004), Namura and Suzuki (2007), Zakeri and Ghorbani (2011) (MATLAB-model), Dimitrovová and Varandas (2009), Varandas et al. (2011), Alves Ribeiro et al. (2015) and Paixão et al. (2016).

As for the 3D FE-models, they can be found in Gallego Giner and López Pita (2009), Nicks (2009), Coelho (2010), Dahlberg (2010), Banimahd et al. (2012), Shan et al. (2013), J. Shi et al. (2013), Shahraki et al. (2015), Chumyen et al. (2022), Ngamkhanong et al. (2020) and Ramos et al. (2022).

In Lei and Mao (2004) the transition zone was modelled as a slope using a continuous spring-damper elastic foundation with one vehicle as the primary loading condition. From this model several parameters were captured under varying slope and stiffness conditions. One of the conclusions of the research conducted was that the differential settlement has more influence on the increase of dynamic forces than the abrupt stiffness. Furthermore, in the research of Z. G. Li and Wu (2008) yet again one single wheel was simulated on a beam-spring system. The transition zone was tested under varying lengths of the slab track and velocities of the wheel. While other research focused on half a vehicle and varying settlement values with the track structure modelled as a Timoshenko beam (Namura & Suzuki, 2007). Varandas et al. (2011) modelled one vehicle on a continuous rail following the Euler-Bernoulli conditions. However, the model itself is non-linear, taking increasing stiffness changes into account with increasing deformation. In a more recent research of Alves Ribeiro et al. (2015) a transition zone model of a culvert was created with backfill as a countermeasure. The results show that the model is in good correlation with the corresponding experimental field measurements and that due to the short calculation time 2D models can be highly efficient. At last, the model of Wang (2018) consists of a complete embankment-bridge-embankment railway structure, resulting in a high computational effort. One of the goals of this research was to investigate if either stiffness or differential settlement contributes more to the increase of track degradation of transition zones on both sides (both embankment-bridge as bridge-embankment transition zones). For the model, use is made of Hughes-Liu beam elements as rails (with UIC54 properties), spring-damper elements in between the rails and sleepers as fasteners with bilinear properties to simulate clamping of fasteners in tension and rail pads in compression. Furthermore, non-linear contact elements between the sleepers and ballast are used to simulate a more realistic behavior as they take into account the the spatial movement of sleepers and ballast stresses. Together with interface elements the penetration of the sleepers into the ballast due to the dynamic forces is prevented. As for the differential settlement an initial settlement is applied over the whole transition zone of 4 mm. Due to the simulated clamping of the fasteners and sleepers and the bending stiffness of the beam elements, hanging sleepers are created. The conclusion from this research was that the differential settlement is the main contributor to the high dynamic loads and therefore the track degradation. Next, it showed that the degradation of the approaching zone (EB) is of more interest than that from the BE transition.

From these papers it becomes clear that none of the models uses the vertical axle box acceleration measurements to investigate the condition of a transition zone.

2.5.2. MBS models

For the multi body simulation software, the research is quite limited. From a literature study, no research has been found on transition zone models using this kind of software. This gives a clear indication of the novelty of this research. In the research of Shen et al. (2016) for example, the effect of wheelset flexibility at crossings is investigated using MBS. More research about crossings and irregularities like squats (high frequency defects) can be found using this kind of software.

Although the MBS software is based upon analysing the vehicle dynamics, certain toolkits within the software exist to simulate more complex situations, for example flexible bridges. This toolkit allows for the creation of a flexible track with the ability to change the properties (stiffness and damping) for every sleeper individually (see chapter 4 for more information). In the research of Bezin et al. (2009), this toolkit is used for the investigation of hanging sleepers and its effect on the vehicle dynamics. The research shows that the effect of sleeper voids give a realistic result in terms of an increase in the dynamic forces of the wheel-rail contact. The sleepers surrounding the void experience higher forces and with an increasing velocity, the dynamic amplification increases as well. Furthermore, this paper suggests that by using this toolkit the creation of a transition zone with the presence of hanging sleepers, could be possible using this kind of software.

<div align="right">

3

</div>

Measurement data analysis

In this chapter the ABA-data is analysed and processed. At first, the location of the field measurements is discussed, and the transition zones present identified. Then, different statistical and mathematical methods are applied on the data using Python to identify trends, patterns, certain anomalies and main frequencies. The goal of this chapter is to find characteristics of transition zones in the data. Through this goal, an answer on the second sub-question is tried to be obtained, 'From the acceleration data, is it possible to indicate characteristics of the transition zones?'. The data comes from the research of Unsiwilai et al. (2023).

3.1. Location description

The trajectory where the axle box acceleration has been acquired is between station Lage Zwaluwe (Noord-Brabant) and Dordrecht (Zuid-Holland). The acceleration data available has been measured with a CTO train (*'Centrum voor Technisch Onderzoek'*) at two consecutive days in 2019, both longitudinal as vertically at multiple wheelsets on both the inner and outer rail. A total length of around 11 kilometers has been made available to analyse. The track consists of a double railway line, with the available data obtained from the East side of the track going in the direction of Dordrecht.

3.1.1. Classification transition zones

Figure 3.1 shows the locations of the bridges and the corresponding transition zones. The bridges cross different roads, waterways, other railway lines and small streams. The section also contains different level crossings and turnouts, therefore their transition zones. However, this will be out of the scope for this research due to the available model.
In table 3.1 nine parts of the trajectory are highlighted showing the embankment-bridge (EB) and bridge-embankment (BE) transition zone. In this research both zones will be analysed and discussed. According to Wang (2018) different behavior exist in both of these zones. While the amplification of the dynamic forces in the EB-zone mostly comes from the change in settlement and pitch movement of the bogie, the amplification of the dynamic forces in the BE-zone can be assigned to the drop and bounce of the bogie. The front bogie of the vehicle drops from the bridge on the open track and due to settlement and stiffness changes, it bounces on the open track increasing the wheel loads. For each bridge the location in kilometers is given together with the average speed of the CTO measurement train used to obtain the ABA data. The average velocity has been taken from the research of Unsiwilai

Figure 3.1: Transition zone locations. In green the ballast to slab track transition zones and in red the ballast bridge decks.

et al. (2023). Next to this, track remarks are given. Some of the transition zones consists of auxiliary rails as countermeasure for the differential settlement (increase of bending stiffness) and others have insulated rail joints (IRJ's) in close proximity which could affect the data in terms of high dynamic wheel loads that could be shown as high peaks in the acceleration data. An important factor to consider is the fact that no current condition is known of this particular track section. With the aid of different techniques anomalies indicating track irregularities can hopefully be observed.

Noticeable are bridge number 3 ('Moerdijkspoorbrug') and 8. Both of them containing a slab track (following the theoretical description of transition zones) while the rest is built up with ballast track (see figure 3.1 for the locations). Especially number 8 will be of interest due to the presence of a slab track and location of the IRJ, which is around 40 meters away from the bridge deck (so less influence on the data). Number 3 will be more difficult to assess due to its long bridge deck of over 1 kilometer. Due to the absence of auxiliary rails and conveniently placed IRJ, bridge number 4 will therefore instead be discussed below. The remaining transition zone data will be analysed as well and can be found in Attachment C. These locations however, do have IRJ's in the near vicinity (within 30 meters).

3.2. ABA data

Here the ABA-data will be analysed and discussed. Different mathematical methods will be briefly explained and its results shown. Due to the extent of the data, bridge numbers 4 and 8 plus the corresponding transition zones will be shown with the aid of graphs and plots (full overview in Attachment C).

From the formula of the excitation frequency (e.g. frequency caused by an outside force), see equation 3.1, the cut off frequency to be used for the Butterworth filter at the filtering process of the data in chapter 3.2.1 can be obtained. With higher frequencies corresponding to short wave track irregularities (e.g. squats, corrugation, et cetera), a lower cut off frequency is desired. By using the sleeper spacing of 0.6 meters a characteristic point in the data can be obtained. The transition zone frequencies are most likely lower (due to the longer length of a transition zone) and therefore the sleeper spacing could act as a maximum in the data analysis, while most peaks are filtered out. The CTO train makes use of an ABA sensor with a 25,600 Hz frequency rate, which makes the filtered results very accurate.

$$f = \frac{V}{\lambda} = \frac{25}{0.6} = 41.67 Hz \tag{3.1}$$

With a cut off frequency of 41.67 Hz (smaller for the lower velocities) an initial analyses can be performed at the data. However, to make sure no information is lost a slightly higher low pass filter of 45 Hz will be used in the data analysis. Noticeable is the changing velocity for the different transition zones. As the only changing variable in equation 3.1 is the velocity, each transition zone will have a different cut off frequency depending on the outcome using the sleeper spacing as wavelength. These frequencies are given in table 3.2.

3.2.1. Statistical analysis

For the detection differences between open tracks and transition zones, it's important to get an idea of the length of a transition zone. Of course, this length is variable and depending on the location and state of the transition zone. In the literature no clear answer to this question can be found either. After gathering information, the following comes up. In the research of Wang (2018) for example, displacement increases until around 4.5 meters before the bridge structure are measured. This same value holds for Le Pen et al. (2014). In Varandas et al. (2011) and Coelho et al. (2010) the transition zone is around 7.2 meters and 8 meters respectively. While in D. Li et al. (2005) the length of 30 meters is taken. The formula used in Wang, Chang, et al. (2018) gives a more substantiated answer:

$$L = \sqrt{1,6 * \Delta(h) * V_e^2} \tag{3.2}$$

In this formula L (meters) will be length of the affected zone (transition zone), with $\Delta(h)$ the displacement (meters) and V_e the velocity of the railway vehicles (km/u). For convenience 0.01

Bridge No.	GPS location (km)	Photo (ProRail, 2023)	Railway track bridge deck	Remarks	V_{ave} (m/s^2)
1	17.272 - 17.297		Ballast track	IRJ (17.243)	22
2	17.423 - 17.431		Ballast track	IRJ (17.436)	22
3	17.834 - 18.936		Slab track	IRJ (17.786) Auxiliary rails	25
4	24.652 - 24.661		Ballast track	IRJ (24.704)	25
5	25.228 - 25.246		Ballast track	IRJ (25.226)	25
6	25.255 - 25.265		Ballast track	IRJ (25.226)	25
7	26.993 - 27.023		Ballast track	IRJ (26.991) Auxiliary rails Station	20
8	27.728 - 27.763		Slab track	IRJ (27.799) Auxiliary rails	15
9	28.414- 28.434		Ballast track	IRJ (28.448) Auxiliary rails	10
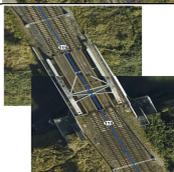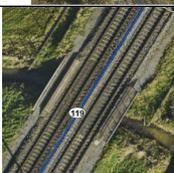
Table 3.1: Detailed information of the transition zones present

Velocity (m/s)	Cut off frequency (Hz)	Frequency range of interest (Hz)
25 (no.4,5,6)	45	5 - 21
22 (no.1,2)	40	4 - 18
17 (no.7)	30	3 - 14
15 (no.8)	30	3 - 12.5
10 (no.9)	25	2 - 8

Table 3.2: Velocities with their corresponding cut off frequency and range of interest for analysis

m is taken as the displacement and 140 km/h as the velocity of the train (Dutch operational speeds), the maximum length of a newly constructed transition zone will therefore be:

$$L = \sqrt{1,6 * 0.01 * 140^2} = 17.7 meters \tag{3.3}$$

However, with different velocities known (table 3.1) the transition zone length will differ from the calculated value. Using the formula again results in lengths of 4.6 up to 11.4 meters. Therefore, further calculations will maintain the 11.4 meters. Again, this is not the final length but will serve as an indicator for different analyses techniques. During this analysis some transition zones could appear to have larger or smaller affected lengths.

3.2.1.1. Magnitude

According to the research of Salvador et al. (2016), the ideal location for axle box accelerations is the first wheelset on a trailer vehicle instead of the motor vehicle. This has to do with the motor-induced vibrations that can interfere with the measurements. However, because the data is acquired with a CTO train, no trailer vehicle is present. The data that is used in this chapter is from the first wheelset of the first bogie. Although this is not the ideal location, the before-mentioned vibrations can be neglected.

The first step in any data analyses is the visualisation of the acquired data. In this case the visualisation shows an acceleration-distance graph as seen in figure 3.2. With the location of the bridges collected in table 3.1 every transition zone can be plotted keeping in mind the corresponding velocities and thus changing frequencies.

From the figure it can be seen that the track consists of high vertical accelerations along the track. These high peak are most likely the result of the presence or IRJ's and small track defects (e.g. track irregularities like squats and corrugation). Also the variation in speed can be a cause for the fluctuations in density along the zero acceleration axis.
By applying a signal processing filter data can be filtered both in the high or low band (active filter). Doing so unwanted components in the data can be removed and only a certain frequency range can be acquired. With this purpose in mind the Butterworth filter is applied. The Butterworth filter is able to reshape the frequency spectrum of the signal with a flat frequency response as result. After selecting the desired passband, the range of frequencies that is
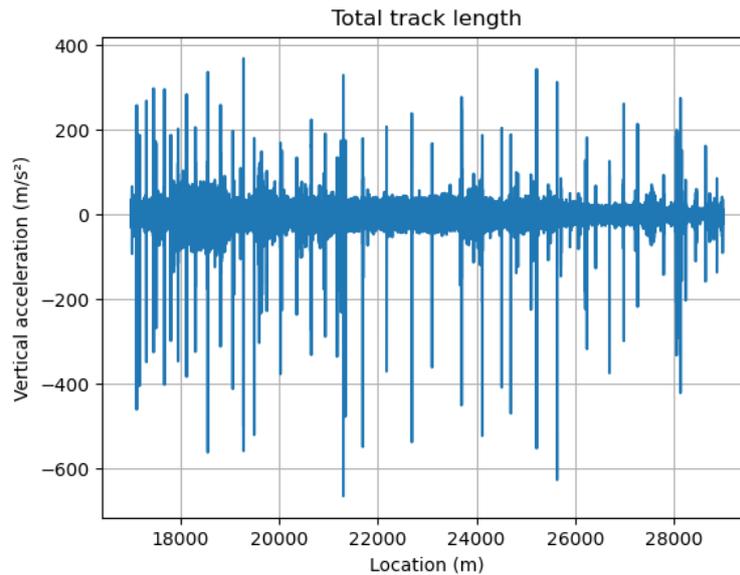
Figure 3.2: Plotted acceleration data from Lage Zwaluwe to Dordrecht

allowed to pass through the filter, an order has to be selected. The higher the order, the more complex the calculation will be, however, more precise as well (increase in stopband response). The Butterworth filter is a commonly used filter due to the lack of ripples in the output and its roll-off. This is the part where the filter is at its stopband (cut off frequency) and thus in a so called transition band. Here, the filter has the advantage of keeping the signal smooth during this transition, unlike other filters that can have an abrupt transition. Another advantage of the Butterworth filter is the flat frequency response. When using a low pass filter, all the frequencies within the given passband are still there but attenuated in amplitude. In the end, the same factor is used for each frequency present in the passband which results in a flat frequency response. So in short, the Butterworth low pass filter removes high frequency noise from the input and preserves low frequency content in the output.

The formula for the transfer function can be expressed as following:

$$H(j\omega) = \frac{1}{\sqrt{1 + \varepsilon^2 (\frac{\omega}{\omega_C})^{2n}}}$$

(3.4)

With H being the transfer function, ε as the maximum passband gain, ω as the operating frequency, ω_C as the cut off frequency (rad/s) and n the order of the filter (Electronics, n.d.). This formula describes the frequency response of the Butterworth filter principle. The filter's characteristics are determined by this function. Such as the flat frequency response, magnitude of attenuation and the smooth or abrupt roll-off.

As discussed above a Butterworth filter of the fourth order with a cut off frequency of maximum 45 Hz (depending on the velocity) is used to get a better visualisation of the data from figure 3.2 using Python. In figure 3.3 bridge number 4 and 8 are plotted, with and without the filter. In these figures the bridge locations are highlighted with grey areas and red lines, the data here

(a) Bridge 4   (b) Bridge 8
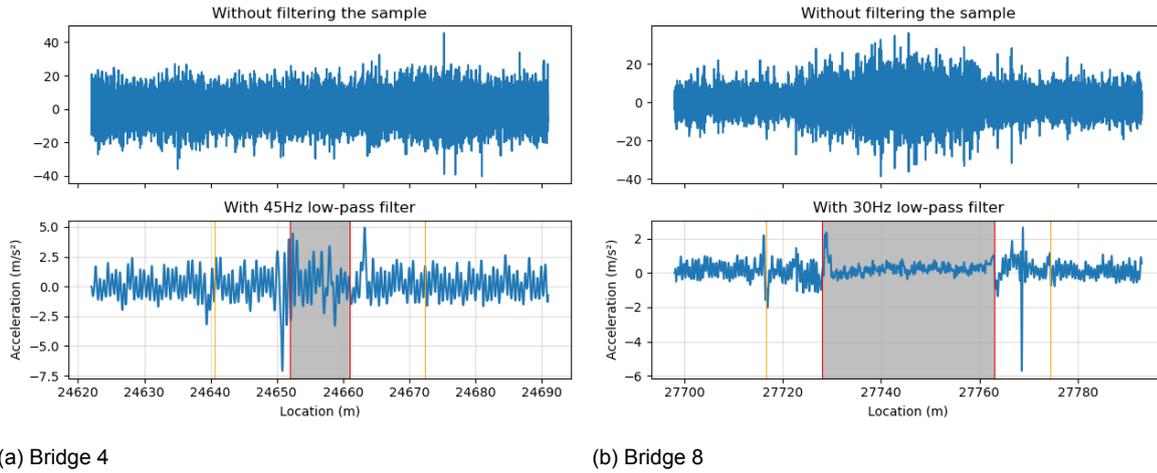
Figure 3.3: Selected data from bridge 4 (a) and 8 (b). The red lines mark the start and end of bridge and orange lines mark the start and end of the transition zone

is not considered. The orange vertical lines show the beginning and ending (as estimation) of the transition zones as calculated before. In both cases there are some clear peaks visible at -2.5 m/s^2, -7.5 m/s^2 and 5 m/s^2 for bridge 4. For bridge 8 the peaks are visible at -2/+2 m/s^2 and -6 m/s^2. While the amplitude stays overall the same. For bridge 4 the data ranges from -7.5 to 2.5 m/s^2 and for bridge 8 from around -2 to 2 m/s^2. However, the peaks on their own don't show the condition of the transition zone or ability of the ABA data on itself. They do give an idea of the track geometry at particular time stamps. Some of these peaks for example, can indicate small defects or track irregularities. Especially the peak at bridge 4 close to the bridge can indicate the presence of degradation or hanging sleepers.

3.2.1.2. Normal distribution

The transition zone can be selected for each bridge using the length calculated in 3.2. After looking at the magnitude, the normal distribution (the Gaussian distribution) can give a better representation of the data in terms of assessing variability, infer patterns and making predictions. The normal distributions main function is the probability density function $f(x)$:

$$f(x) = \frac{1}{\sigma\sqrt{2\pi}} e^{-\frac{1}{2}(\frac{x-\mu}{\sigma})^2} \text{ for } -\infty < x < \infty \tag{3.5}$$

With σ being the standard deviation and μ as the mean (Dekking et al., 2005).

From figure 3.4 the normal distribution is plotted for both the transition zones shown in orange and the open tracks shown in blue. The normal distribution for bridge 4 indicates a higher standard deviation for the transition zones than the open track. It shows a sigma of 0.93 against 0.50 and 0.84 against 0.43 for the EB and BE zones respectively (figure 3.5). This can be interpreted as a section of track with outliers and anomalies which as well indicate certain track irregularities. Figure 3.4b (bridge 8) has a more equal pattern with the open track in terms of the normal distribution for the EB zone (as well as the standard deviation), however the same conclusion as before is drawn for the BE zone. The EB zone of bridge 8 could be interpreted (based upon only these values) as a transition zone in good condition (not many outliers in the dataset). Next to the standard deviation, the kurtosis could be of interest. The standard
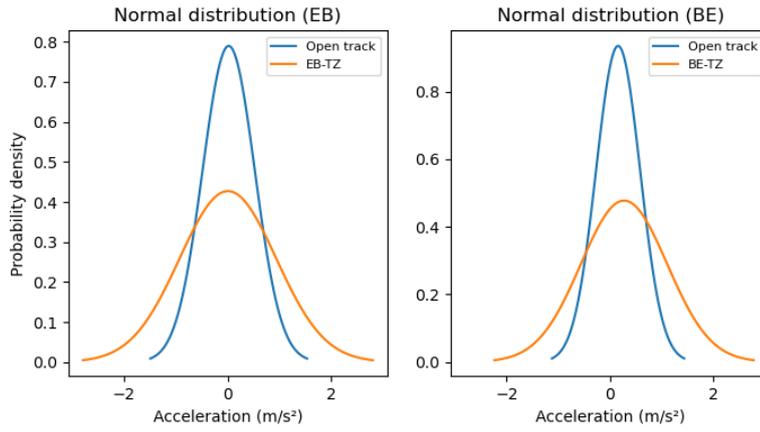
(a) Bridge 4
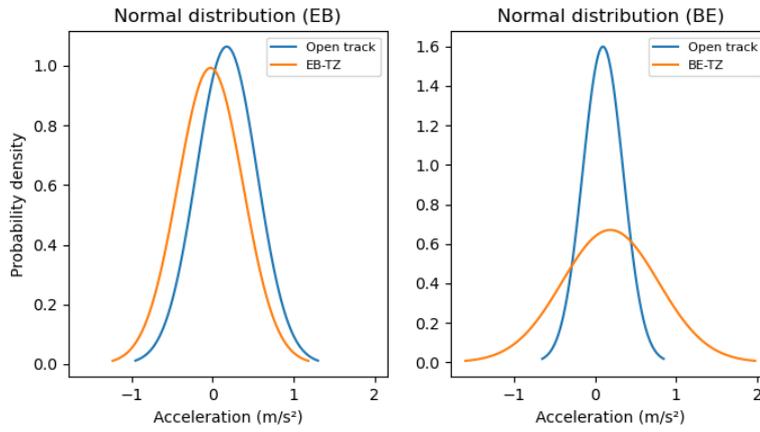
(b) Bridge 8

Figure 3.4: Normal distribution from open track and transition zone
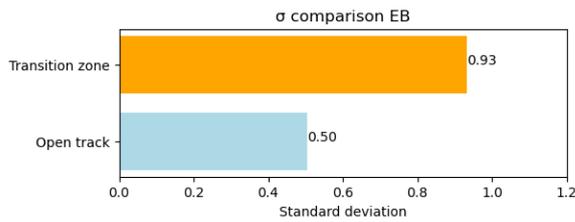
(a) EB zone bridge 4
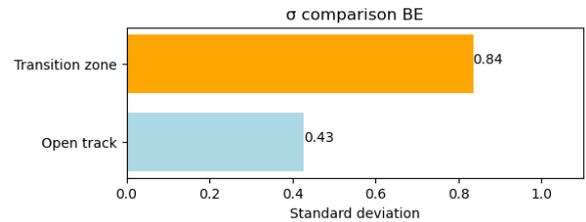
(b) BE zone bridge 4
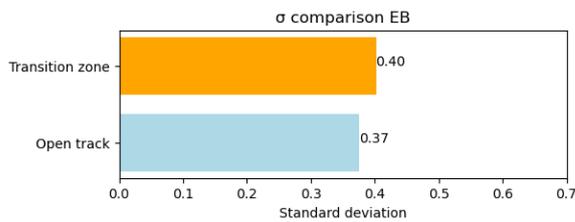
(c) EB zone bridge 8
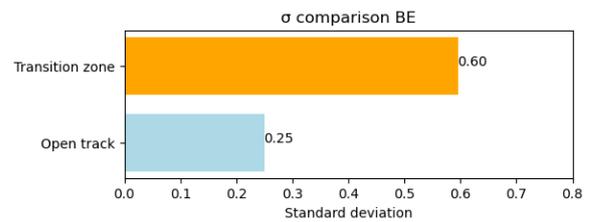
(d) BE zone bridge 8

Figure 3.5: Standard deviation from open tracks and transition zones

deviation can be compared between transition zones and open track and it is expected that the standard deviation (how much it deviates from the mean) is higher at transition zones due to higher dynamic amplifications and thus track degradation. The kurtosis on the other hand, a degree of peakness of the distribution, could give information about anomalies in the data set. High values for the kurtosis should indicate peaks in the signal, while lower values should indicate a more equal signal. Attachment B describes the kurtosis principle in more detail. However, resulting from the use of this analysis method on the data set, it indicates that the values does not seem to match the expected results. The kurtosis values are based upon the expected number of outliers, which means that if a dataset has a lot of outliers, the kurtosis value will not indicate them (e.g. in the case of transition zones). It would be denoted as *normal* for the data set. Also, the sample sizes plays an important factor.

3.2.2. Frequency analysis

For the frequency domain analyses, different mathematical methods can be used. With the data being in the time domain a better understanding of what happens at the track can be given though frequencies as discussed in chapter 2.4. From here it is concluded that the most used methods are the Fourier Transform (FT) and Continuous Wavelet Transform (CWT). To get a basic grasp of the frequencies in the data, the FFT is used. Be aware that the FFT is a discrete transformation, while the data is continuous. However, this would give a clear suggestion of what frequencies occur while not being entirely accurate mathematically. For now this can be neglected.

3.2.2.1. Fourier Transform

The graphs in figure 3.6 show the frequency domain of the data sets of bridge 4 and 8. The vertical axis is normalized in order to remove the redundancy of the magnitude level and to make both graphs more comparable. The horizontal axis shows the frequencies. First thing to notice is the peak at around 42 Hz and 26 Hz for bridge 4's and 8's transition zone, respectively. With the velocities known from table 3.1 the corresponding wavelength equals around 0.6 meters for both, which is the sleeper spacing. At bridge 4 multiple smaller peaks are obtained, all less than approximately 27 Hz. These peaks can correspond to the bogie length, the distance of two separate bogies of the vehicle, or higher wavelengths irregularities. They indicate wavelengths of 3 meters or more which are according to the NEN-EN 13848-1:2019 corresponding to the *D1* wavelength range ($3 < \lambda \leq 25 meters$) (NEN, 2019). Commonly hanging sleepers, differential settlement and differential stiffness are irregularities with a wavelength of 1.2 meters up to 5 meters (TU Delft, 2020b). These wavelengths are chosen over the NEN indications due to the fact that wavelengths of 25 meters are far out of range for the purpose of this research. By looking at figure 1.3 the length of a transition zone is at least several sleepers wide, making the before mentioned wavelength a good indicator for this investigation.

For bridge 8 the highest peaks are more concentrated below 10 Hz, while the magnitude remains very small in comparison to bridge 4. This would correspond to a wavelength of 3 meters or more which is in line with the before mentioned wavelengths as well. As already discussed, although the Fourier Transformation gives a first impression about the magnitude of the different common frequencies, it does not give an indication of the location in time of these frequencies. Also, using a lower cut off frequency would magnify the lower frequencies in terms of magnitude and lower the sleeper spacing peak. This could help in identifying the

peaks more accurately if needed.

(a) Bridge 4   (b) Bridge 8
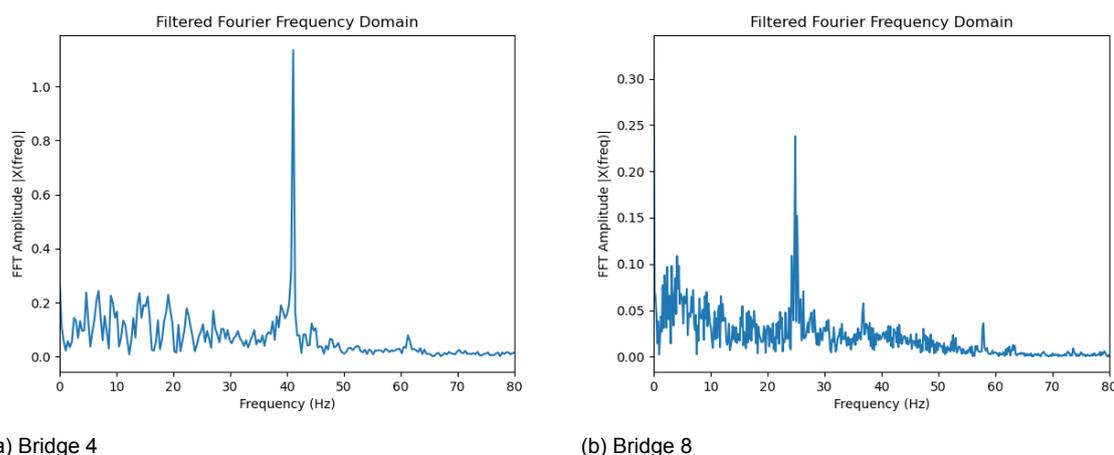
Figure 3.6: Fast Fourier Transform of filtered data

3.2.2.2. Continuous Wavelet Transform

As stated in chapter 2.4, the Continuous Wavelet Transform gives a better understanding of the frequency domain, as it considers the location of the frequencies as well. From the scalogram, the visual interpretation of the CWT's outcome, a fast visual condition assessment could be obtained. A scalogram can be seen as a heat map in which the frequency strengths are shown in terms of a color magnitude. With the location on the horizontal axis and frequency response on the vertical axis. The colour map *jet* is used for the scalogram in order to fit other research with acceleration related scalograms.

Figure 3.7 gives the results of the CWT coefficients. with the knowledge obtained so far, the vertical axis is limited by the frequency of the sleeper spacing. Below this value the relevant frequencies for the condition assessment of the transition zone can be found (the bigger the wavelength, the lower the frequency of interest). Although the data from the bridge itself is not considered in this research, the sudden disappearance of the sleeper spacing frequency at bridge 8 shows the presence of the slab track. Here no sleeper spacing is present due to the absence of sleepers (bridge 4 contains ballast track).

Looking at the EB-transition zone, greater frequencies can be seen at bridge 4. However, from table 3.1 it is known that the CTO train had a higher velocity at bridge 4 than at bridge 8. With higher velocities, also higher energy excitation's are expected and thus a stronger ABA-responses. This is clearly the case with the vertical acceleration measurements. The peak frequency just before the bridge at figure 3.7a is coming from a rather small wavelength track irregularity (less than 1 meter), which could indicate damage to the track at the point of transition. With the same magnitude (power) at bridge 8 at the location of embankment to bridge transition, it could be argued that the moment of transition (e.g. the abrupt stiffness change) can be clearly visible in the ABA signal using a scalogram. With the value depending on the velocity and the condition of the transition zone, a stronger power value could be an indication of the presence of abrupt stiffness change and differential settlements. This would be in line with the location of these track irregularities as well.

Next to the higher magnitude peaks also more light coloured concentration areas around 10 Hz for bridge 4 and around 5-10 Hz for bridge 8 are present. By keeping in mind the
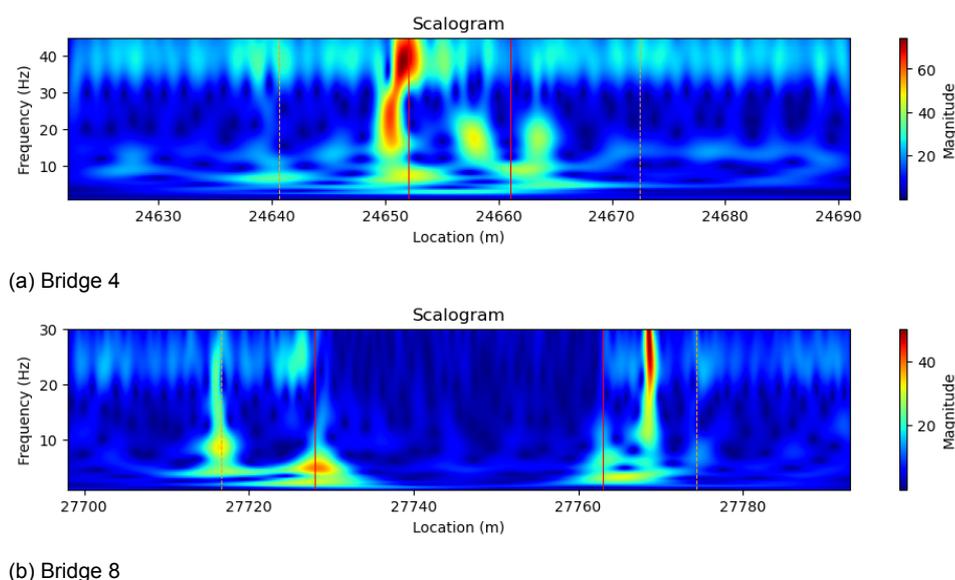
(a) Bridge 4

(b) Bridge 8

Figure 3.7: Continuous Wavelet Transform of filtered data. Red lines show bridge location, orange lines show assumed transition zone beginning and ending, respectively

1.2 - 5 m wavelength range and the corresponding velocities of each bridge, frequencies of around 5-20 Hz and 3-12.5 Hz for bridge 4 and 8 respectively are of particular interest. These frequency peaks are clearly visible within the light coloured frequency concentration areas on both scalograms. This indicates not only the presence of the transition zone, but also of a certain differential settlement or hanging sleeper. The BE transition zones also show light colored concentration areas for both frequency ranges. The transition from bridge to open track however, gives less magnitude of the frequencies compared with the EB transition. This could be explained due to the moving behavior of the bogie. At the end of the bridge it more or less glides off the bridge and drops and bounces on the open track, the bogie does not follow the same movement when running onto the bridge. At bridge 8 (EB) a strong frequency concentration can be seen at around 25 Hz. The location of this frequency response coincide with the ending of the auxiliary rails. Another reasonable cause could be the presence of a fish plate joint.

Now by using the global wavelet power spectrum principle, the average of the scalogram can be plotted at different time intervals (in this case locations). In figure 3.8 the global power spectrum of the bridges are plotted. Figure 3.8a shows the total track length until start of the bridge (4), while figure 3.8b shows the total track length starting at the end of the bridge (4). The same holds for bridge 8. First thing to notice at the plots of bridge 4 is the peak of the sleeper spacing at around 40 Hz. This same peak is visible in the graphs of bridge 8 at around 25 Hz. By looking at the EB transition zone of bridge 4 a peak with almost the same energy in magnitude as the sleeper spacing is present at around 15 Hz which is inside the region of interest. Also, the overall power of the frequencies is higher for the transition zone than for the open track especially in the region mentioned. For bridge 8 (figure 3.8c) the same phenomenon is visible with a peak around 4 Hz. The open track however, also shows large peaks around the same frequency. This frequency could be assigned to the vehicle motion, but with wavelengths of 1.9 and 3.8 meters uneven ballast settlement is more likely. Ultimately, differential settlement is not limited to transition zones. A big distinction between bridge 4 and 8 is the power in which these frequencies exist. For bridge 4 the overall power is far greater than for bridge 8 which again falls in line with the conclusion that the EB transition zone of

(a) Bridge 4, EB transition zone

(b) Bridge 4, BE transition zone

(c) Bridge 8, EB transition zone

(d) Bridge 8, BE transition zone
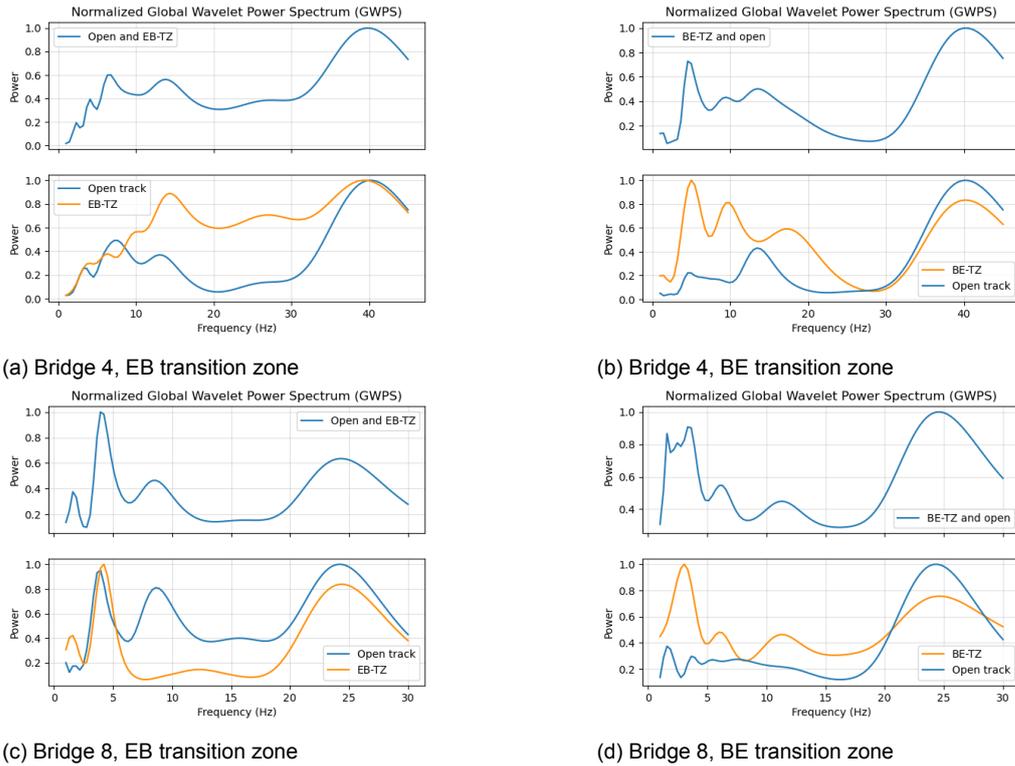
Figure 3.8: Global wavelet spectrum

bridge number 8 can be in better condition than EB transition zone of bridge number 9. Next, by looking at the BE transition zones similar conclusions can be drawn. For bridge 4 (figure 3.8b) again the peaks of the transition zone frequencies exist only in the region of interest. For bridge 8 (figure 3.8d), a similar high peak at around 3 Hz exist which still falls in line with the before mentioned region. Again, the overall power of bridge 4 is greater than for bridge 8. Frequencies coming from the length of the wheel base of the bogie or car body (2.5 m and 20 m) are not significant in this data set. The rest of the transition zones are plotted in Attachment C.

3.3. Conclusion

In conclusion, the CWT's coefficient plotted within the scalogram give a good visualisation of how the transition zone is acting during a train pass in terms of frequencies. Making use of the global wavelet power spectrum in correlation with the scalogram gives a more complete picture of what is happening inside a certain region. High frequency peaks can be easily spotted together with the location, length and magnitude of these anomalies. For transition zones the wavelength between 1.2 - 5 meters seems to be correct in order to find long wave track irregularities. Besides, the GWPS shows in most of the cases a larger power overall of the transition zone frequencies than for the open track frequencies. Next, it is also noted that in almost all of the transition zone GWPS plots, the frequency concentrations differ for the embankment-bridge section and bridge-embankment section. The data from all transition zones considered, shows that the frequencies of the EB transition zone concentrate overall more between the full region within $1.2 < \lambda < 5$ meter. While the BE transition zone is more concentrated at the higher region of these wavelengths (lower frequencies). All of these conclusions confirm that transition zones can be distinguished with certain frequencies based upon differential stiffness, settlements and hanging sleepers.

Overall, the scalogram and GWPS are good indicators to perform a data analyses on vertical acceleration data. An interesting question to ask is if the frequencies for range for $\lambda = 1.2$ - 5 meters will also be present in the results of the numerical simulations and how these frequencies would behave in terms of magnitude/power when a transition zone is in better or worse condition (low versus high degradation)? These questions will be discussed in chapter 4, 5 and 6.

4

Numerical model

Now that the main frequencies of the transition zone are identified, this chapter will present a method to simulate the behavior of a transition zone using a multi body simulation (MBS) software instead of the commonly used finite element analysis software (as in previous research). This chapter will answer the third sub-question, 'Is it possible to simulate the behavior of a transition zone using a multi body simulation (MBS) software?'. At first, the MBS software is explained more elaborately. Second, different methods to obtain a transition zone model are proposed and the results discussed.

4.1. Multi body simulation software

The software used for the simulation of a transition zone is VI-Rail. VI-Rail is a multi body simulation (MBS) software which can be described as a numerical simulation tool in which the motion and behavior of rigid or flexible bodies in a system are simulated and analysed. Unlike finite element analyses, MBS software focuses on the overall movement of a mechanical system (instead of focusing on individual components within the system) and no mesh will be created. Several bodies are connected and interact with each other through a contact model. VI-Rail simulates and analysis the behavior of the railway vehicle. With the moving track analysis, the track is modelled as a rigid body and only the vehicle dynamics can be evaluated. The mass of the sleepers moves a long with the location of the vehicle, making the computational time very low. The VI-Rail flextrack plugin allows for the creation of complex track models such as bridges that include the flexible characteristics of the rail (represented by mass less Adam Beams) which is adjustable per individual sleeper. With the aid of flextrack, the interaction between the vehicle and railway can be modelled in situations where the track flexibility should be taken into account (e.g. transition zones) (VI-Grade, 2016). Table 4.1 shows the advantages and disadvantages of the moving track analysis and flextrack analysis. In terms of advantages and disadvantages of MBS and FEM, several major advantages of MBS over FEM are the savings in computational time and the flexibility of the system. It's faster and easier to make adjustments with MBS software. However, also drawbacks exist. The stress distribution for example is easier to interpret using FEM and the main purpose of VI-Rail is vehicle dynamics. Using MBS however, initial knowledge about the behavior of the railway track is needed before running a simulation. For example, when adjusting the sleeper sizes in flextrack, the base bushing (spring and damper) need to be altered as well. The software does not do this automatically.

The experience with VI-Rail shows that the use of MBS represents a reliable and accurate
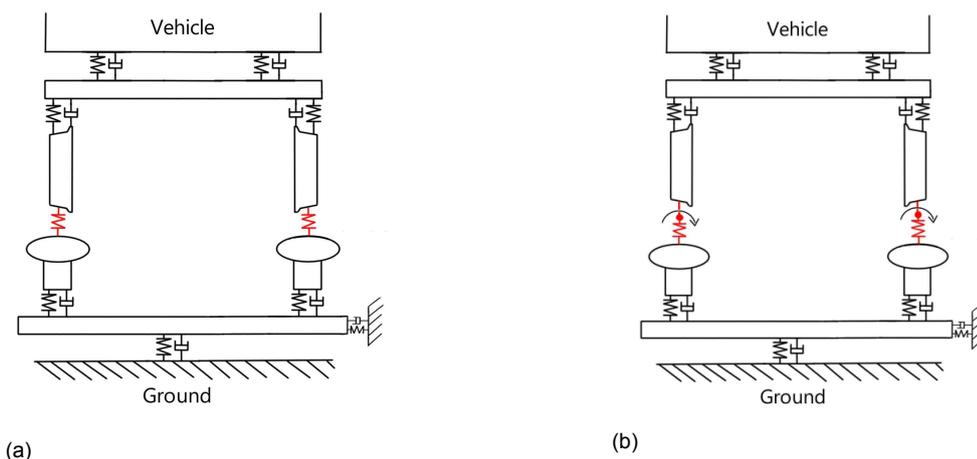
Figure 4.1: Schematic view of the moving track analysis MBS setup (left) and flextrack setup (right)

representation of reality and it could be promising to investigate the behavior of transition zones using the flextrack. An important aspect to notice is that VI-Rail is specifically designed to investigate the vehicle dynamics. Although it can be difficult to implement a realistic behavior of the transition zone, the vertical acceleration of the vehicle is part of the vehicle dynamics VI-Rail is designed for.

	Moving track	Flextrack analysis
Advantages	- Fast and reliable simulations - Easy implementation of settlements	- Ability to adjust parameters per sleeper individually (e.g. stiffness, damping, et cetera) - Possible to create complex tracks - Allowing to create hanging sleepers
Disadvantages	- Only vehicle dynamics can be adjusted - No options to change track parameters - Good understanding of the behavior of railway tracks is needed	- Not being able to introduce settlements - Longer simulation times - Good understanding of the behavior of railway tracks is needed

Table 4.1: Advantages and disadvantages moving track vs flextrack analysis

As MBS software is based on the interaction between different models, these different models need to be defined first. Often three models are needed to complete a simulation. One as the vehicle model, the other as the track model and last the contact model between the latter mentioned models. Figure 4.1 gives a schematic view of the setup of the model. The bogie and car body interact with each other trough springs and dampers (e.g. secondary and primary stiffness). The track model consists of base bushings (sleeper to ground connection) and rail bushings, the rail pads and fasteners (rail to sleeper connections). The contact model between both is shown in red. As for the flextrack toolkit (figure 4.1b, the schematic view is changing slightly. Next to the translational degrees of freedom, also rotational degrees of freedom are present at the location where the Adam Beams act as the rails. These beams are flexible in longitudinal direction and behave as Timoshenko beams. The moving track principle contains rigid rails.

4.1.1. Vehicle model

For the vehicle the standard benchmark model called Manchester Passenger Wagon is used. This vehicle model is provided by the software and consists of a car body, two bogies and four wheelsets (see figure 4.2). As stated before, the models are multi body systems connected by dampers and springs, with the wheelset connected to the bogie (primary suspension) and the bogie connected to the car body (secondary suspension). While the measurements from 3 are obtained using a CTO train this research's main focus is on the track geometry instead of the vehicle model. The only adaptation to the vehicle model that has been made are the added acceleration output requests on the axle box of the front bogie (both left and right).

4.1.2. Contact model

For the contact model the VI-Rail software provides several options. The contact model describes the wheel-rail contact in terms of the kinematics of one wheel relative to one rail. For the use of flexible track only WRGEN elements are available. This General Contact Element uses the wheel and rail profile as input and computes the actual contact kinematics for each step during the simulation. This element gives the most accurate results of the wheel-rail contact while it is still computational efficient. Therefore it is the most suitable element for dynamic simulations. More information can be found in VI-Grade (2022).
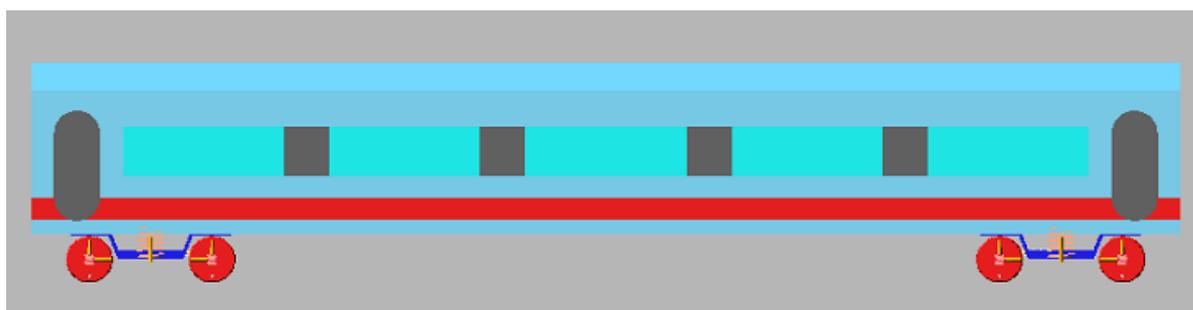
Figure 4.2: Vehicle model

4.1.3. Track model

The track model consists of both the ballast/rail properties and track geometry. For the track properties the stiffness and damping values are derived from studies done at the university (see attachment D). For the track geometry use is made of a windows command file that can be imported within the VI-Rail environment to automatically generate a pre-programmed track. The advantage of using this method is the ease to adjust certain parameters, the reference to certain values, the length of the track and the properties of each sleeper individually. Also, the location of irregularities and settlements can be added in this script. Without using a file to automatically create the track model, the procedure is not only very time consuming it is also prone to error and almost impossible for larger tracks. Changing objects manually in the software is far more difficult and most likely result in errors when starting a simulation than using this type of script. The rail profile UIC60 has been chosen which in the Netherlands is used at the HSL line and Betuweroute. This profile is selected for convenience as VI-Rail does not by itself contain the UIC54 profile (more commonly used at regular routes in the country).

4.2. Model simulations

To test the ability of the flextrack tool and to be able to answer the sub-question stated for this chapter, several cases are simulated to analyse the responses. The different models are discussed and its relevance is explained. Two main ways of testing the ability of the MBS software are elaborated below. For all simulations holds that use is made of a Gstiff integrator method with a maximum allowed integration step (Hmax) of $2x10^{-4}$. The simulation velocity is set at 25 m/s (as this is the maximum speed of the available measurement data and will be useful for chapter 5) with time steps of $1x10^{-3}$. The bridge length depends on the model but will be great enough for the whole vehicle model. The open track that will be investigated next to the transition zone, will be 40 meters for both the EB and BE models. Due to the extent of the investigation multiple sections will be shown and discussed in attachment F, referred to later on in this chapter.

4.2.1. Flextrack

The first way to test the ability of the MBS software is purely focused on the use flextrack only. Figure 4.3 shows the model plan for the different models. After reaching model number 2a, the introduction of the settlement curve, the flextrack analysis results in simulation errors. Although method 1 fails to reach its intended goal, the knowledge obtained from the results and models help in understanding the basics for method 2 (section 4.2.2).
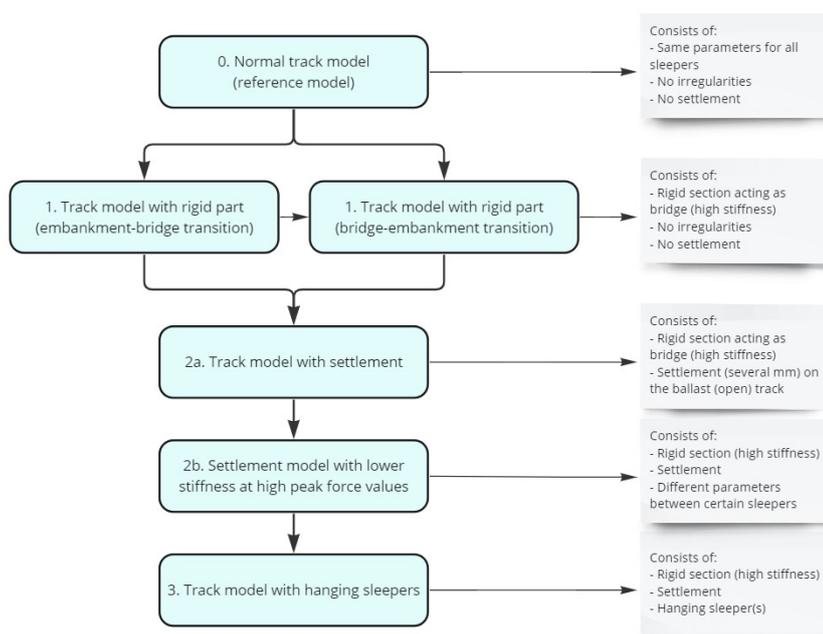
Figure 4.3: Track models. Each new model consists of the old model including its adjustments

First, a track without any settlement or irregularities is used to analyse the wheel force and vertical accelerations over time even as displacements for a general understanding of the results (called the normal track model or zero model). This model will act as a reference to the later created models, at the same time it will give an indication of how long the track should be made in order to damp out vibrations from the vehicle. Next, this model will be validated in order to make sure the results are correct.

Second, a rigid section simulating a railway bridge is inserted (model 1). The rigid section uses a much higher ballast stiffness (the bushing of figure) which simulates an engineering structure that is not influenced by any settlement. Two models will be created here, one acting as the embankment bridge transition zone, and the other acting as the bridge embankment transition zone.
These models will be presented and discussed in attachment F.

Third, settlement is introduced (model 2a). This settlement of several millimeters will act as the differential settlement causing transition zones to deteriorate faster than open track. Only one model will be made here, a longer but similar track according to model 0. The goal of this model is to see how the software reacts to the settlement and where the highest forces arise. This location will be marked and the bushing stiffness of the sleeper will be lowered for model 2b (both EB and BE models) to simulate the degradation of the transition zone.

Finally, after investigating the results of the latter mentioned models, hanging sleepers are simulated on the locations where the lower stiffness is introduced (model 3). At these locations the sleepers are experiencing the most forces/stresses and therefore will be the first to create a void in the ballast underneath the sleeper.

Normal track model - model 0

Starting with the normal track model a track with a length of 160 meters is tested. For the flextrack analysis to work it is important for the simulation that both the start and the end sections are fixed. In other words, both sections have to be modelled as rigid. These sections are made 30 meters long, long enough to make sure the vehicle is completely positioned on this initial rigid track to enable a smooth simulation start. Figure 4.4 shows the track model with both the rigid parts at end and beginning and the normal track in the middle. After running the simulation, the vertical contact force of the front wheel (figure 4.5a) shows the distance it takes for the vehicle to completely damp out any vibrations (caused by the rigid part). Although the noise to signal ratio is very low, it takes around 125 meters to get a constant signal. With this conclusion, the next track models will be made longer. Also, figure 4.5b shows the vertical acceleration signal of the vehicle bogie (ABA signal). This signal will be used as a reference signal for the later simulations. The peaks at the beginning and end are related to the stiffness change of the rigid section to the open track (and vice versa). These peaks will not be discussed any further but will be visible in later results. Figure 4.5c gives the scalogram of the vertical acceleration. With the knowledge obtained in chapter 3 only the frequencies below 45 Hz will be considered. As the figure shows, the frequencies above this value are not relevant.
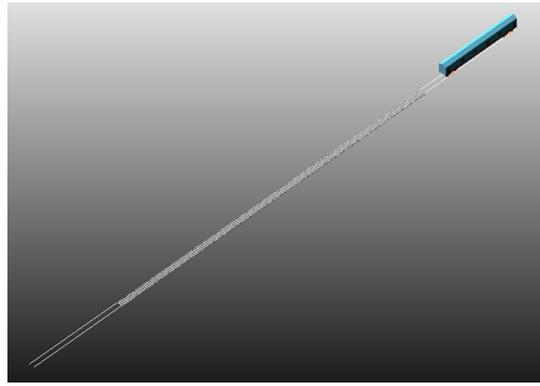
Figure 4.4: Initial track model

(a) Vertical wheel-rail contact forces

(b) Vertical acceleration

(c) Scalogram of the acceleration results
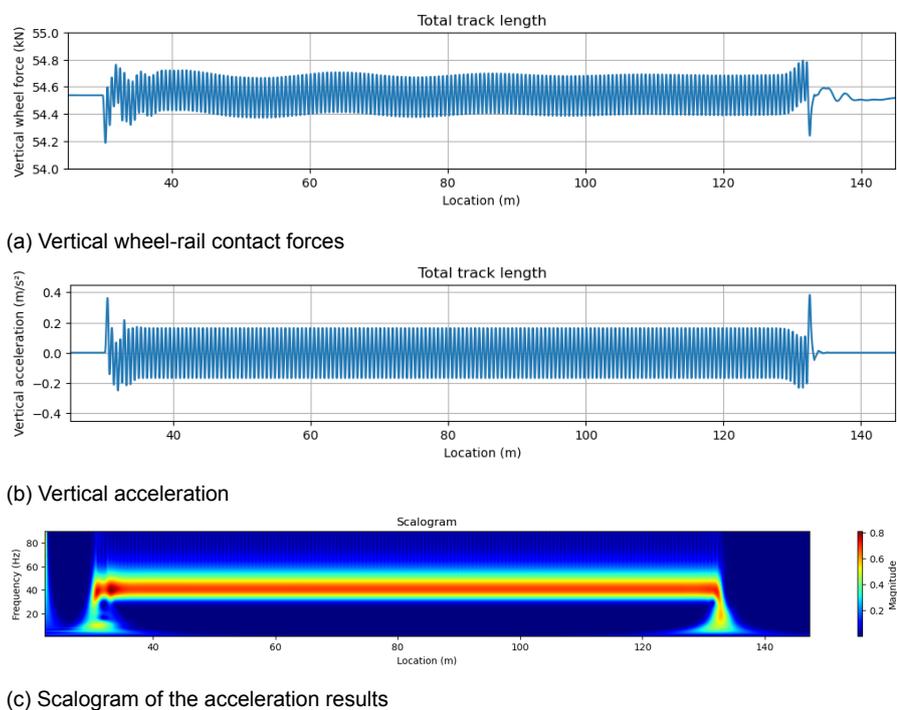
Figure 4.5: Results from the normal track model

Model validation

To continue the model adjustments, the results need to be validated. At first, a visual validation is done. With the total mass of the vehicle known, the wheel forces coincide with the expected results of forces around 54.5 kN. Without any irregularities on the track like differential stiffness or differential settlements, the amplitude of the forces (figure 4.5a) seem in order. With only a first bump of the fixed section towards the open track a low signal-to-noise ratio is expected to damp out over time. This can be clearly seen in the figures. Next to the forces, also accelerations can be validated. The accelerations are in the range of 0.2 m/s^2 which is in line with the research of Wang (2018).

Although, the results do look rather discrete and less natural this could be assigned to the

fact that the track is perfectly straight with no influences acting on it except from the vehicle dynamics.

After a visual validation, the Zimmermann model can also be used to validate the model. Here, a comparison of the rail deflection between the simulation results and the Zimmermann's beam formulation is given. For a complete explanation of the Zimmermann model a reference is made to attachment E. Figure 4.6 shows both sleeper deflections plotted in the same graph. The close proximity between both models gives a good indication of the accuracy of the MBS software.
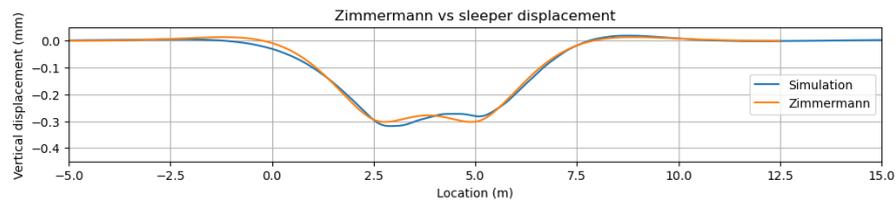
Figure 4.6: Analytical Zimmermann calculation vs the sleeper displacement of the normal track model

Differential settlement model - model 2a

In model 2a the track settlement is introduced (no bridge section is present). After construction of a railway track, the ballast immediately settles, this settlement is about 4 mm. For this reason, a differential settlement of 4 mm is introduced in the model. The settlement uses a transition of around 7.5 meters in length with a slope of 1:1875 (figure 4.7). In the industry a slope of 1:600 or more is compulsory. The reason for the length is based upon the size step the settlement curve is interpolated with. If the length is too small, the MBS is not able to converge to a solution, being too long however, the transition would be too smooth to be able to notice any changes in the results.
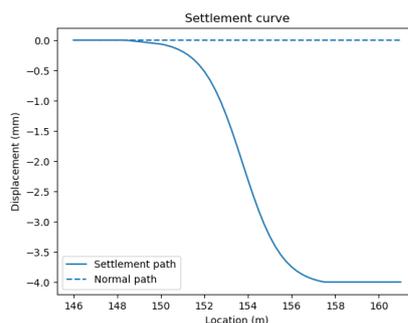
Figure 4.7: Introduced settlement curve starting at 150 meters (BE transition zone)

From a trial and error approach, the s-curve for the settlement is the best option to use. Implementing the settlement linearly from 0 to 4 mm gives a clear nod in the settlement curve and creates a two-point contact for the wheel-rail contact. The software is not able to interpolate these settlement curves. Implementing a more smoother line, like an s-curve, works better for the software.

(a) Vertical wheel-rail contact forces

(b) Vertical acceleration

(c) Scalogram of the acceleration results
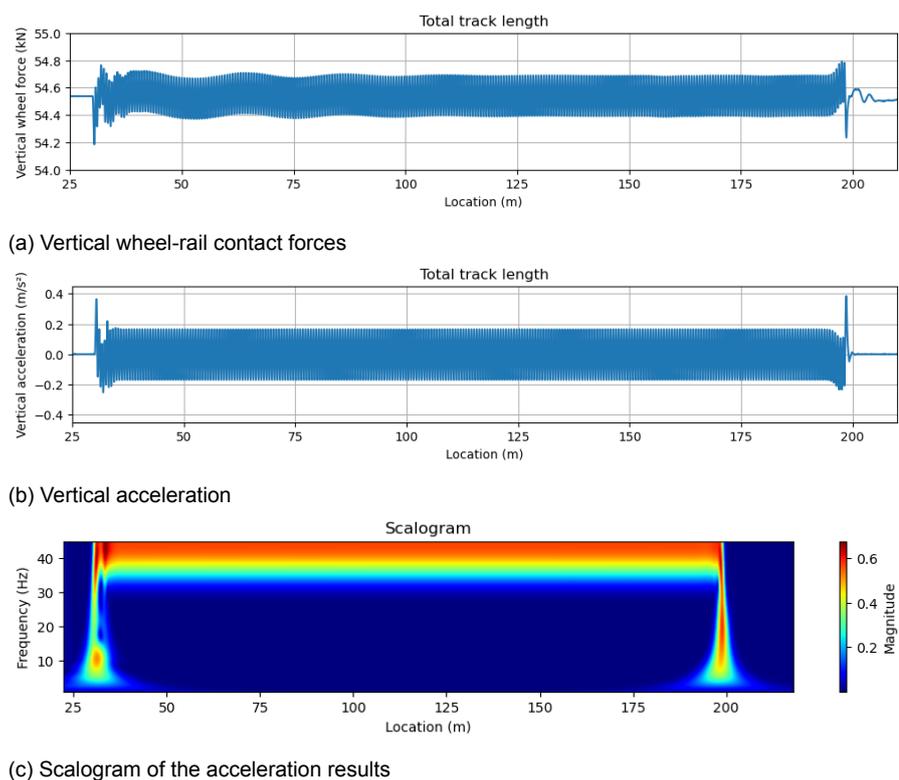
Figure 4.8: Results from the differential settlement model

With the differential settlements applied, it is noticeable that the settlement does not appear to be taken into account in the software. The settlement curve is implemented in the track file however, neither the forces nor the accelerations seem to pick it up (figure 4.8). No peaks are visible in the graphs and no frequency concentration is present in the scalogram apart from the first and last part of the track. A peak in force that slowly declined to zero with a sinusoidal wave was expected. After running several simulations with different lengths of the settlement curve, smaller steps for the interpolation, smaller time steps for the simulation and changing between the two ways the settlement can be implemented in the track file (both analytic 'vertical path' and through 'measurement path'), the conclusion can be taken that the flextrack is not able to process settlements in the track geometry.

Following this conclusion a quick simulation is set up in the moving track analysis of VI-Rail. Here, less degrees of freedom are present and no flexibility of the rails is available. By applying the same parameters and settlement curve, the results are given in figure 4.9. It is clear from the wheel-rail contact force that the settlement should indeed be visible in the data. Not only the forces change over time as expected with a decreasing sinusoidal wave, also the vertical acceleration from the axle box changes. Why the flextrack does not show this is unclear, however, it is a strong proof that flextrack is not as accurate as the software implies it is. Different methods have been tried to bypass this error. First, to see if the flextrack reads the track files correctly, a different track file is implemented. A model with a curved track shows that flextrack does read the track file correct. Second, a time step of 10^{-4} is assigned to the simulation. Not only does this make the simulation time almost 6 hours, it also results in a simulation failure for different settlement curves. Third, section breaks were applied in the settlement file. With this method VI-Rail creates a spline between points, however, this is often used at the rail configuration and not at the vertical path where the settlements are

defined. Again, this results in a simulation error. Considering all of these reasons, it can be concluded that the first method of achieving a transition zone with the MBS software fails. It is not possible to get an idea of where the biggest forces occur using the flextrack due to the settlement and thus, it is not possible to replace the sleepers at this location (as this is unknown) with weaker sleepers (in terms of vertical stiffness) and voided sleepers for the next models.

(a) Vertical wheel-rail contact forces

(b) Vertical acceleration
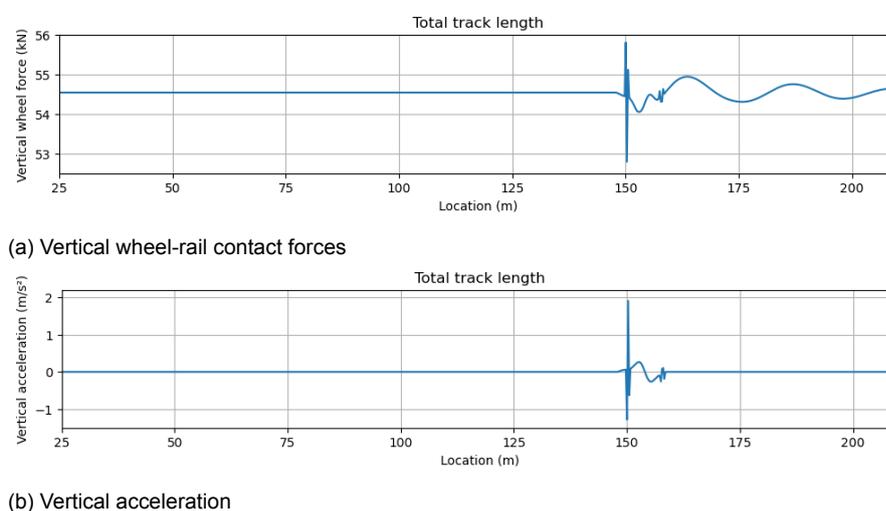
Figure 4.9: Results from the differential settlement model using the moving track

Although it's not possible to simulate the settlement in the flextrack model, it is proven that differential stiffness is picked up by the flextrack analysis and settlements at the moving track analysis. Stiffness and settlement are proportional related and this relationship can be used for achieving correct results with the MBS software. Based upon this conclusion a second method is proposed.

4.2.2. Flextrack vs moving track

A second way of testing the ability of the MBS software is focused on both the flextrack toolkit as the moving track analysis. As discussed above, the moving track shows the differential settlement in both force and accelerations outputs, while the flextrack shows the differential stiffness only in these outputs. By modelling different cases with only settlements in the moving track, and only stiffness differences in the flextrack, the behavior of a transition zone could be simulated and compared. This assumption is based upon the relationship between settlement and stiffness, as stated above. These parameters are proportional to each other. Figure 4.10 shows this relationship.

With an increasing force or settlement, the stiffness increases as well. This graph contributes to the idea of changing the stiffness properties in flextrack in such a way that they resemble the desired settlement of the track. In other words, by lowering the vertical ballast stiffness of each sleeper individually, the forces of the vehicle model cause the settlement to occur in a numerical way. The other way around, by implementing settlements, the forces of the vehicle cause the vertical stiffness to change. This latter mentioned principle can be used for the moving track. Here, the properties of the track can not be changed, the vehicle and track move together in the same plane. The rail, rail pad, fastening system and sleeper properties are not represented. This principle is purely focused on the vehicle dynamics. What is possible to change, and what is visible in the results, is the settlement of the track. Tuning the settlement
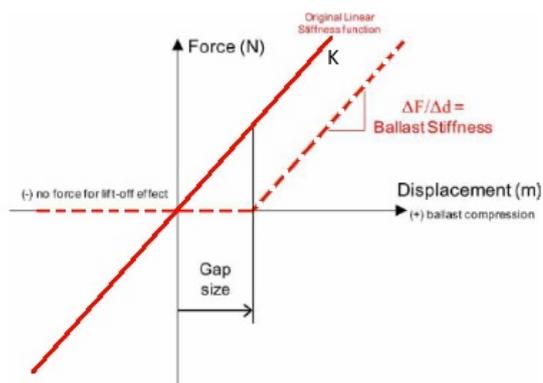
Figure 4.10: Relationship deformation and force (Bezin et al., 2009)

curve in such a way that it represents a settlement that can be seen at transition zones, can be used in the moving track simulation.

In short, the second method focuses on two aspects. Changing the stiffness for the flexible track and changing the settlement for the moving track. These values of both are obtained using Matlab. With the aid of a script based upon the Zimmermann method (see attachment E), written and used in the course TU Delft (2020b), the axle load, different stiffness properties, track length and bending stiffness can be adjusted. In figure F.1 an overview is given of the different models that will be created. Again for each of the models the results are presented and briefly discussed below. Notice, the results of the moving track simulations will act as a guidance. As seen in section 4.2.1, flextrack offers more useful results than moving track itself.
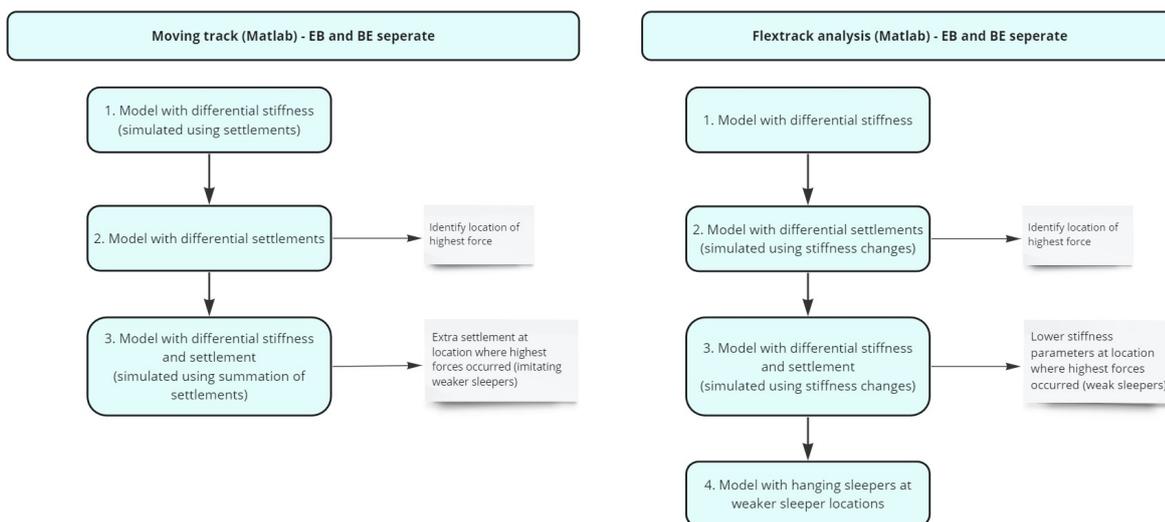
Figure 4.11: Analysis method for moving track using Matlab (left) and analysis method for flextrack using Matlab (right)

First, a calculation is made in Matlab for the differential stiffness. As output the Matlab script results in a certain settlement curve that will be implemented in the moving track model. This

model will be made twice, both for the embankment-bridge model and the bridge-embankment model. As for the flextrack analysis, these models are already discussed in figures F.2 and F.3 and can be found in attachment F (both the moving track analysis as the flextrack analysis)

Second, the differential settlements will be introduced. Again, using the Matlab file the stiffness from the open track will be lowered in order to obtain a settlement of 4 mm. This settlement curve will be used for the moving track (both transition zones). The values for the vertical stiffness will be implemented in the command file of flextrack (where it assigns the correct properties to each sleeper) at the correct locations. The goal of these models is to acquire the locations of the biggest forces right before and/or after the bridge section in the transition zones. At these locations weaker sleepers exist. The Matlab file makes use of the foundation coefficients (see figure 4.12) instead of the ballast and rail stiffness that are needed for the flextrack file. With the following relationship between the foundation coefficient k and the vertical stiffness k_d of the spring, the foundation coefficient can be calculated. Where the 600 comes from the sleeper spacing in mm.

$$k = \frac{k_d}{600} \tag{4.1}$$

Next, the foundation coefficient acts as the total vertical stiffness, while in the flextrack model both the vertical ballast stiffness ($k_z^{ballast}$) as the vertical rail pad stiffness ($k_z^{railpad}$) exists. To overcome this, the formula of equivalent stiffness is used.

$$\frac{1}{k} + \frac{1}{k} + \dots + \frac{1}{k} = \frac{1}{k^{total}} \tag{4.2}$$

$$\frac{1}{k_z^{ballast}} + \frac{1}{k_z^{railpad}} = \frac{1}{k_d^{total}} \tag{4.3}$$

By maintaining the vertical rail pad stiffness constant, the only variable is the vertical ballast stiffness. This is the stiffness parameter that will be changed to simulate the settlement. These models (both the moving track as the flextrack analysis) will be discussed in attachment F.

Third, a combined model of both the differential settlement as the differential stiffness is made. For the moving track this means a settlement curve with higher values. Here, an increase in settlement is made at the locations highlighted from model 2 (the highest force). For the flextrack on the other hand, this means a lower stiffness value for the ballast. Again, this lower stiffness value is implemented only at the locations where the highest forces from the differential settlement results occurred.
Again, these models (for the flextrack analysis only) will be discussed in attachment F.

At last, hanging sleepers are simulated for the flextrack analysis only. These sleepers will be placed at the location where the weaker sleepers are situated (resulting from the latter mentioned model). Here, the sleepers experience the highest forces and will therefore be prone to degradation. For the moving track, no option to create these sleepers is available. This model is therefore only applicable for the flextrack analysis.
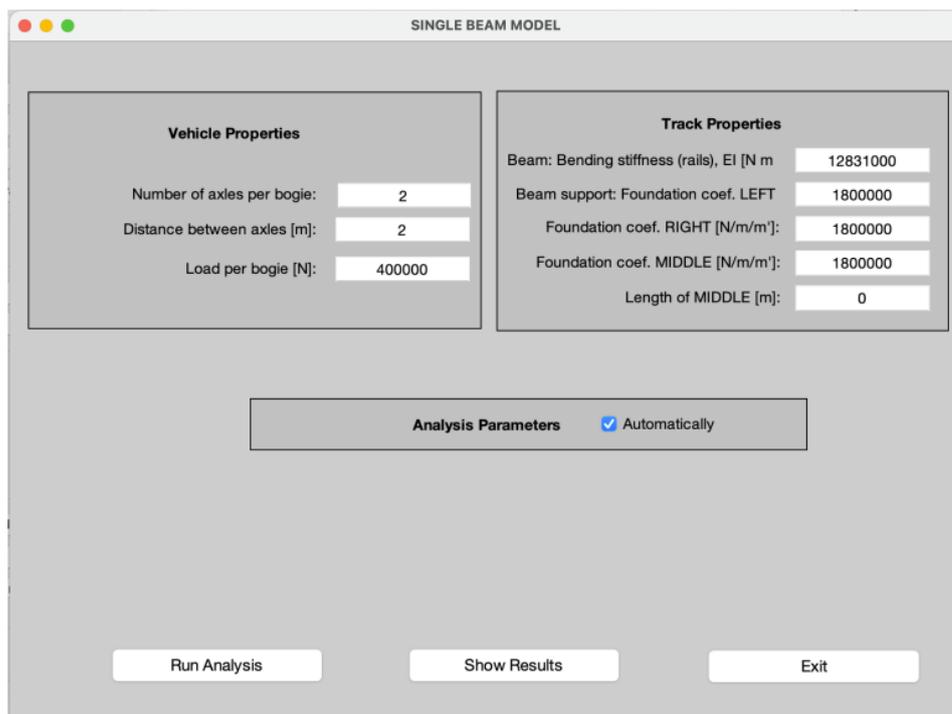
Figure 4.12: Matlab file used

The Matlab file that has been used is shown in figure 4.12 (the parameters shown are arbitrary). Multiple variables in the script can be adjusted depending on the desired simulation. The most important ones are on the right hand side. Here the different foundation coefficients (K1, K2, and K3) can be set according to the principle of figure 4.13. Here, Q defines the wheel load, w the vertical deformation and EI the bending stiffness of the rails. By making K1 rigid and setting the correct parameters at K2 and K3, a transition zone can be recreated. The outcome of the script is obtained in the form of a settlement curve.
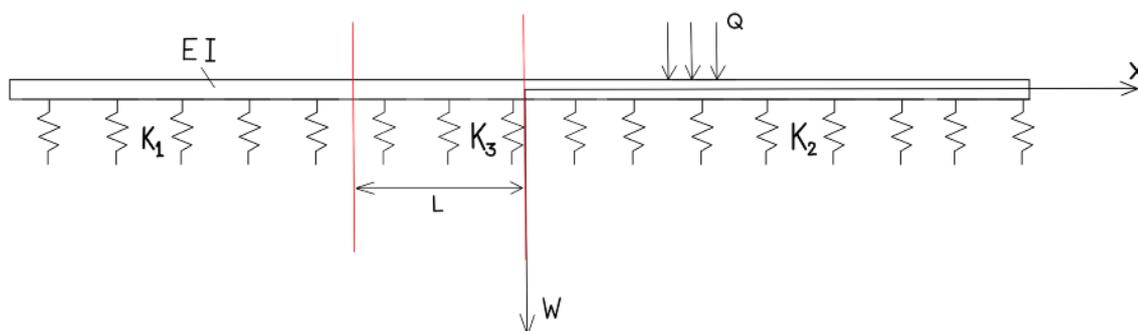
Figure 4.13: Matlab principle (Zimmermann)

Combined model moving track - model 3
The last model for the moving track is model 3. Here, the identified locations of the high forces (attachment F) are modelled with extra settlement to simulate a weaker part of track. Using Matlab new settlement curves are created and implemented in the simulation. An example of the new settlement curve is shown in figure 4.14. The settlement will go up to 6 mm and back to 4 mm again for the rest of the track (vice versa for the EB model). By comparing the dynamic wheel forces, the force of the EB transition zone is indeed much greater than the BE transition zone (figures 4.15a and 4.16a). As for the vertical acceleration of the BE model, two peaks can be noticed. These results look rather odd. A high peak in the beginning was expected but not followed by a second peak. This peak could be the result from an integration error in the software when applying the settlement curve. The first peak corresponds to the movement of the bogie of the vehicle when it hits the settlement and goes back up again (drop and bounce). For the EB model these two peaks are less significant due to the very high amplitude at the beginning of the bridge (180 meters). Also, especially for the EB model the acceleration peaks as well are very high (up to 15 m/s^2) due to the fast elevation of the vehicle. The scalogram shows a clear frequency area in which the differential stiffness and settlement together are concentrated at the lower frequency range. The scalogram of the EB model gives a more logical output than the BE model does. Both models however, look rather discrete in the results.
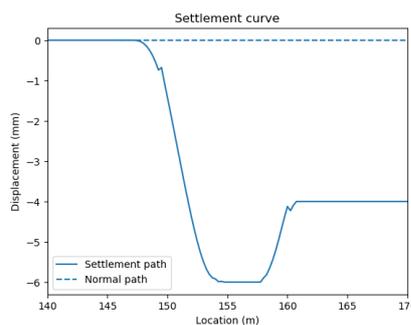
Figure 4.14: Introduced settlement curve starting at 150 meters (BE transition zone)

Transition zone flextrack with hanging sleepers - model 4
The last model that is made using flextrack is model 4. Model 4 contains all the same parameters and properties as the models before (attachment D). However, the main difference here is the introduction of the hanging sleeper that flextrack is able to simulate. When a train passes a hanging sleeper, the sleeper is pushed down but makes no contact to the ballast. Because of this, the wheel-rail forces are distributed along the adjacent sleepers. These sleepers endure higher forces and degradation from this and eventually start hanging as well. The voids in the flextrack simulation are modelled as non-linear functions based upon the value of the void. When the bogie passes the sleeper, no forces are present in opposite direction until the gap between the ballast and sleeper is closed. If this gap is closed, a vector force element proportional to the displacement is activated and pushes against the sleeper. The assigned properties for the base bushing corresponding to these hanging sleepers are halve of the calculated values used (see attachment D and F) (Bezin et al., 2009) (VI-Grade, 2022).

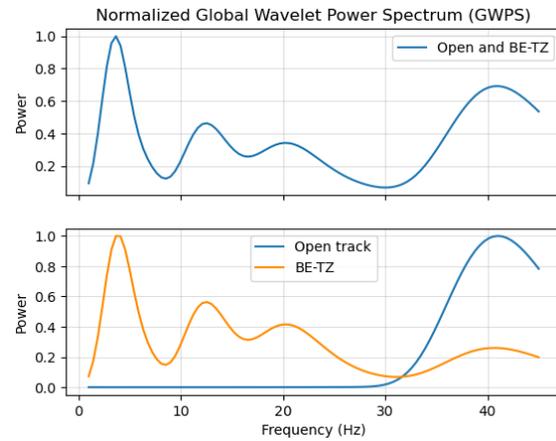Figure F.14 shows the locations of the hanging sleepers in both models in light blue. In red
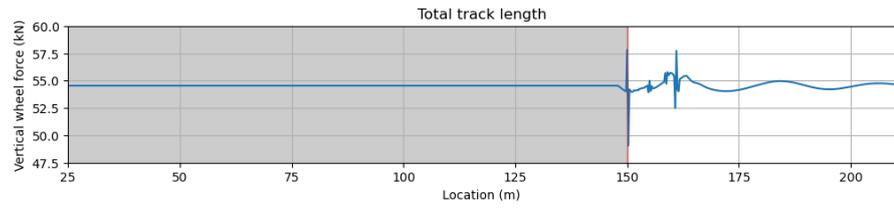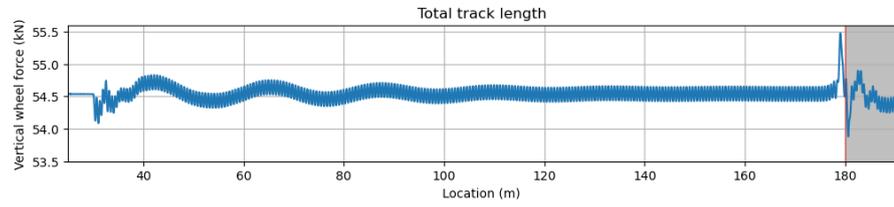
(a) Vertical wheel-rail contact forces
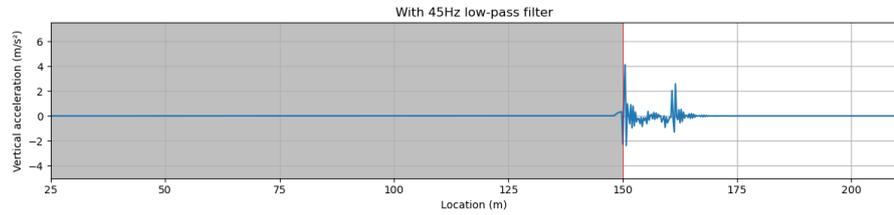
(b) Vertical acceleration
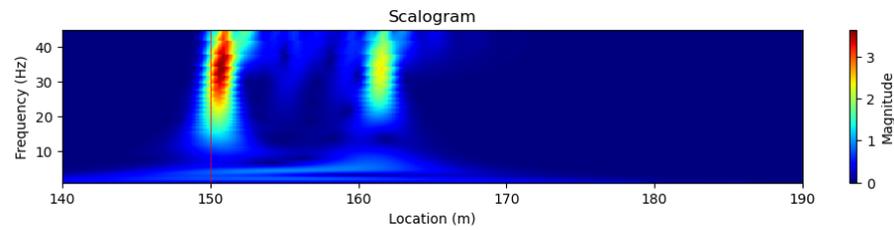
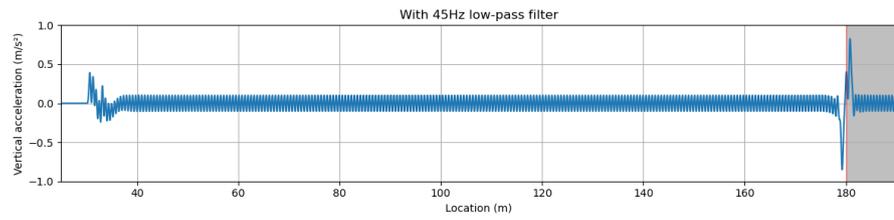(c) Scalogram of the acceleration results. The red line marks the bridge ending

Figure 4.15: Results from the BE model 3 using moving track. In gray the rigid bridge section is plotted
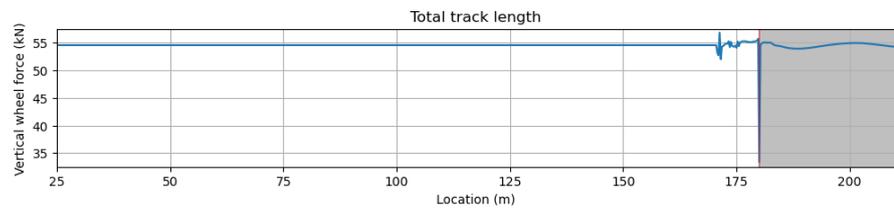
(a) Vertical wheel-rail contact forces
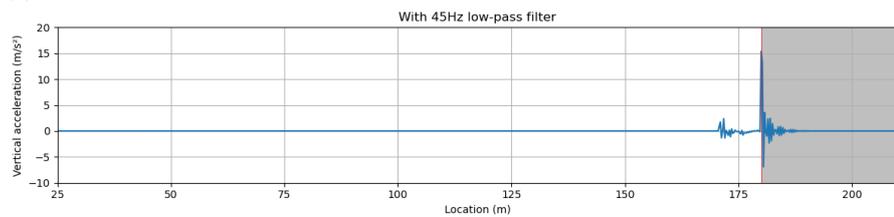
(b) Vertical acceleration
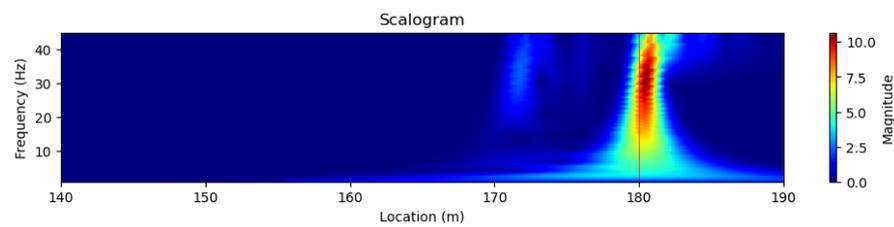
(c) Scalogram of the acceleration results. The red line marks the bridge beginning

Figure 4.16: Results from the EB model 3 using moving track. In gray the rigid bridge section is plotted

the bridge section is highlighted, in silver the open track (where the stiffness corresponding to 4 mm settlement is maintained), and in yellow the weaker sleepers. The hanging sleeper have been given a void with a gap of 1 mm (arbitrary value).

Figures 4.18 and 4.19 give the results for model 4 of both the EB and the BE transition zones. Starting at the wheel-rail dynamic contact forces of the BE model (figure 4.18a, the first thing to notice are the multiple peaks at the beginning of the open track (around 150 meters). These peaks are a direct result of the weaker sleepers in combination with the hanging sleeper since they were not shown in model 3. This is also evidence for the distribution of loads to the adjacent sleepers due to the hanging sleeper as explained above. As for the vertical acceleration, the same peaks are visible. The data here varies from -0.5 to 0.5 m/s^2, which is higher than model 2 and 3. The scalogram of the BE model clearly shows the concentration of frequencies in the lower area due to the differential stiffness and hanging sleeper. The GWPS confirms that most of the frequencies are in the region between 5 and 20 Hz. From the scalogram the transition zone (starting at 150 meters) looks to be around 10-12.5 meters in terms of the concentrated frequency area. For the EB model similar conclusions can be drawn. Both the vertical contact forces as the vertical acceleration values are slightly higher, while the transition zone in length looks to be smaller. Which is in line with the theory about EB transition zones. As for the GWPS results, again the frequencies are concentrated in between 8 and 24 Hz.

When comparing these graphs with the results obtained from the previous models (attachment F), the differences that arise when using different stiffness parameters (weaker sleepers) are evident. Especially the combination with simulating hanging sleepers, the frequency concentration at the transition zone locations become larger and greater (in length and magnitude) than for only differential stiffness and/or settlement. Comparing the results of model 4 of the flextrack analysis with the results of model 3 from the moving track, differences and similarities emerge as well. First thing to notice is that the results of the flextrack look more as expected and the data more continuous than the results coming from the moving track. For the EB model (figure 4.16c and 4.19c) the moving track analysis gives rather odd results with two peaks in both the graphs and the scalogram. It is possible here that the settlement curve is not correctly integrated in the software. The flextrack on the other hand, gives more expected results that are in line with the research of Wang (2018). With one clear peak at the beginning of the transition zone instead of two. As for the BE model (figure 4.15c and 4.18c), the results are more similar in a way that the frequency locations are more or less concentrated at the same values. However, the very high peaks at the acceleration and force results from the moving track are not shown for the flextrack analysis.
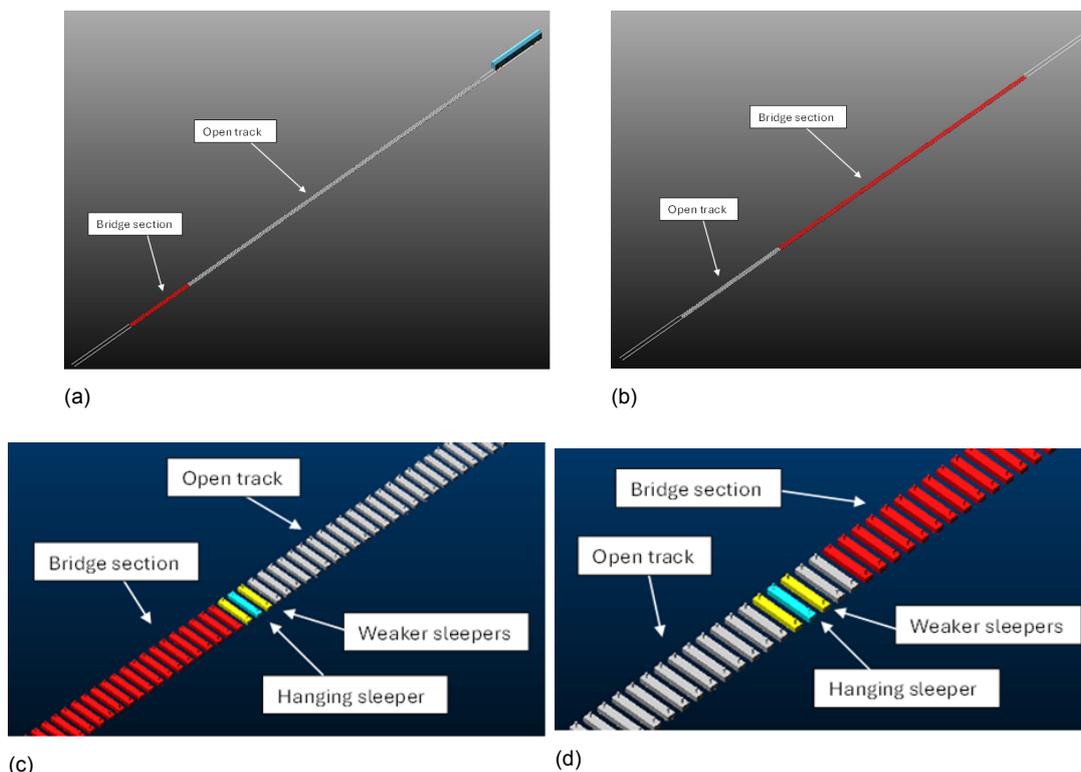
Figure 4.17: (a) Embankment-bridge model and (b) Bridge-embankment model. Close up for model 4 of the (c) EB and (d) BE transition zones

4.3. Conclusion

After running the simulations of method 1 it can be concluded that introducing differential settlement at the flextrack toolkit fails in leading to proper outcome results. When comparing the outcome results of method 2 between the moving track analysis and the flextrack analysis, it becomes clear that the moving track can result in rather discrete and irrational results. A reason for these results can arise from the fact that the moving track analysis is meant for the investigation of the vehicle dynamics only and not for the interaction between vehicle and track. From the research of Wang (2018) it is shown that the differences between the EB and BE transition zone in particular is concentrated at the length of the affected zone and magnitude of the dynamic wheel-rail contact forces. With higher forces but shorter zones for the EB transition zone and lower forces but longer zones for the BE transition zones. These conclusions can be seen at model 3 and 4 of method 2 flextrack analysis. From these findings it can be concluded that the flextrack toolkit is indeed capable of showing differential stiffness and settlement (in terms of stiffness) changes. Also, the main occurring frequencies are in line with the findings from chapter 3. More about these frequencies in chapter 5.
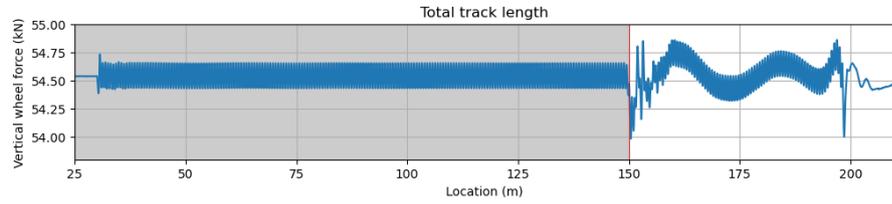
(a) Vertical wheel-rail contact forces
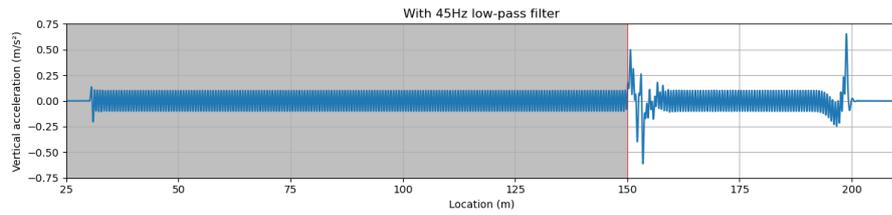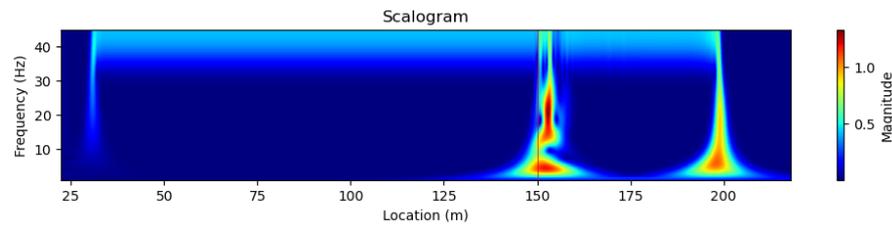
(b) Vertical acceleration

(c) Scalogram of the acceleration results. The red line marks the bridge ending

(d) GWPS of the acceleration results

Figure 4.18: Results from the BE model 4 using flextrack. In gray the rigid bridge section is plotted

(a) Vertical wheel-rail contact forces

(b) Vertical acceleration
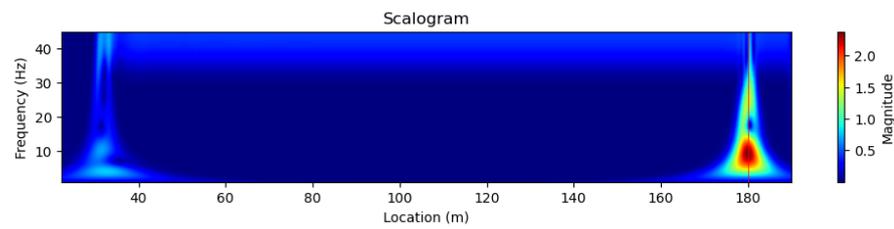
(c) Scalogram of the acceleration results. The red line marks the bridge beginning
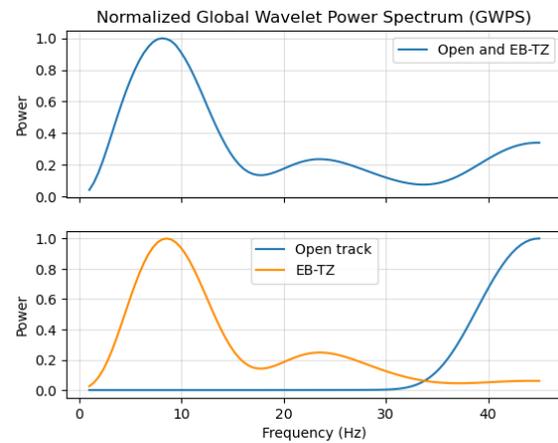
(d) GWPS of the acceleration results

Figure 4.19: Results from the EB model 4 using flextrack. In gray the rigid bridge section is plotted

<div style="text-align: right; font-size: 3em;">5</div>

Measurement and simulation data comparison

With both the measurement data from the CTO train and the simulation results from the MBS software analysed and discussed in chapter 3 and 4 respectively, this chapter will discuss these results compared to one another. Herewith, an answer to the fourth sub-question 'How do the measurement ABA-data and simulation data relate to each other?' will be obtained.

5.1. Data comparison

The data obtained from the CTO train and analysed in chapter 3 only consists of the vertical acceleration of a certain track with the corresponding locations. No knowledge about the condition of this section of the railway track is available. Due to this reason it is not feasible to only compare the state or condition of the transition zones through the acceleration curves, but rather between the occurring frequencies and amplitudes within the data of the vertical acceleration. As the frequencies coincide, it can be confirmed that the higher wavelength frequencies are indeed corresponding to abrupt stiffness changes and differential settlements (and hanging sleepers). From chapter 4 the conclusion is obtained that the flextrack analysis gives the most accurate results for the simulation of the transition zones. Therefore, the models presented with this analysis will be compared to the data from the CTO train. The comparison of which CTO train measurement data depends on the velocity. Since the simulation results are obtained using a velocity of 25 m/s^2 the locations of bridge 4 and 6 will be selected as the CTO train made use of the same velocity when obtaining these measurements.

Figure 5.1 shows the comparison between the vertical acceleration simulation data and measurement data. For the simulation data, model 4 from method 2 is used (model with differential stiffness, settlement and a hanging sleeper). As expected are the simulation results significantly lower than the measurement data. This can be attributed to several factors. First, although the measurement data has been filtered, a lot of noise is still present in the data. This noise can be caused by certain track irregularities, weather effects, temperature effects, other passing trains, et cetera. The simulation data on the other hand is only subjected to the irregularities the model has been assigned, like differential stiffness, and settlement. Second, the simulation data is obtained using a Benchmark Manchester Passenger vehicle. This vehicle differs in properties and parameters from the CTO train that has been used for the measurement data. Next, it's also possible that the CTO train measured the track with

more than one vehicle connected to each other, while the simulation has been done with one wagon only.

By taking a closer look at the EB comparison for bridge 4 (figure 5.1a), the peak values from the simulation data at around 178 meters are visible at the measurement data as well, only these are significantly lower. This same conclusion holds for the other transition zones except for the EB transition zone of bridge 6. Here, the simulation peaks do not coincide with the measurement data.
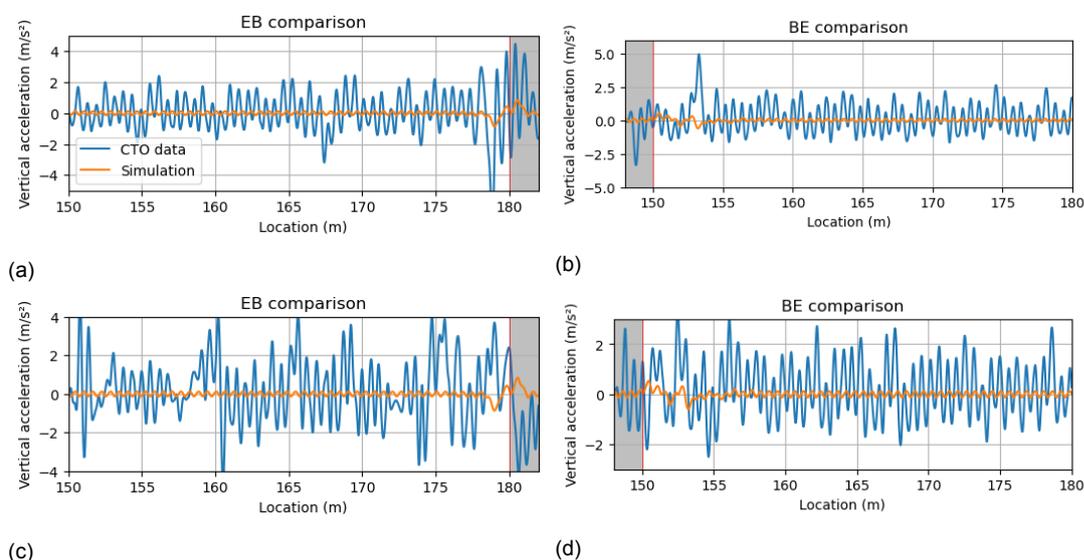
Figure 5.1: Comparison of the simulation and measurement data for (a) bridge 4 EB transition zone, (b) bridge 4 BE transition zone, (c) bridge 6 EB transition zone, (d) and bridge 6 BE transition zone

As the above mentioned results were expected, the main focus should therefore be the comparison between the occurring frequencies. From chapter 3 it became clear which frequencies matter in terms of recognizing the transition zone characteristics like differential settlement and stiffness. These frequencies varied in the order of $1.2 < \lambda < 5$ meters (in wavelength). This frequency region of interest could tell more about the condition assessment of a transition zone in chapter 6.

In figure 5.2 the scalogram of both model 4 from the flextrack analysis (EB and BE) and bridge number 4 are shown. Due to the noise in the measurement data the resemblances are not immediately visible. However, the lower frequency concentrations can be seen at the transition from open track to bridge (and vice versa) when comparing the measurement results and the simulation data. The change in magnitude of the frequencies could be assigned to the noise and unknown configuration of the vehicle order. As concluded in chapter 3, the GWPS gives a more clear picture of the frequencies that are present inside the regions. In figure 5.3 the global wavelet power spectra of bridge 4, 6 and the simulations are plotted. From these graphs the high peaks in the lower frequency region is visible for all of the transition zones. In most of the cases, except for a peak at 3 Hz at the EB of bridge 6, the transition zone frequencies are higher than the open track inside the region of interest, suggesting the presence of differential stiffness and settlement possibly in combination with hanging sleepers. The peak at 3 Hz for bridge 6 could suggest that the transition zone is longer than suggested. For the simulation results, the lengths of the transition zones are taken as they can be seen on the scalogram (figures 5.2c and 5.2d). The transition zone starts (and ends) by where the frequencies from a magnitude of 0 transition towards a frequency with a higher magnitude (in color this means

from blue to any other color).

From the results of chapter 4 it was shown that the frequencies present for the EB zone for the differential stiffness and settlements are in the order of 6 - 25 Hz (1 < λ < 4.2 meters). For the BE zone this is 5 - 12 Hz (2.1 < λ < 5 meters). There is no significant difference between differential stiffness and differential settlement. A reason for this could be the fact that the differential settlement is simulated using stiffness changes. The model containing hanging sleepers differ only slightly for the BE zone, where the frequencies become 5 - 20 Hz (1.25 < λ < 5 meters). The EB zone stays here at 8 - 24 Hz (1 < λ < 3.1 meters). So, it can be concluded that the initial zone of interest (1.2 < λ < 5 meters) does give a good indication of the presence of a transition zone in the data. While there is no significant change in frequencies between differential stiffness and settlement, there is a change in frequencies when hanging sleepers are introduced. Especially for the BE zone. Without hanging sleepers the frequencies here are lower than with badly supported sleepers. These frequencies can be seen in figures 5.3e and 5.3f.

(a) bridge 4

(b) bridge 6

(c) EB model 4

(d) BE model 4
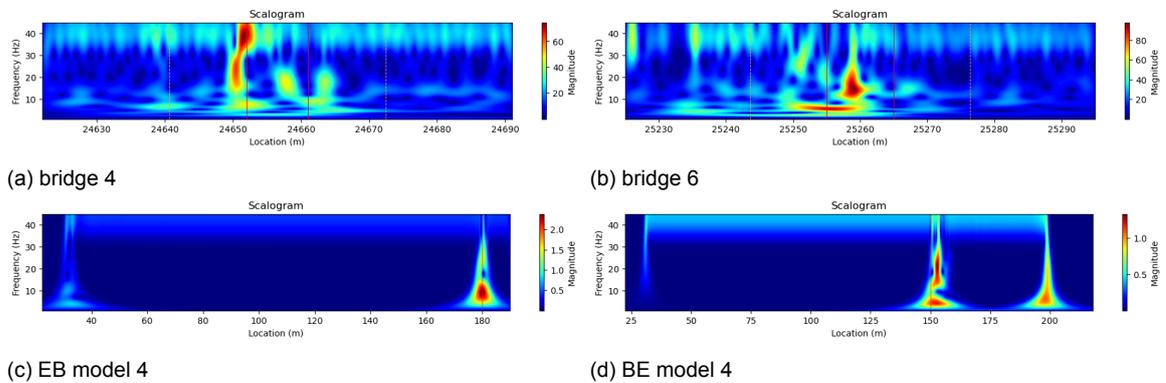
Figure 5.2: scalogram comparison between (a) bridge 4, (b) bridge 6, (c) EB of model 4 of the flextrack analysis and (d) BE of model 4 of the flextrack analysis
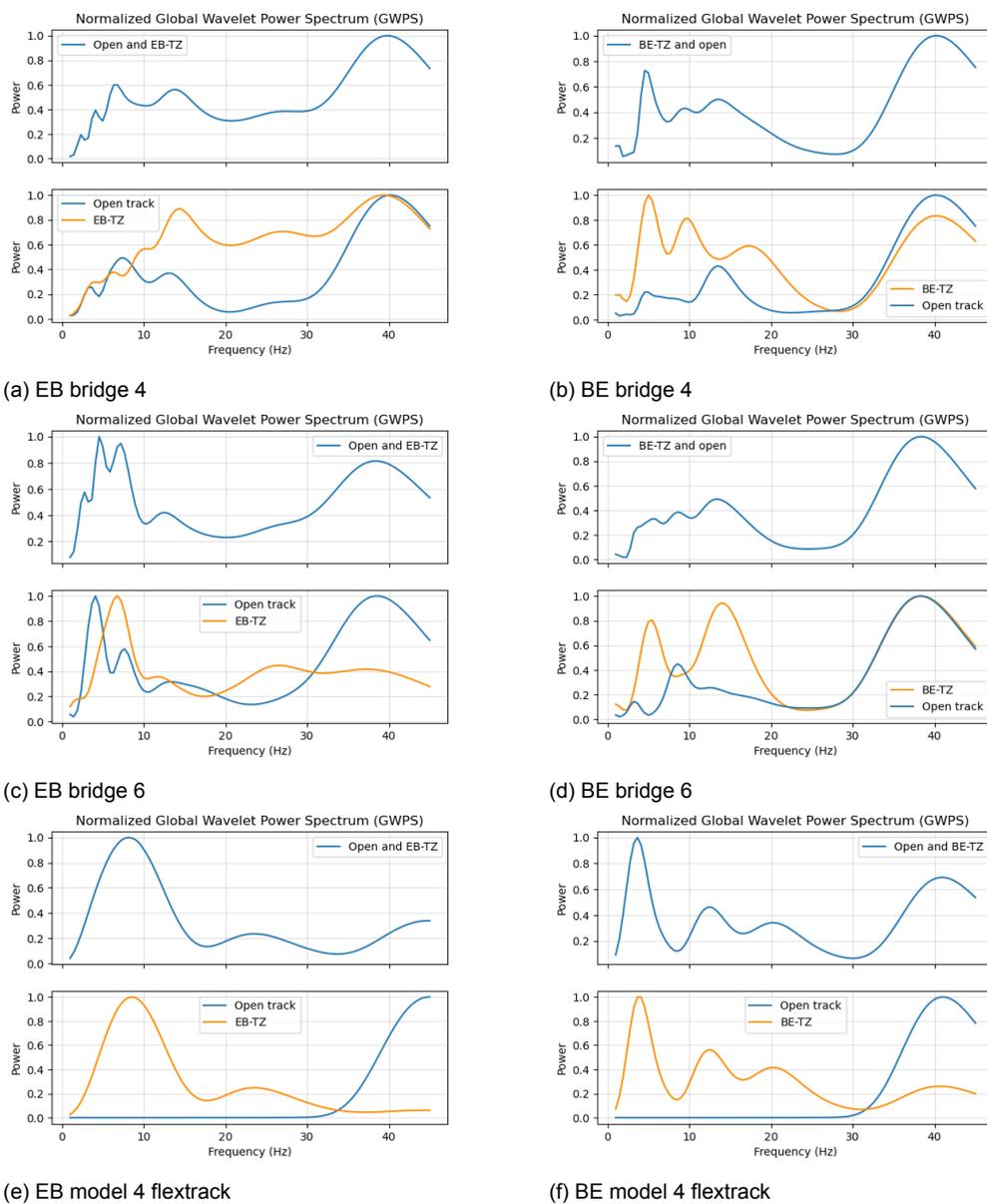
Figure 5.3: GWPS comparison between (a) EB of bridge 4, (b) BE of bridge 4, (c) EB of bridge 6, (d) BE of bridge 6, and (e) EB of model 4 of the flextrack analysis and (f) BE of model 4 of the flextrack analysis

6

Condition Monitoring

In this chapter the flextrack model from chapter 4 is used with different parameters in order to test if a condition assessment can be made with the aid of vertical acceleration results. This chapter will give an answer to the fifth and final sub-question 'What does the vertical acceleration tells about the condition of a transition zone using MBS software?'. Three situations are proposed, for each of these situations a MBS model is presented. The results of the models are plotted and the effect of the ABA output is discussed.

6.1. Condition assessment cases

Below three models are presented. These models are simulated using a vehicle velocity of 140 km/h (Dutch operational speeds). From past research conclusions were made stating that a greater velocity will also result in a higher energy exaction of the vertical axle box acceleration measurements (Unsiwilai et al., 2023). Each model represents a certain phase of the service life of a transition zone ranging from a good to worse condition. The first model will be a *new* transition zone with a differential settlement only of 4 mm (the ballast compaction after construction). The second model represents a transition zone that already has been used for some time and where damage starts to occur. The last model of the transition zone will be in the worst state and will experience the most differential settlement.

With the knowledge of the previous chapters the main frequencies with a wavelength between 1.2 and 5 meters will be the region of interest for the condition monitoring of the transition zones using vertical axle box accelerations. The most useful analysis for the detection of these frequencies is the global wavelet spectrum. In chapter 3, 4 and 5 use is made of the normalized GWPS to make comparisons between the different models presented to overcome the possible chance of very low frequency responses that could otherwise not be seen. In this chapter however, the magnitude of the frequency responses will matter to make a good comparison and condition assessment of the three cases.

6.1.1. New track

The first model consists of a transition zone in good condition. The model is similar to the previous models with the EB and BE transition zones split in two models to make sure no noise

from either transition zone is present at the other transition zone. Again, on the open track a 4 mm differential settlement is introduced with no other irregularities except for the bridge. The value of the base bushing is set at $1.35\text{E}10^7 N/m$ to achieve this settlement. Figures 6.1 and 6.2 show the results of the wheel-rail contact force, the vertical acceleration, the scalogram, the GWPS and the standard deviation of the acceleration signal. Comparing the vertical force between the EB and BE transition zone, the forces at the EB are higher as expected. The fast elevation of the vehicle results in a high peak just before the bridge. On the other side, the vehicle drops of the bridge and bounces back on track (explaining the downwards peak). The location of the impact of the wheels depends on the velocity. The upward peaks at the BE suggest this bouncing movement. The highest forces at the EB zone occur at the first three sleepers before the bridge. For the BE zone the highest forces occur at the fourth and fifth sleeper from the bridge. The vertical acceleration behaves the other way around. At the EB transition zone the vertical acceleration is negative due to the climb of the bogie. At the BE transition zone, the bogie accelerates as is comes down on the track. The scalogram shows therefore a longer frequency concentration at the BE transition zone of around 12 meters. While the affected zone for the EB transition zone is around 8 meters long. Notice the low-pass filter of 70 Hz for the acceleration values. Above this value no frequencies of interest are present. By looking at the GWPS, the EB model shows more extensive frequencies than the BE model. With a velocity of 140 km/h, the frequencies of interest are in the region of 7.8 - 32.5 Hz. For both models this is the case as well. The power of the frequencies are similar (vertical axis GWPS), however, the lower frequencies are of interest for the BE zone (7 - 16 Hz) and the higher frequencies for the EB zone (9 - 35 Hz). Although this difference, both peaks of the GWPS lay around 8 Hz. At last, the standard deviation for both models is higher at the transition zone than it is at the open tracks. This is a direct results from the peaks at the transition zone.

6.1.2. Used track

For the second model a differential stiffness of 8 mm is introduced. This settlement is achieved by a base bushing value of $5.4\text{E}10^6 N/m$. This model represents a medium degraded transition zone with one hanging sleeper at the location of the highest force on both the EB model and BE model. For the EB model this is the second sleeper before the bridge starts, while for the BE model this is the fourth sleeper after the bridge. Figures 6.3 and 6.6 show the results of the simulations. Most of the conclusions from the first model holds for the second model as well. The wheel-rail forces at the EB zone are significantly higher while the affected length for the BE zone is greater. The vertical acceleration at the EB model encounters a higher downwards peak suggesting a larger elevation for the vehicle. The acceleration at the BE zone are significantly increased by the larger settlement and hanging sleeper. Generating a longer affected zone than the EB zone (15 meters vs 8 meters). Both the scalogram plots clearly show the lower range of the frequencies of interest. Especially the BE transition zone shows the frequency concentrated area of around 20 - 25 Hz corresponding to the hanging sleeper. As for the GWPS, both models show similar results compared to the transition zone in good condition. Lower frequency peaks for the BE zone (5 and 17 Hz) and more extensive frequencies in range for the EB zone (8 - 20 Hz). Again, the frequencies are more or less in the region of interest. The peak at 5 Hz from the BE model corresponds to a wavelength of 7.8 meters which, according to TU Delft (2020b), falls in line with large soil settlements. Compared to the transition zone in good condition (section 6.1.1), the magnitude of the GWPS frequency plot is also significantly greater. Although the magnitude in the first model was the same for both EB and BE models, the magnitude for the degraded model differs. For the EB transition

zone the magnitude is slightly higher than for the EB zone. This suggests a higher frequency concentration due to the high dynamic force at the moment the vehicle hits the bridge.

6.1.3. Heavily used track

At last, the third model is created. This last model represents a condition zone in bad condition. A high differential settlement of 12 mm is introduced with three hanging sleepers on both sides at the locations of the highest forces. For the EB model this are the first three sleepers before the start of the bridge. For the BE model, sleepers three, four and five are taken. The differential settlement is simulated using a base bushing stiffness of $3.0E10^6 N/m$.

Most of the conclusions stated before hold for the last models as well. The vertical wheel-rail contact forces are significant compared to other models and the vertical acceleration, due to the presence of the hanging sleepers, consists of a lot of peaks especially at the BE transition zone. The fast elevation of the vehicle in the vertical acceleration at the EB model has increased by a 1000% compared to the transition zone in good condition. The presence of hanging sleepers results in a propagation of forces to the adjacent sleepers, as can be seen as higher forces move more away from the bridge section. The length of the affected zone however, is decreased at both sides according to the scalogram plots. With only 6 meters at the EB transition and 13 meters at the BE transition. No straightforward reason can be given for this phenomenon. With higher velocities and larger differential settlements, also larger affected zones were expected. It turns out that the frequencies stay more concentrated instead of spreading out. For the acceleration and force data however, the peaks at the BE transition zone do move more away from the bridge compared to the earlier results. For the GWPS plots the power of the occurring frequencies have increased significantly as well. With frequencies ranging from 8 - 18 Hz for the EB transition zone and 5 - 18 Hz for the BE transition zone, the peaks are as expected. Again, the magnitude of both EB and BE models differ. The magnitude for the EB transition zone is almost 2.5 times higher than for the BE transition zone. This leads to the conclusion that the EB transition zones are often in worse condition than the BE transition zones, due to the high dynamic impact force.

6.2. Conclusion

From the models presented above two important conclusions can be taken. First, it can be concluded that the multi body simulation software is able to simulate transition zones in different conditions. Second, the potential of the vertical acceleration from the axle box accelerations to assess the condition of transition zones is there. Especially the frequency indicators that can be taken out of the acceleration data are of great value for this condition assessment. More degraded transition zones show higher power of the long wavelength frequencies.

Moreover, the conclusion from chapter 3 can be seen here as well. The frequency concentrations differ for the embankment-bridge section and bridge-embankment section. The simulation data shows that the frequencies of EB transition zone concentrate overall more between the full region within $1.2 < \lambda < 5$ meter. While the BE transition zone is more concentrated at the higher region of these wavelengths (e.g. the lower frequencies).
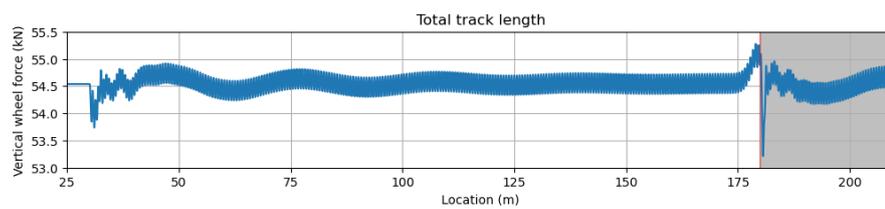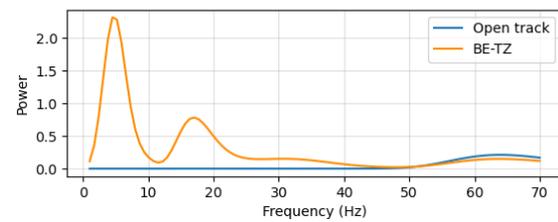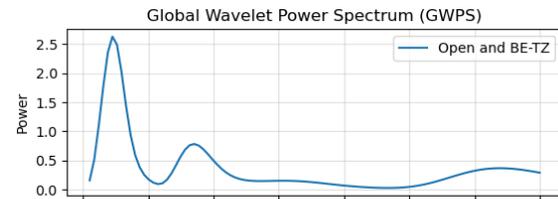
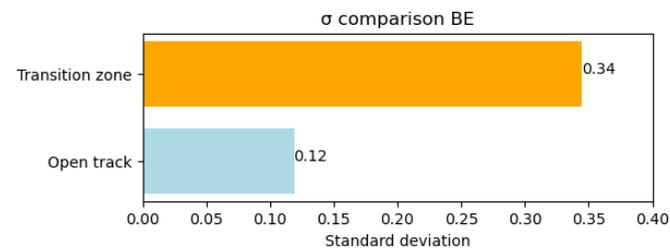(a) Vertical wheel-rail contact forces
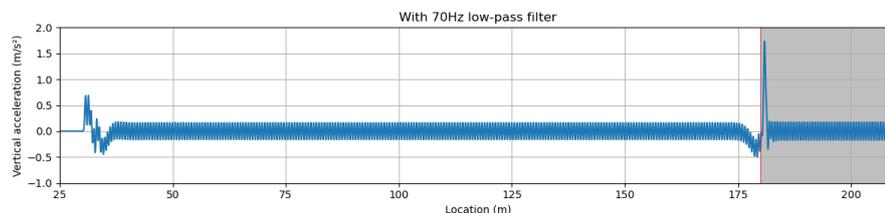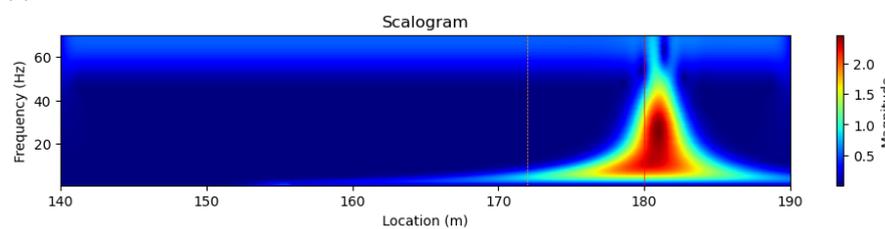
(b) Vertical acceleration

(c) Scalogram of the acceleration results. The red line marks the bridge beginning, the orange line the transition zone
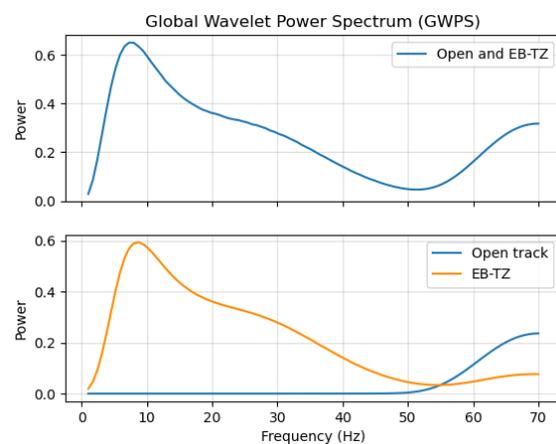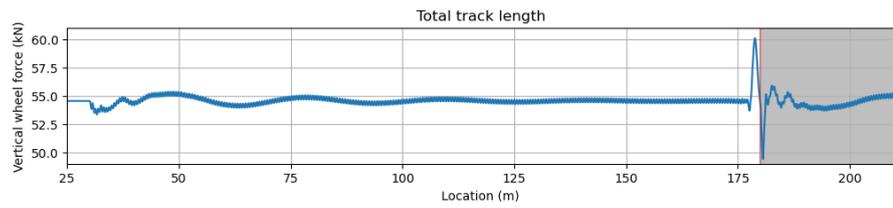

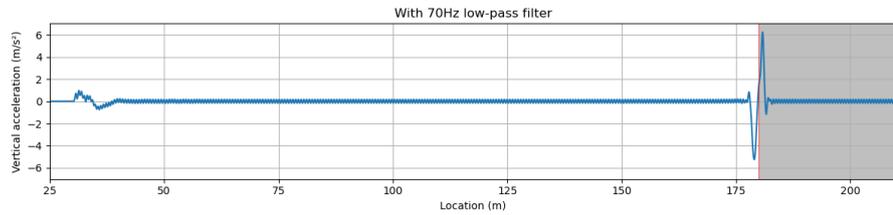
(d) GWPS of the acceleration results
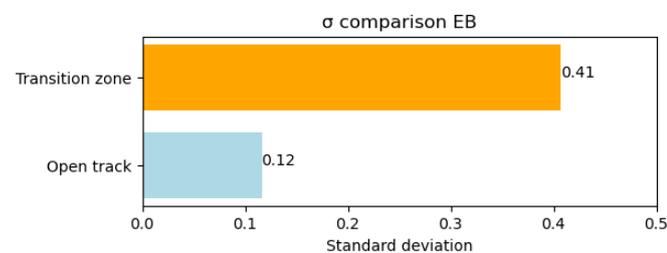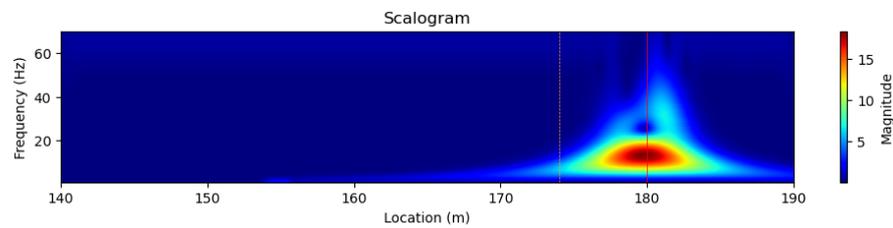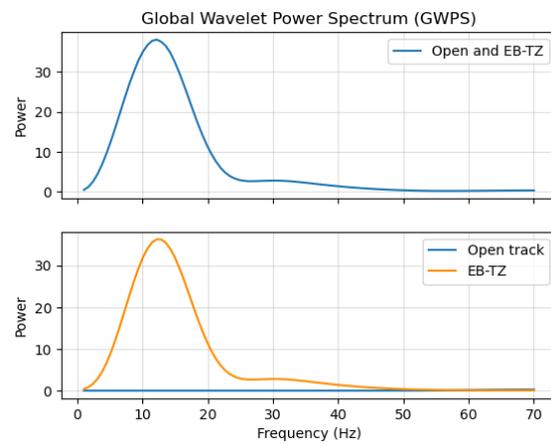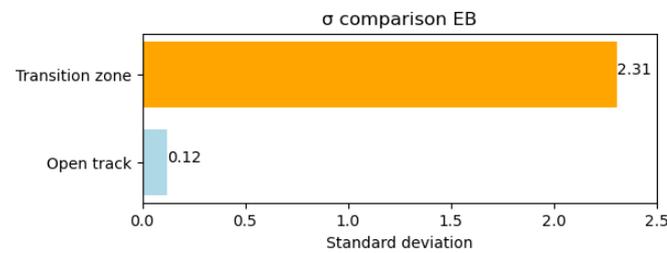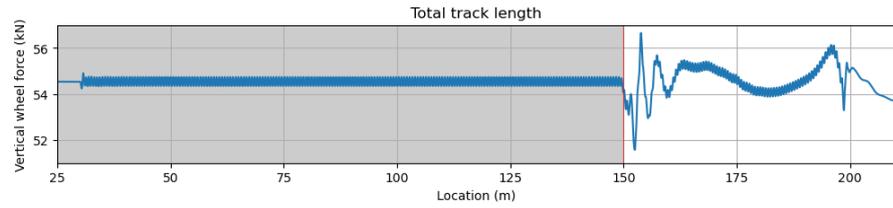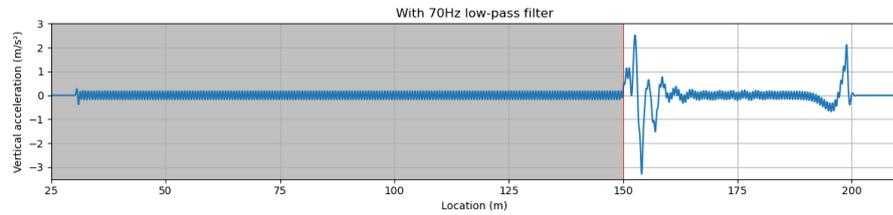

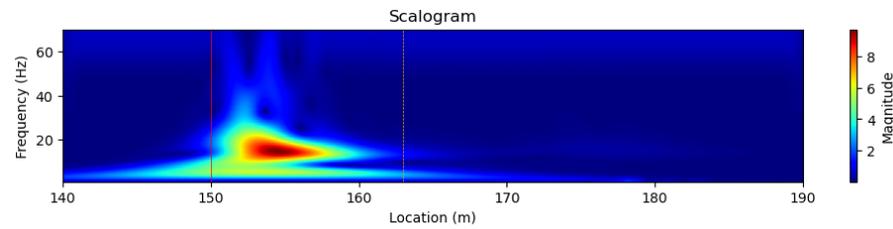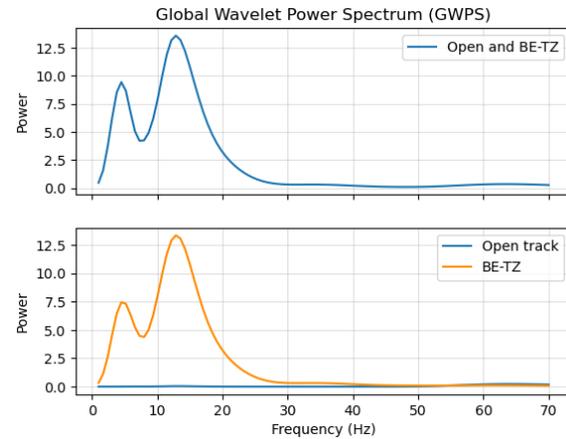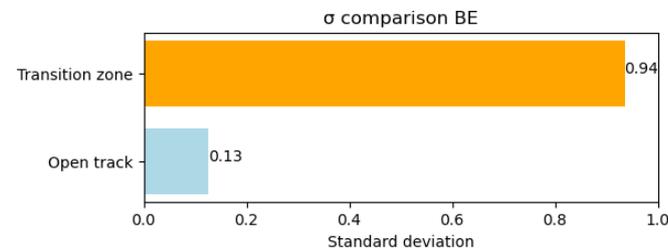(e) Standard deviation of the acceleration results

Figure 6.1: Results from the transition zone in good (new) condition (EB). In gray the rigid bridge section is plotted
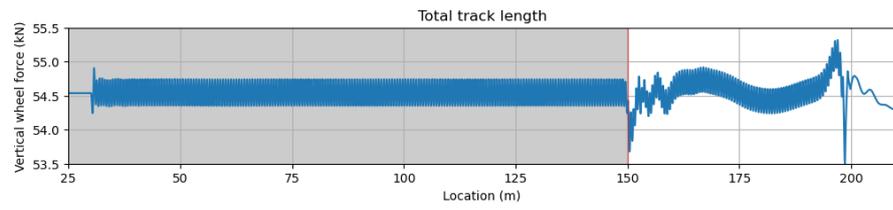
(a) Vertical wheel-rail contact forces
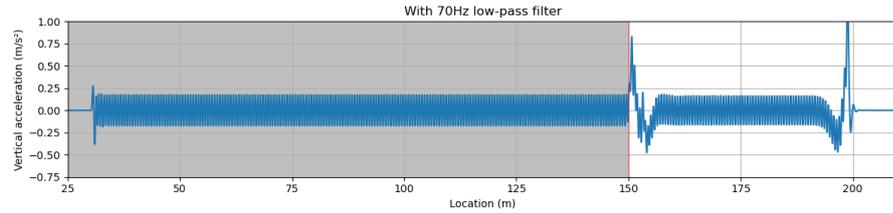
(b) Vertical acceleration
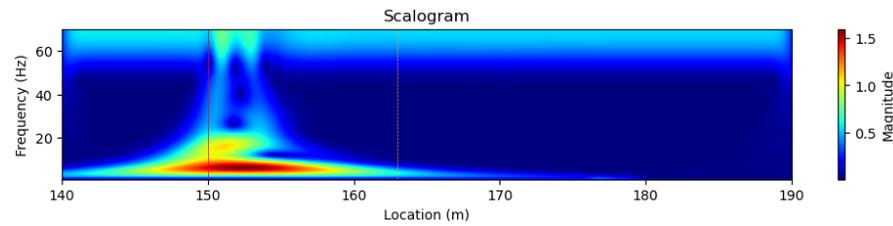
(c) Scalogram of the acceleration results. The red line marks the bridge ending, the orange line the transition zone
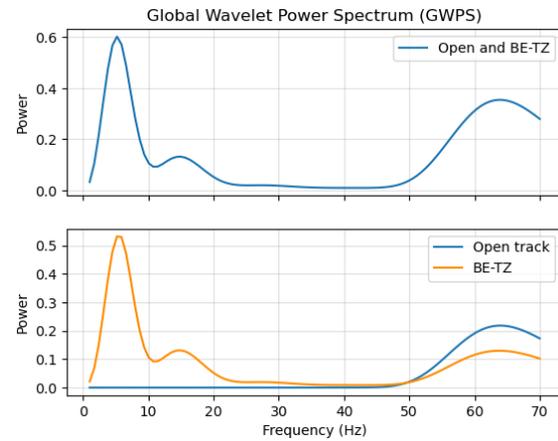
(d) GWPS of the acceleration results
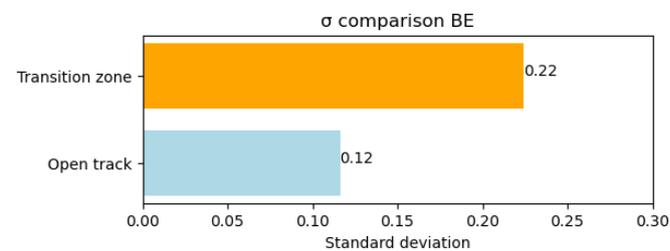
(e) Standard deviation of the acceleration results

Figure 6.2: Results from the transition zone in good (new) condition (BE). In gray the rigid bridge section is plotted
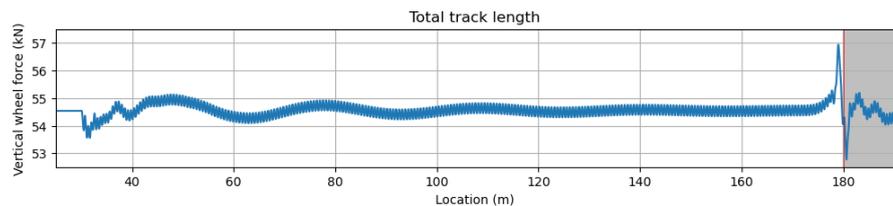
(a) Vertical wheel-rail contact forces
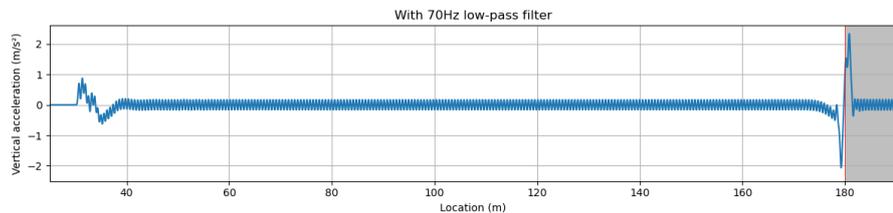
(b) Vertical acceleration
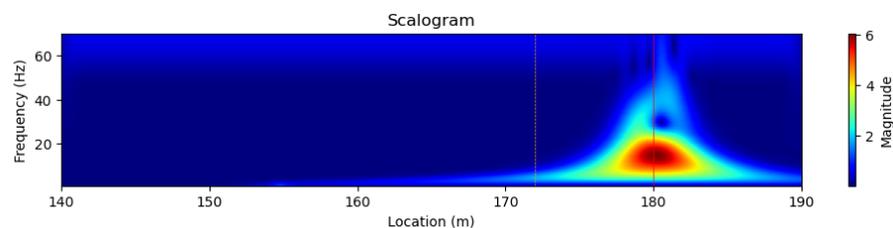
(c) Scalogram of the acceleration results. The red line marks the bridge beginning, the orange line the transition zone
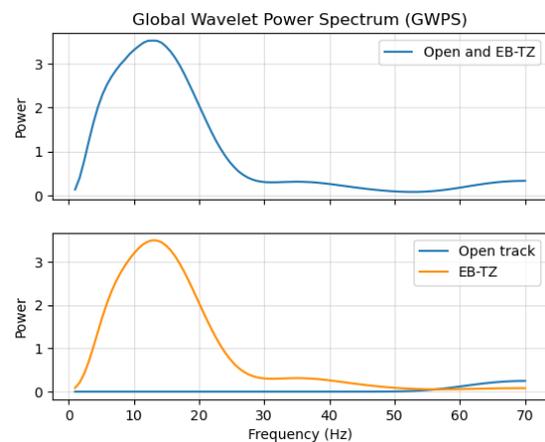
(d) GWPS of the acceleration results
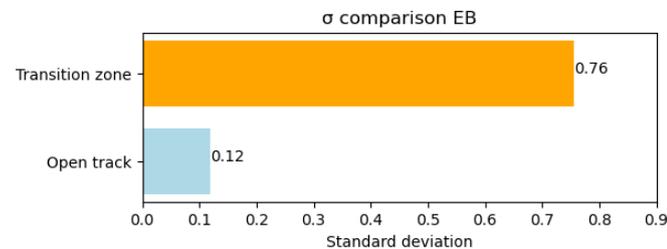
(e) Standard deviation of the acceleration results

Figure 6.3: Results from the transition zone in degraded (used) condition (EB). In gray the rigid bridge section is plotted
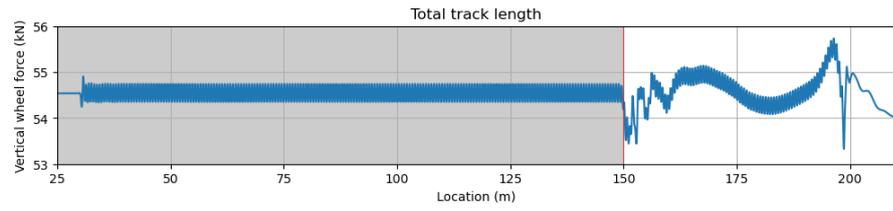
(a) Vertical wheel-rail contact forces
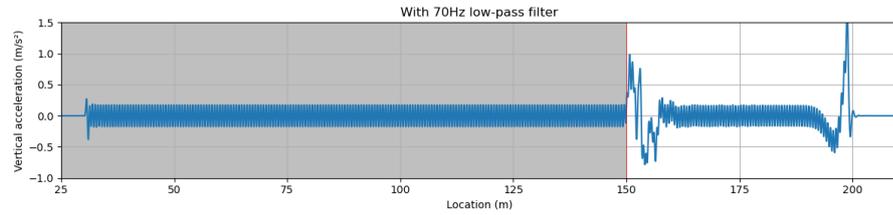
(b) Vertical acceleration
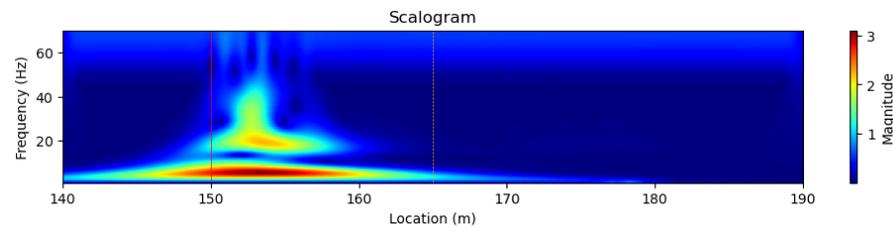
(c) Scalogram of the acceleration results. The red line marks the bridge ending, the orange line the transition zone

(d) GWPS of the acceleration results

(e) Standard deviation of the acceleration results

Figure 6.4: Results from the transition zone in degraded (used) condition (BE). In gray the rigid bridge section is plotted

(a) Vertical wheel-rail contact forces

(b) Vertical acceleration

(c) Scalogram of the acceleration results. The red line marks the bridge beginning, the orange line the transition zone

(d) GWPS of the acceleration results

(e) Standard deviation of the acceleration results

Figure 6.5: Results from the transition zone in heavily degraded (used) condition (EB). In gray the rigid bridge section is plotted

(a) Vertical wheel-rail contact forces

(b) Vertical acceleration

(c) Scalogram of the acceleration results. The red line marks the bridge ending, the orange line the transition zone

(d) GWPS of the acceleration results

(e) Standard deviation of the acceleration results

Figure 6.6: Results from the transition zone in heavily degraded (used) condition (BE). In gray the rigid bridge section is plotted

7

Conclusion

7.1. Conclusion

Now that all sub-questions have been answered, a final answer can be given to the main question of this investigation, 'How can ABA-data serve the condition assessment of transition zones?'. Below the main findings are highlighted using bullet points. Together they form an answer to the main question.

- From the literature it is clear that ABA-data is mostly used for the detection and condition assessment of short wave track irregularities (high frequency defects).

- The characteristics of the transition zones are hidden in the frequencies of differential stiffness and settlements within the vertical acceleration data.

- It is shown that the potential for axle box acceleration data to assess the condition of a transition zone is there. Investigating the frequency region with longer wavelengths of $1.2 < \lambda < 5$ meter gives a powerful insight in the condition monitoring of transition zones. This shows that ABA is a powerful non-invasive monitoring technique.

- The multi body simulation software in combination with the flextrack toolkit provides results that are in line with the theory known about transition zones. Higher dynamic forces at the embankment-bridge zone and longer affected lengths at the bridge-embankment zone. No previous research is found using this kind of software to model engineering structures in combination with the investigation of the vertical acceleration data.

- The MBS software is capable of modelling different stages of the transition zone's service life and provides potential results.

- Using the ABA-data, more degraded transition zones show higher concentrations of the long wavelength corresponding frequencies, which makes it a good indicator for not only short wave track irregularities but also long wave irregularities (like settlements).

- The frequency concentrations differ for the embankment - bridge section and bridge - embankment section. Both the measurement data and simulation data show that the frequencies of EB transition zone concentrate overall more between the full region within $1.2 < \lambda < 5$ meter. While the BE transition zone is more concentrated at the higher region of these wavelengths (e.g. the lower frequencies).

Overall, it can be concluded that ABA is promising technique for the condition monitoring of transition zones.

7.2. Points of discussion

The points of discussion for this research are:

- The ABA-data from the CTO train is analysed without any knowledge about the condition of that particular railway track. A more accurate comparison could be made by knowing what the state of each transition zone was at the time of measurement.

- The ABA-data is acquired using a CTO train while the MBS models make use of the Benchmark Manchester Passenger vehicle. To obtain a more accurate comparison, the same parameters and properties for the train model as the CTO train should be used.

- The MBS models make use of UIC60 rails. The more commonly used railway profile in the Netherlands is UIC54.

- The calculated stiffness values through the analytical approach using a Matlab model based upon the theory of Zimmermann could be acquired in a more realistic manner through real life or laboratory tests.

7.3. Future work

As for the future research, interesting topics could be but are not limited to:

- Comparing and combining multi body simulation models and finite element models in order to create a more realistic behavior of the ballast in the MBS software in terms of stiffness and damping.

- The investigation if the axle box accelerations from passenger trains (like NS) could replace the measurement ABA-data from the CTO train. How does quantity weigh up against quality? And how often does a transition zone needs to be monitored?

- Creating algorithms to automatically extract the frequencies that highlight the condition of transition zones.

<div align="right">

A

</div>

<div align="right">
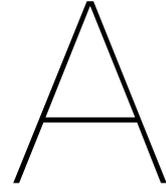
Attachment A

</div>

Measurement techniques

This section gives an overview of the existing measurement techniques for railway track measurements.

VGS/DIC

VGS (video gauge system) (see figure A.1a) is an optical measurement method that uses DIC-technique (digital image correlation) ((Liu et al., 2018)) to accurately measure transient displacements using a high-speed camera. A reference image is taken beforehand and with targets applied on the rails and sleepers a camera creates a video file during train passes. This file is converted to images that through an image correlation technique is analysed to identify patterns in the data (described in Bowness et al. (2007)). With this process a transient displacement can be obtained relative to the initial image to capture dynamic profiles of a railway track, like in the research of Wang, Markine, and Liu (2018) and Le Pen et al. (2014). One of its main advantages is the direct measurement of settlements without obstructing the track availability.

Optical level

Another instrument is the optical level, a more conventional level instrument that measures height differences in a horizontal plane. These height differences can be used to quantify the permanent settlement of a railway track. However, research using optical level instruments at railway tracks is limited. D. Li et al. (2005) used the method to conclude that transition zones indeed endure greater settlement over time than open tracks.

Geophones

Geophones are small seismic sensors used to monitor velocity through vibrations (figure A.1b). The instrument consists of a magnetic core inside a coil of wire. The core is able to freely move together with the housing it's attached to. The coil and housing of the geophone are attached through leaf springs (to sustain higher loads). Geophones can be either installed underground (substructure) or on the structure (for example on sleepers) (Iskander, 2018). During train passes vibrations occur and the core moves relative to the coil which stays in place. Due this movement an output voltage proportional to the velocity is monitored (Bowness et al., 2007). Geophones give large displacement amplitudes at low power supply, however, only frequencies above its natural frequency can be monitored (around 10 Hz, so, no small

characteristic axle load frequencies for example) (Iskander, 2018) (Kouroussis et al., 2015). The measured data can be translated to displacement through one integration (filtering out additional noise). In Coelho et al. (2010) it has been implemented at a transition zone.

Accelerometers

Accelerometers are used to measure accelerations through vibrational forces (in terms of railway: coming from any rail related irregularity) (Falamarzi et al., 2019). These type of sensors exist in a variety of versions, with the piezoelectric accelerometer as one of the most highly utilized in the civil industry. Just like geophones, accelerometers can be installed at sub- or superstructure level, though the working principle differs. An accelerometer (figure A.1c) is an electromechanical sensor consisting of an piezoelectric element attached to a mass (known as a mass spring system). During a vibration the mass produces a force on the piezoelectric element initiating an electrical charge proportional to the acceleration force (Newton's Second Law). This charge is converted to a voltage which can be read (multiple configurations exist such as uniaxial or triaxial) (OmegaEngineering, 2020) (Yoder & Adams, 2014). The output can be integrated (twice) to displacement (filtering out additional noise). However, double integration to obtain dynamic displacement data is highly sensitive to errors. Unlike geophones, only frequencies below their natural frequency can be monitored (Iskander, 2018). Accelerometers are easy to install, are low in costs, have good sensitivity and offer a wide frequency range. For lower frequencies, piezoresistive accelerometers are used. Piezoresistive accelerometers are based upon strain gauge principle and it measures stress. The piezoresistive element deforms due to a force and the change in resistance is measured (Yoder & Adams, 2014). In Coelho et al. (2010) it has been implemented at a transition zone.

(a)   (b)   (c)

Figure A.1: a) VGS/DIC device set up (Wang, Markine, & Liu, 2018) b) Geophone (Le Pen, L., et al., 2018) c) Accelerometer (Vukušičová, D., 2017)

LVDT

Linear variable differential transformers, in short LVDT (figure A.2a), is a technique to measure both permanent and transient displacements of the railway track, reliable and accurate (array of LVDT's are called Multi-Depth Deflectometers - MDD). The sensor can be described as an electromechanical passive inductive transducer. This means that it is both electrical and mechanical (electromechanical), not capable of generating energy (passive), stores energy as an electromagnetic field (inductive) and converts energy (transducer) (RealPars, 2022). With a push rod attached to a ferromagnetic core inside multiple cylindrical coils it measures linear displacements as a function of the output voltage created (i.e. the LVDT converts linear motion into an electrical signal). The output voltage is linearly related to the displacement of the core. With no frictional forces to distort the readings and no fatigue due to zero mechanical connections, the sensor is attractive to use. However, the operating range of a LVDT is limited by the size of the sensors coils (Yoder & Adams, 2014). In Stark and Wilk (2016) it has been implemented at a transition zone.

Strain gauge

strain gauges are small sensors that can be bonded to a surface to measure the (micro-) deformations of a material. From an arbitrary external or internal force (heat, pressure, et cetera) the material of a strain gauge can change its electrical resistance which can be measured (proportional to the strain applied to the surface) (see figure A.2b). A typical strain gauge is made up in three layers. A protective top layer, a thin metallic sensing element in the middle and a plastic film base on the bottom (Omega, n.d.) (Castillo-Mingorance et al., 2020) (Kouroussis et al., 2015). As the name suggests, the strain gauge can both measure contraction as expansion. With a lot of capabilities there are certain drawbacks like electromagnetic interference, fragility, and high dependence on the temperature (Omega, n.d.). In Paixão et al. (2018) strain gauges has been implemented at a transition zone.

PSD

A position sensitive detector, in short PSD, is a laser-based monitoring system consisting of a transmitter (laser diode) and receiver (PSD module) which can be used to measure track displacement without obstructing the availability of the railway track. The PSD module contains of a light-sensitive area on which the laser generates a current. This current is then split in separate spatial current to determine the position of the center of gravity of the light (Hering et al., 2022). This position can be converted to the vertical displacement of the railway. Figure A.2c shows the PSD module on the rail with a laser module on a tripod in front of it. This measurement equipment is mostly used at high-speed railway lines (including transition zones) due to its high accuracy and resolution (Paixão et al., 2014) (Pinto et al., 2015).

(a)   (b)   (c)
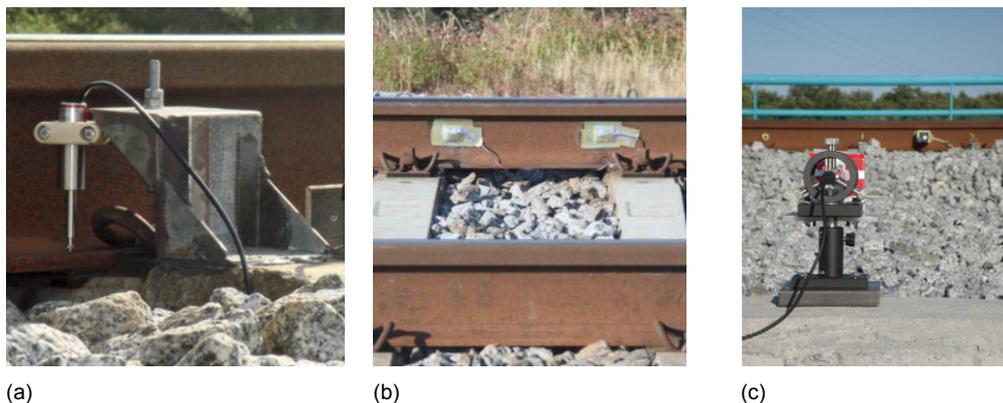
Figure A.2: a) LVDT (Paixão, A., et al., 2015) b) Strain gauge (Paixãoa, A., et al., 2018) c) PSD (Paixão, A., et al., 2014)

InSAR

InSAR short for Interferometric Synthetic Aperture Radar, is a satellite radar based measurement system (figure A.3a). With one or multiple satellites SAR images of the same surface area are taken (at the same time or with different time intervals) and the deformation of the targets can be obtained through InSAR techniques. The principle is based upon radar pulses transmitted under an angle of the nadir from the satellites antenna. Ground targets (e.g. rails) with strong scattering reflection are able to be observed from the satellite and a deformation can be extracted. The system has millimeter precision, has no need for on-site equipment, but is costly to use (Wang, Chang, et al., 2018) (D'Amico et al., 2020). In Wang, Chang, et al. (2018) InSAR has been used for the monitoring of a transition zone.

GPR

GPR (Ground penetrating radar) is a monitoring technique measuring a variety of parameters at railway structures with the main goal of analysing its subsurface conditions and mapping the substructure. The thickness of railway layers (and properties), moisture content, mud pumping, and layer deformation are among the output of GPR. By using radio wave sources pulses of electromagnetic energy are transmitted into the railway structure from an onboard antenna (figure A.3b). The reflected energy is received and the changes in time, amplitude and signal attenuations are recorded. GPR is a continuous monitoring technique able to measure at high speeds without obstructing the availability of the track (Wang et al., 2017). See the research of Wang et al. (2017) for further information.

Smartphones

A relative new measuring technique is the use of smartphones and tablets as continuous acceleration monitoring. Most smartphones and tablets nowadays consists of accelerometers, GPS, camera's and Wifi (taking into account the measurement range of the device, amount of measurements per second of device/software). With these techniques, onboard measuring can be performed which is fast, less complex and more economical profitable than standard measuring equipment. However, the technique is not yet implemented on a big scale and still needs to prove itself, especially when performance and precision stays behind compared to conventional techniques (Rodríguez et al., 2021) (Falamarzi et al., 2019). In the research of Rodríguez et al. (2021) a tablet is used to monitor a transition zone showing its feasibility to measure ride comfort, track condition and locating track irregularities.

(a)   (b)
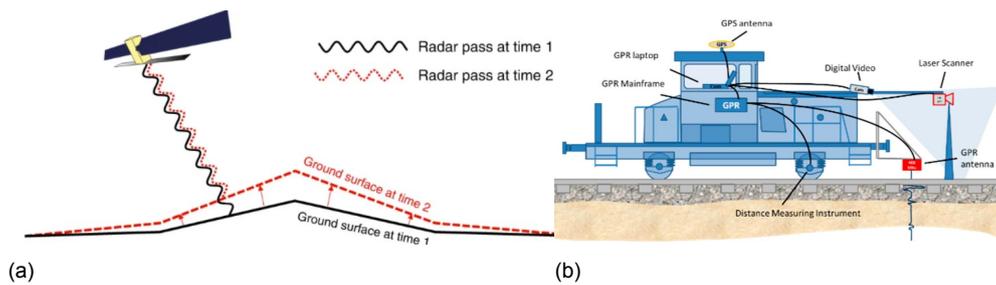
Figure A.3: a) InSAR principle (Biggs, J., et al., 2020) b) GPR principle (Wang, H., et al., 2017)

Attachment B

Kurtosis

Here, the kurtosis principle is explained. It is tried to give an answer to the question if the kurtosis values can be helpful for the analyses of vertical acceleration data. Kurtosis is a statistical measure for the heaviness or lightness of the tails and peak of a normal distribution (e.g. degree of peakness). A lower kurtosis denotes a lighter tail (less peak), thus less likely to have extreme values in the data. In the case of transition zones, a higher kurtosis would suggest the presence of outliers, while a lower value suggest the shape of normal distribution with no irregularities. The main difference between kurtosis and standard deviation is that the standard deviation calculates the dispersion of points around the mean while the kurtosis gives an indication of the shape of the distribution, indicating the presence of extreme values or not.

To get a better understanding of the kurtosis principle, figure B.1 shows the three possible phases. With higher peaks and shorter tails for a positive kurtosis and lower peaks and longer tails for a negative kurtosis. The value of kurtosis for a normal distribution should be around 3. A negative value is considered lower than 3 and a positive higher than 3. For convenience zero is taken as the break between positive and negative. The values discussed here have been adapted to this value.
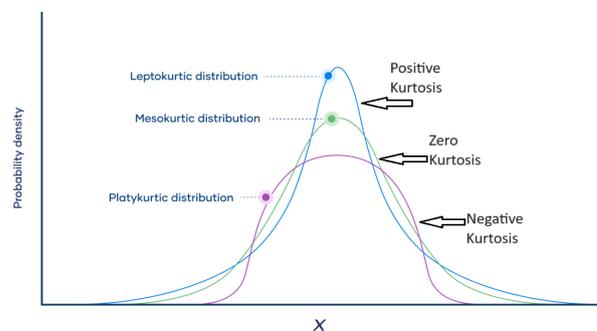
Figure B.1: Kurtosis principle

In the case of transition zones, a higher kurtosis value would be expected for zones in bad condition. This would indicate outliers that can occur due to track irregularities like differential settlement or hanging sleepers. A negative or zero kurtosis is expected at transition zones in good condition. Meaning, no significant outliers are present in the data.

In figure B.2 the kurtosis values are plotted using a histogram of the data, both the open track and transition zone together. At bridge 4, the kurtosis value is high for both sides of the bridge (6.20 and 3.29 respectively). As stated before, this indicates a strong outlier in the data set which can come from certain track irregularities. These outliers can also be seen in figure 3.3. The values for the open track on the other hand are more close to zero, indicating less to no outliers. As for bridge 8, the kurtosis of the EB transition zone is almost zero. With a negative to zero kurtosis implying no outliers, this falls in line with the conclusion that the condition of the transition zone could be rather good. Wile the value of the BE zone is again very high which is in line with the strong peaks in that data set.
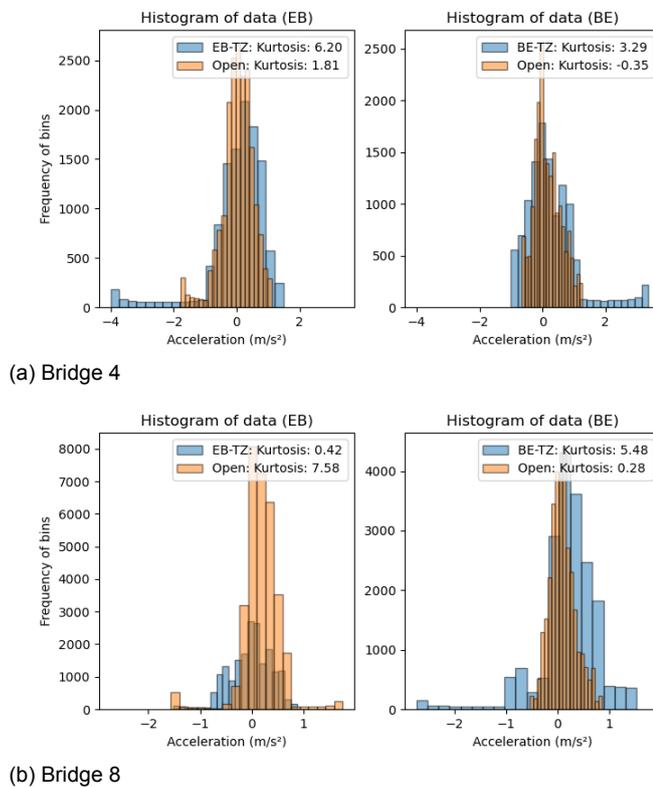
(a) Bridge 4

(b) Bridge 8

Figure B.2: Kurtosis values from open track and transition zone

However, when looking at the other bridge numbers and their corresponding transition zones, these conclusions can not be drawn. While for bridge 4 and 8 the values were positive (indicating outliers) the values for the other bridges lean more towards zero and a negative value. This is probably a result of the kurtosis measure is expecting an outlier in the data set or not. Figure B.4 shows the different values for the kurtosis. By plotting the data (figure C.1) it can be seen that outliers exist in both open track as transition zones. By taking a look at bridge 2 for example, two clear peak can be seen at the open track and some smaller
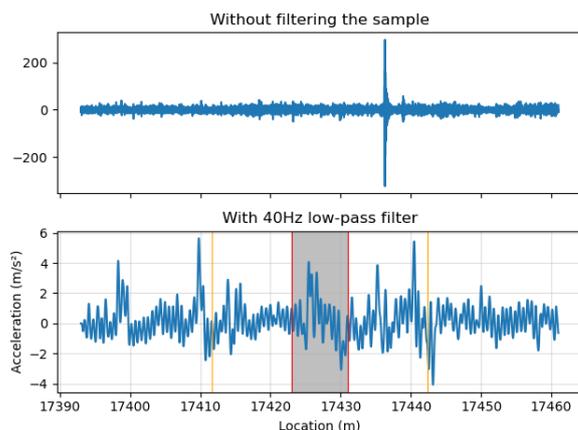
Figure B.3: Bridge 2

amplitudes at the EB transition zone (figure B.3). The value of the kurtosis of the open track is bigger than for the transition zone (2.93 against 0.24) because the two peaks were picked up as anomalies (not expected by the kurtosis measure) in the bigger data set. Which falls in line with the expectation. However, for the BE transition zone, two clear peaks are identified and one smaller at the open track. Here, the values of the kurtosis do not match the first expectation of a high value at the transition zone and a lower one at the open track. In reality it's 0.41 for the transition zone and 2.37 for the open track. This probably has to do with the fact that the kurtosis principle expects another anomaly in the transition zone after the first one, due to its limited sample size. For the open track only one occurs and is therefore marked as an anomaly. Thus, when there are more outliers in the transition zone, the kurtosis will see this as a normal phenomenon and gives a relative low value instead of the expected larger value.

In conclusion, the kurtosis value does not give the expected nor desired outcome. With a higher standard deviation for almost all of the transition zones, it was expected that this would be complemented in the values of the kurtosis. However, in most cases it is the other way around, with the open tracks having a higher kurtosis value than the transition zones. The most likely reason for this is the difference in sample size between the open tracks and transition zones. With less outliers in the longer open track than in the shorter transition zones the value becomes bigger for the open track. While at the same time, the kurtosis *expects* the outliers in the transition zone and due to their presence, gives a lower value. Therefore, the kurtosis is a less suitable statistical measure than the standard deviation as it does not actually indicates the presence of outliers. Finally, it can be argued that the kurtosis does give a good measure between transition zones (same sample sizes). Here the values can say something about the condition of the zones between themselves.

(a) Bridge 1

(b) Bridge 2

(c) Bridge 5

(d) Bridge 6
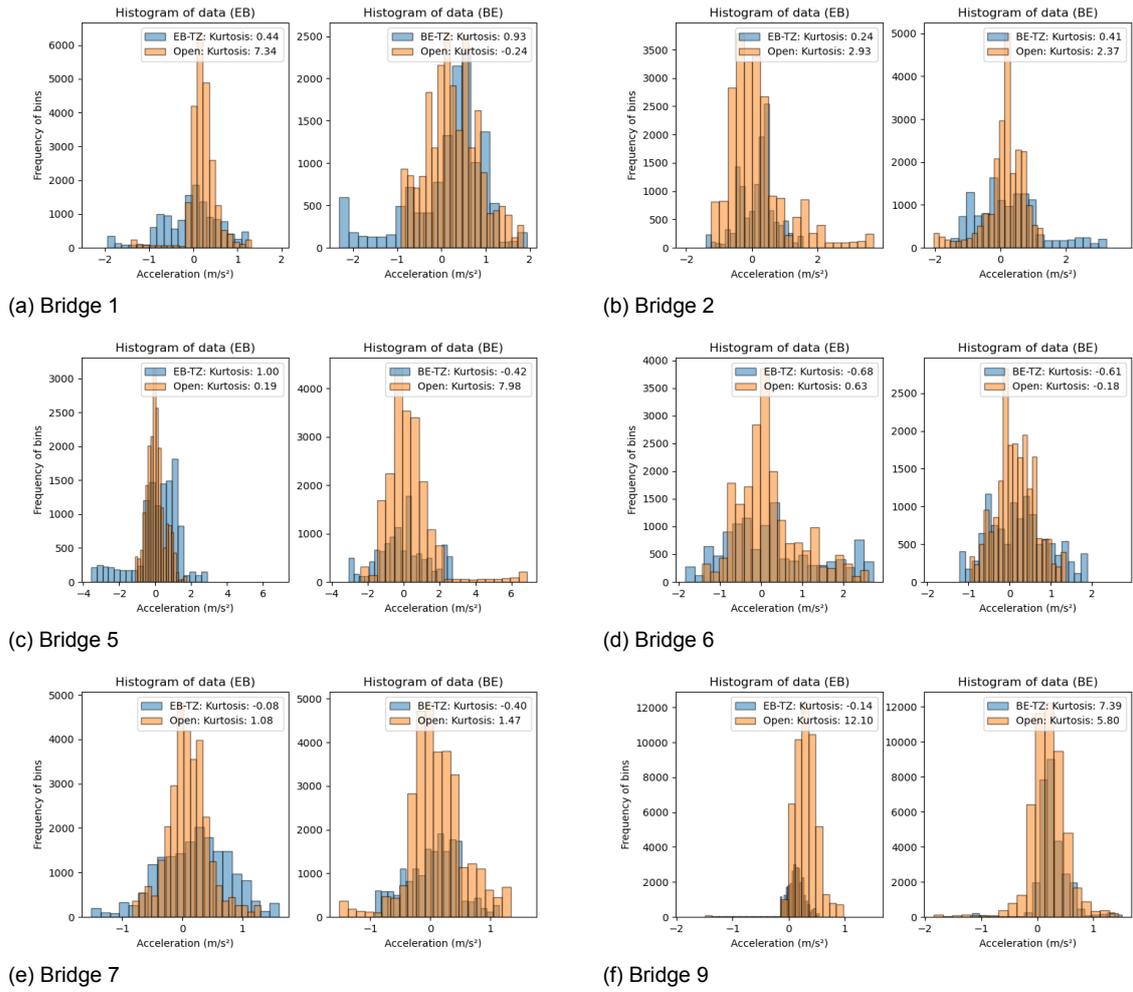
(e) Bridge 7

(f) Bridge 9

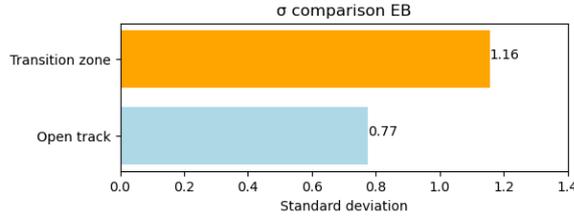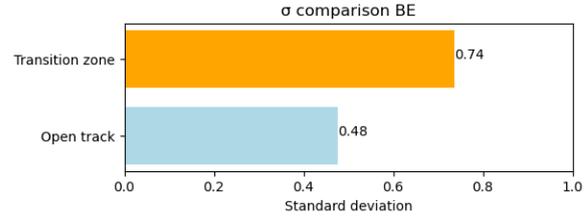Figure B.4: Kurtosis and skewness values of bridge 1 (a), 2 (b), 4 (c), 6 (d), 7 (e) and 9 (f). Both open track as transition zone

C
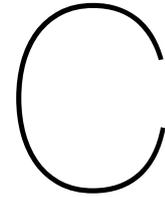
Attachment C

Data analyses remaining bridges

The results of bridge number 1, 2, 5, 6, 7 and 9 and their corresponding transition zones can be found here. Together with the plotted data each transition zone will be briefly discussed. Bridge 3 is taken out of consideration due to its length.

From figure C.1 it can be seen that most of the EB transition zones have an increase of the amplitude of the signal (between the orange and red vertical stripes). Most of them within the limits of the absolute value of 2 m/s^2. Bridge 1 (figure C.1a) gives a good example of such an increase. However, not all data shows this pattern which can be a direct result of IRJ's in the near vicinity if the bridge which can influence the signals amplitude. At bridge 5 for example, the peaks resulting from the IRJ are clearly visible at 25226 meters. As for the BE transition zones, this phenomenon is less visible. Again, bridge 1 demonstrates a decrease in amplitude, but bridge 2 does the opposite.

The standard deviation values as can be seen in figure C.3 are in most of the cases higher for the transition zones than for the open tracks (both EB and BE zones), suggesting an increase of the amplitude of the signal. With the biggest value for bridge 5 which could be an effect of the IRJ in near vicinity. In two cases however, bridge number 2 and 9, the opposite applies (bridge 7 BE is considered equal). Figure C.2b and C.2f shows the normal distributions of these signals. Here the open track has more outliers than the transition zone. This could be appointed to several possibilities. For all data sets the misalignment of had been corrected by the location of the IRJ's. However, for bridge 2 these joints where not visible in the data. For this reason, the value of misalignment has been taken from bridge 1 due to is proximity. As for bridge 9, one reason for the lower standard deviations could be the location of the bridge. The bridge falls in between two IRJ's which can affect the data. Another reason can be the low low-pass filter (25 Hz) that is applied on the data. The velocity of the vehicle here was very low due to the vicinity of a station. By taking all these factors in consideration, it can be stated that the standard deviation is indeed a good measure to identify transition zones on the track. But it is easily affected by any irregularities on the track.

Next, both Fourier Transform and CWT are plotted, figure C.4 and C.5 respectively. Because the CWT gives a better understanding of the condition, only these scalograms are briefly

73
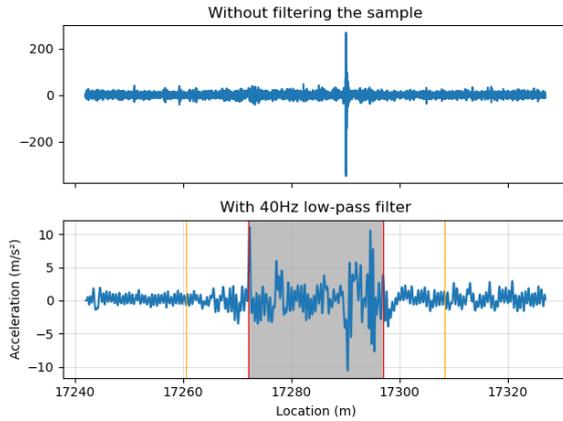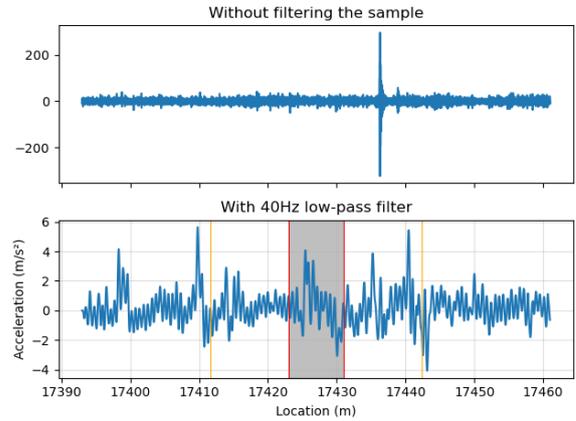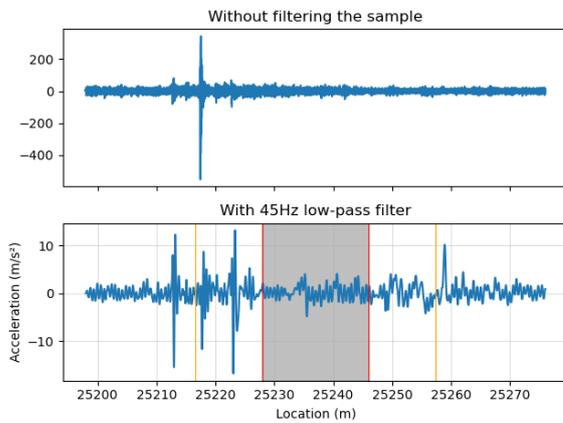
(a) Bridge 1
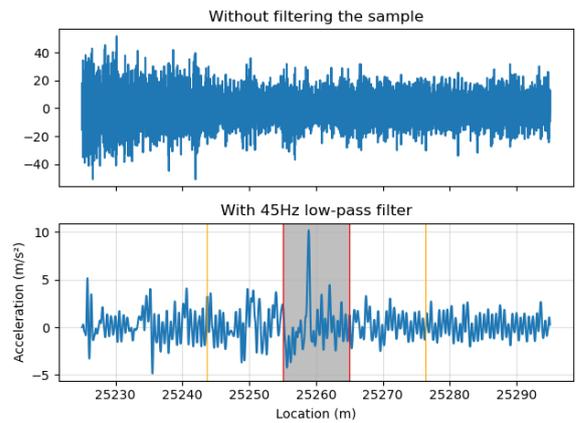
(b) Bridge 2
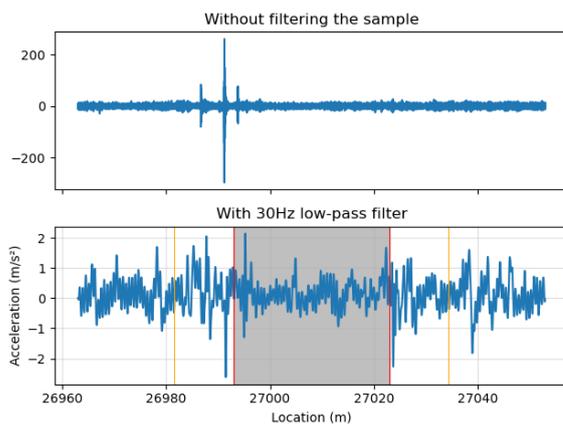
(c) Bridge 5
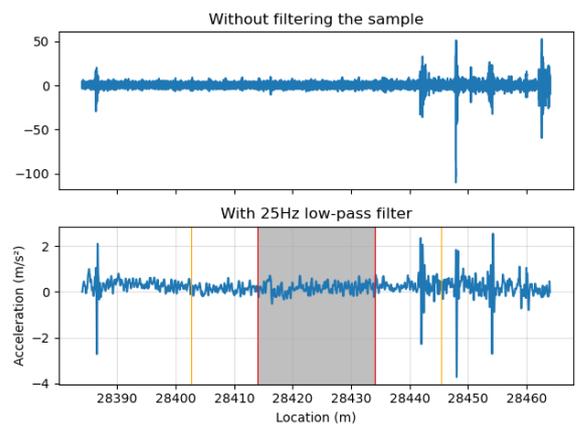
(d) Bridge 6

(e) Bridge 7

(f) Bridge 9

Figure C.1: Selected data from bridge 1 (a), 2 (b), 4 (c), 6 (d), 7 (e) and 9 (f). The red lines mark the start and end of bridge and orange lines mark the start and end of the transition zone

Figure C.2: Normal distribution curve of bridge 1 (a), 2 (b), 4 (c), 6 (d), 7 (e) and 9 (f). Both open track as transition zone
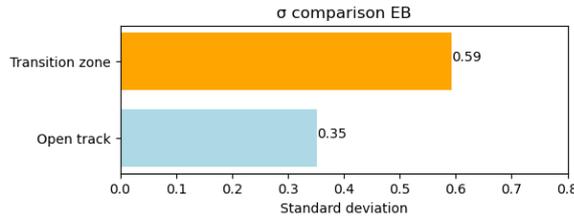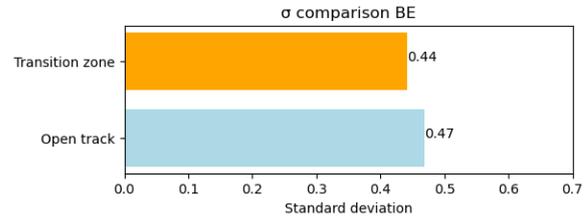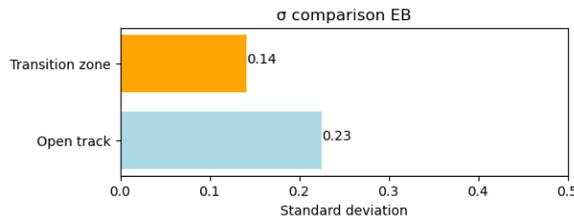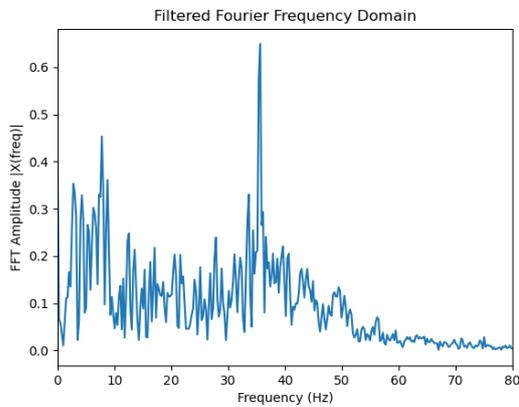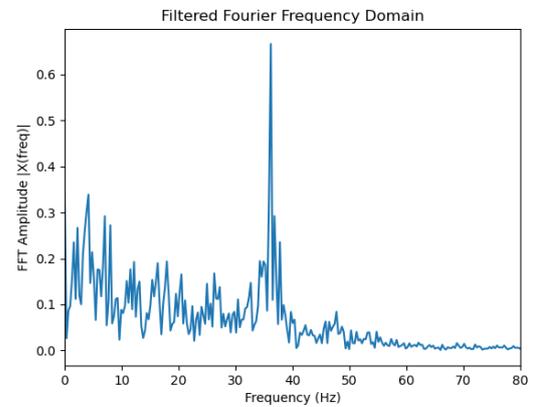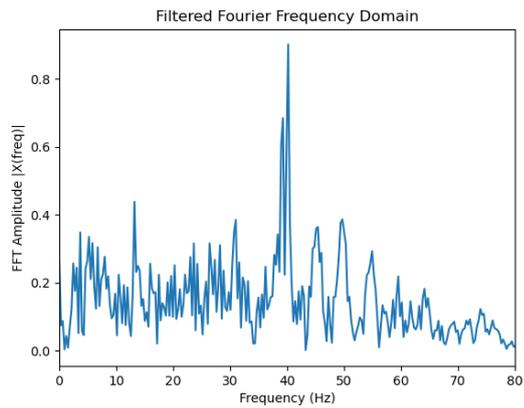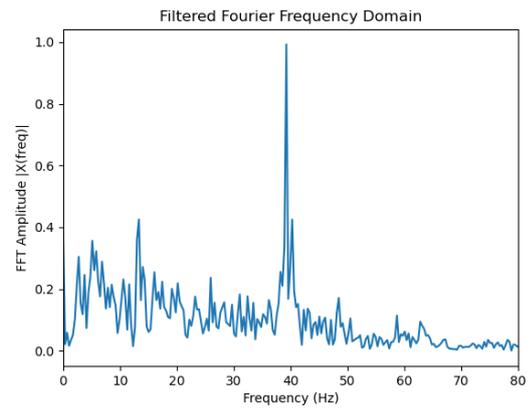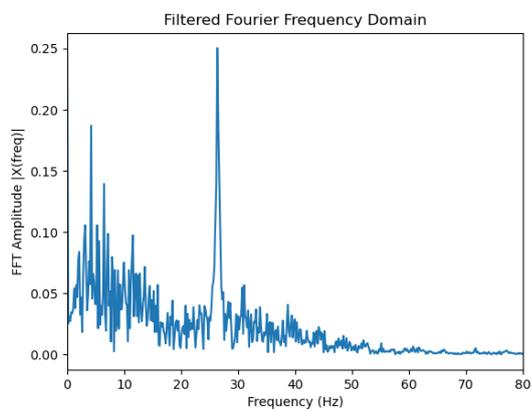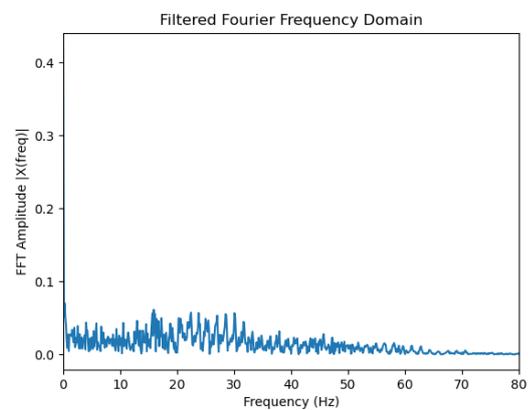
σ comparison EB

Transition zone — 1.25
Open track — 0.50

Standard deviation

(e) Bridge 5

σ comparison BE

Transition zone — 1.40
Open track — 1.31

Standard deviation

(f) Bridge 5

σ comparison EB

Transition zone — 1.16
Open track — 0.77

Standard deviation

(g) Bridge 6

σ comparison BE

Transition zone — 0.74
Open track — 0.48

Standard deviation

(h) Bridge 6

σ comparison EB

Transition zone — 0.59
Open track — 0.35

Standard deviation

(i) Bridge 7

σ comparison BE

Transition zone — 0.44
Open track — 0.47

Standard deviation

(j) Bridge 7

σ comparison EB

Transition zone — 0.14
Open track — 0.23

Standard deviation

(k) Bridge 9

σ comparison BE

Transition zone — 0.28
Open track — 0.33

Standard deviation

(l) Bridge 9

Figure C.3: Standard deviation σ of bridge 1 (a), 2 (b), 4 (c), 6 (d), 7 (e) and 9 (f). Both open tracks as transition zones

Filtered Fourier Frequency Domain

(a) Bridge 1

Filtered Fourier Frequency Domain

(b) Bridge 2

(c) Bridge 5

(d) Bridge 6

(e) Bridge 7

(f) Bridge 9

Figure C.4: Fourier Transform (FFT) of bridge 1 (a), 2 (b), 4 (c), 6 (d), 7 (e) and 9 (f)

Velocity (m/s)	Cut off frequency (Hz)	Frequency range of interest (Hz)
25 (no.4,5,6)	45	5 - 21
22 (no.1,2)	40	4 - 18
17 (no.7)	30	3 - 14
15 (no.8)	30	3 - 12.5
10 (no.9)	25	2 - 8

Table C.1: Velocities with their corresponding cut off frequency and range of interest for analysis

discussed with their corresponding GWPS (figure C.6). First thing to notice is the fact that for all bridges the scalograms are quite different from each other. Bridge 1, 2, 6 and 7 show frequency concentrations at the EB and BE transitions (the moment when the bogie is moving on and off the bridge). By looking at C.1, the region of interests are met in bridge 1 (mostly EB), 2, 5 (BE only), 6 (mostly EB) and 7. By taking for example bridge 7, high frequency concentration is located at around 5 - 14 Hz at the EB transition zone. This falls perfectly in line with the region of frequency interest of 3 - 14 Hz. With the higher standard deviation values as well, it's likely that differential settlements exist at this location. Bridge 2 shows high concentration areas at around 5 Hz over a longer period of time. Here, it can be possible that the a differential settlement extents longer than the suggested length of the transition zone. Bridge 9 does not seem to show any frequencies at all. Here the GWPS can give more answers.

For the final analyses, the GWPS are plotted in figure C.6. These plots should give the most information of what is happening within a transition zone and open track. Like before, for every bridge the total length of the track is plotted until and from the bridge. Below these plots, the open track and transition zone are plotted separately. From the scalograms it was concluded that most transition zones do show the abrupt stiffness change and have high frequency concentration areas in the region of interests. From the GWPS it can be seen that for every track the sleeper spacing peak is easy to be distinguished. By starting at bridge 1, the region of interest (5-21 Hz) is well present within the EB and BE transition zone. However, for the BE transition even lower values seem to exist. These can be assigned to the length of the car body. For bridge 2, the region of 4-18 Hz is present in the frequencies for both EB as BE transition zone. The BE zone for bridge 5 has higher frequencies in the range of interest, but almost no frequencies in that region at the EB zone. This falls in line with the scalogram conclusion. The high standard deviation are resulting from peaks with higher frequencies (20 Hz and up). These frequencies come from small track wave irregularities. It is possible that a certain corrugation or squat is present at the rail head of the EB at bridge 5. Next, bridge 6 falls in line with the region of interest and shows a higher frequency power overall. Bridge 7 follows this pattern. At last bridge 9, here the GWPS picks up more than the scalogram for the EB zone and shows a peak at 5 Hz which sits in between the 2 - 8 Hz of interest for this bridge. However, the BE zone does not show much which is probably due to the station and IRJ in the vicinity. Also the auxiliary rails could be a reason for the small frequency concentrations at the EB transition zone.
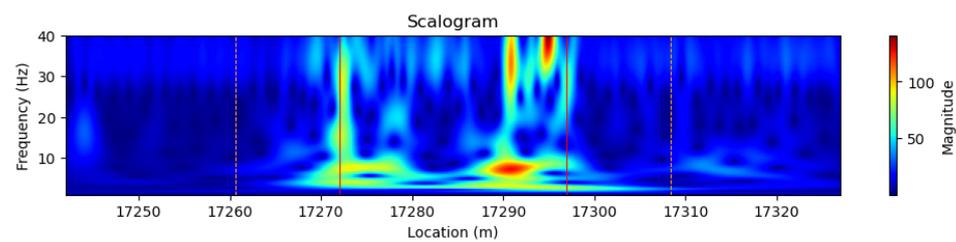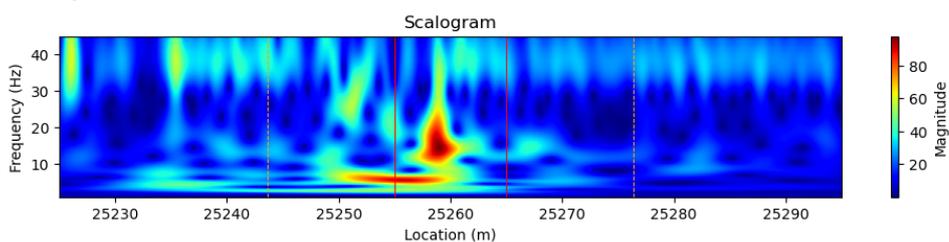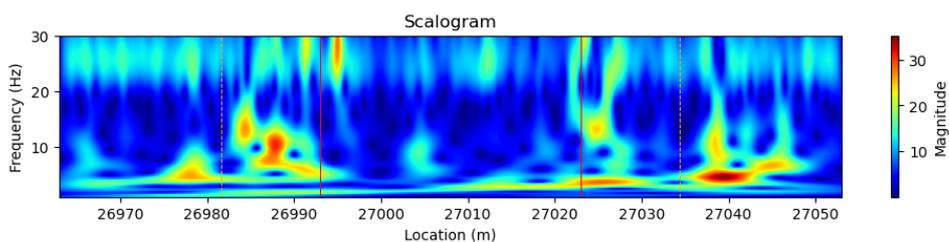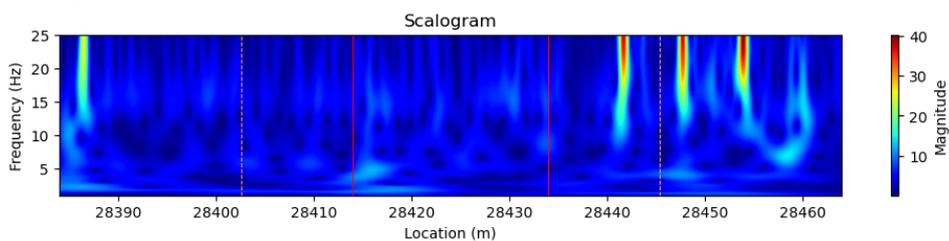
(a) Bridge 1
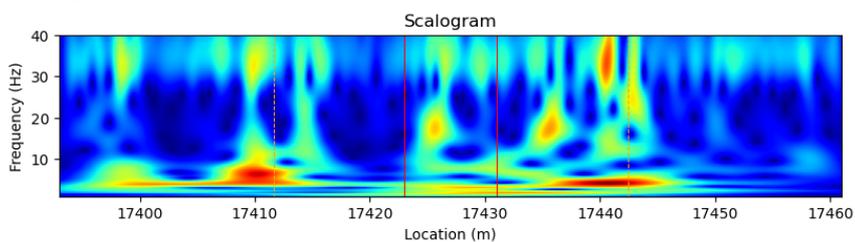
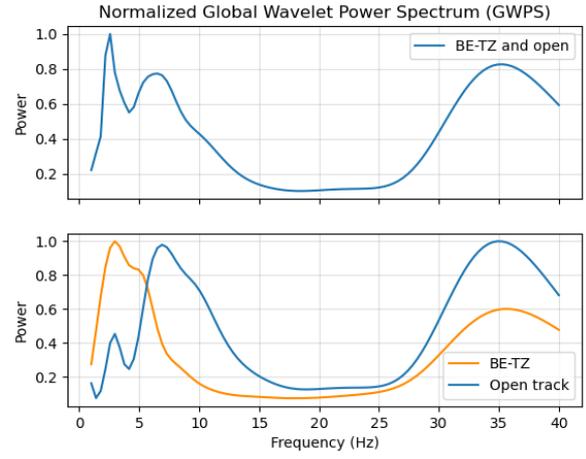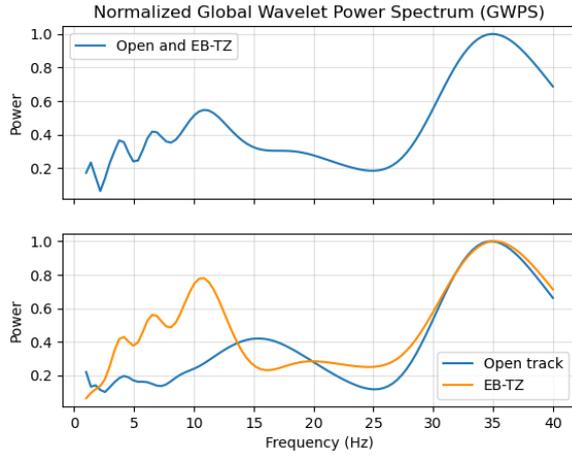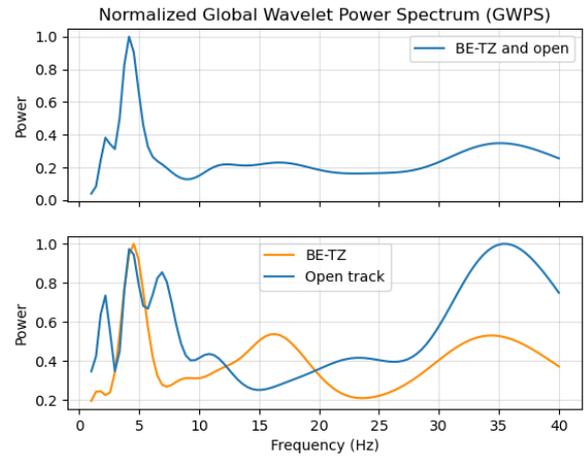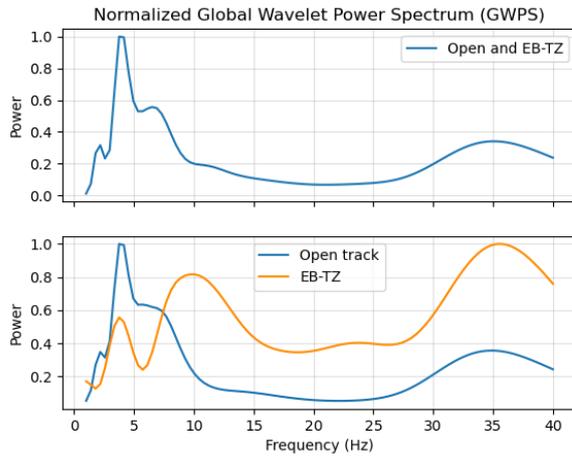(b) Bridge 2
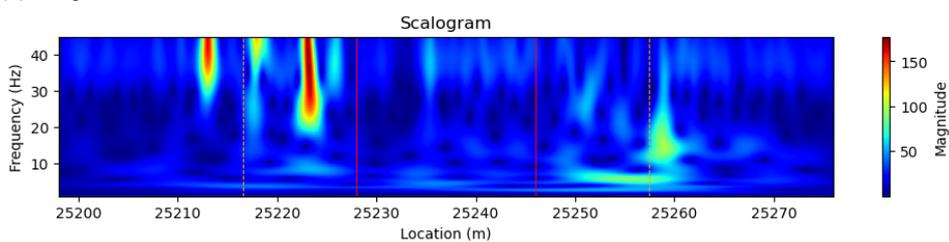
(c) Bridge 5

(d) Bridge 6

(e) Bridge 7

(f) Bridge 9

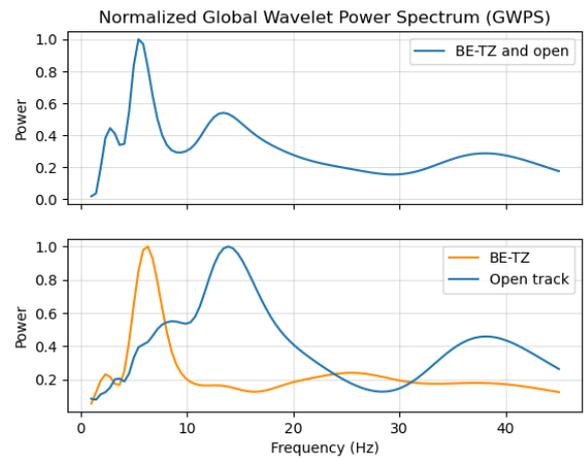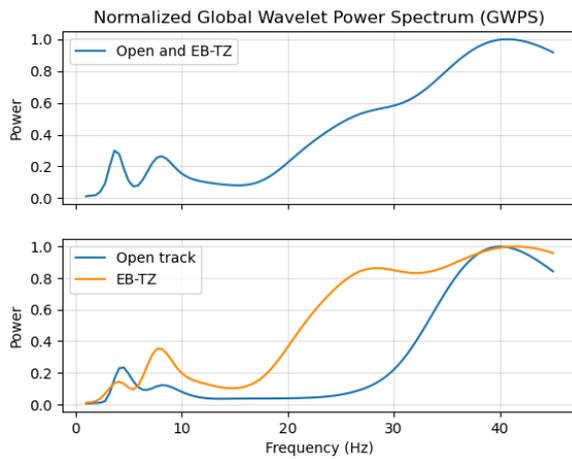Figure C.5: Scalogram of bridge 1 (a), 2 (b), 4 (c), 6 (d), 7 (e) and 9 (f)

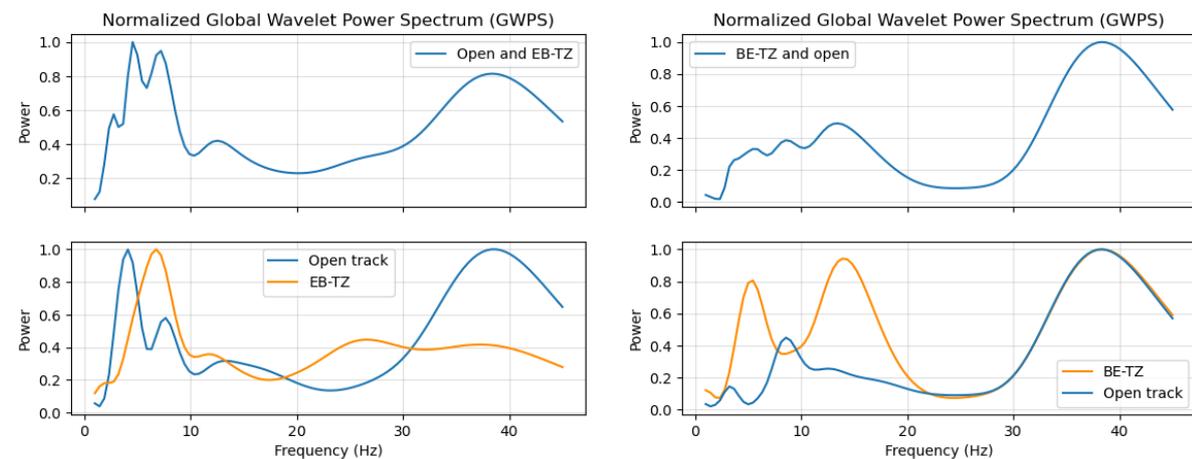(a) Bridge 1

(b) Bridge 1

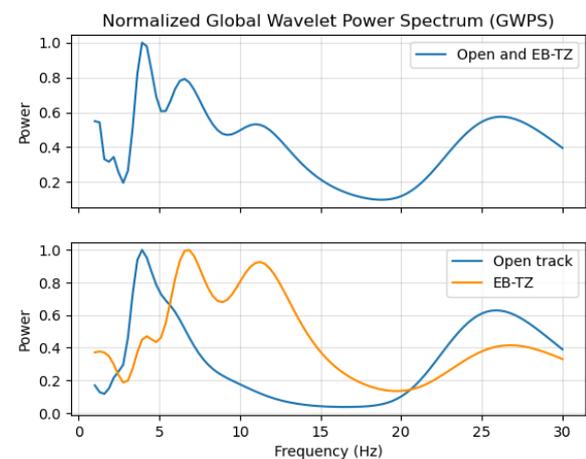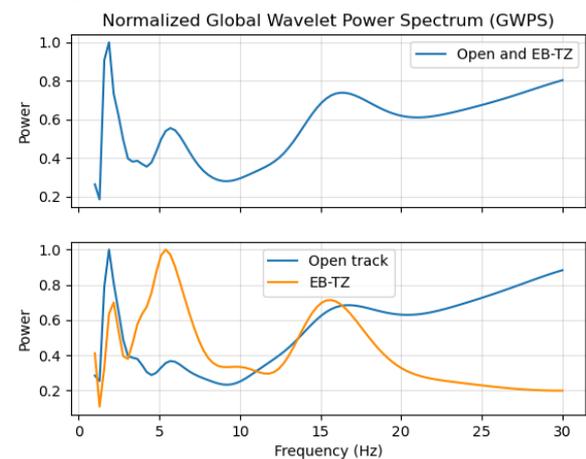(c) Bridge 2

(d) Bridge 2

(e) Bridge 5

(f) Bridge 5

(g) Bridge 6

(h) Bridge 6

(i) Bridge 7

(j) Bridge 7

(k) Bridge 9

(l) Bridge 9

Figure C.6: Scalogram of bridge 1 (a), 2 (b), 4 (c), 6 (d), 7 (e) and 9 (f)

In conclusion, in almost all of the situations the frequencies of the transition zones meet the expected frequencies. Also, the frequency power overall of the transition zones is in most of the cases greater than of the open tracks (for all the EB zones, and 4 out of 6 BE zones). This confirms the fact that transition zones can be distinguished with certain frequencies based upon differential settlements and hanging sleepers. The scalogram and GWPS are good indicators to perform a data analyses on vertical acceleration data.

D
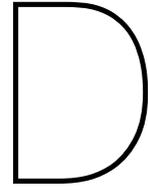
Attachment D

Simulation parameters

Parameters used for the track model based upon Shen et al. (2016) and TU Delft (2020b). According to the formulas for the spring constant of the rails, the parameters are in line with a track in good condition. This holds for the rail properties as well. These are in line with the known values for UIC60.

Parameter	Value
Mass rail	60.3 kg/m
Mass sleeper	244 kg
Ballast	
K_y (lateral)	$1.2x10^8$ N/m
K_z (vertical)	$9.0x10^7$
K_x (rolling)	$1.3x10^8$
C_y	$4.0x10^4$ Ns/m
C_z	$6.4x10^4$
C_x	$2.9x10^5$
Rail	
K_y (lateral)	$2.8x10^8$ N/m
K_z (vertical)	$1.3x10^9$
K_x (rolling)	$3.6x10^8$
C_y	$5.8x10^4$ Ns/m
C_z	$4.5x10^4$
C_x	$3.9x10^5$

Table D.1: Content of the frp file which contains the values of the stiffness and damping parameters.

Parameter	Value
Sleeper distance	0.6 m
Sleeper height	0.2 m
Sleeper width	0.3 m
Rail height	0.172 m
Rail Ixx	$1.75x10^{-6}m^4$
Rail Iyy	$3.055x10^{-5}m^4$
Rail Izz	$5.12x10^{-6}m^4$
Rail area	$7.67x10^{-3}m^2$
Rail Young Modulus	$2.1x10^{11}N/m^2$
Damping ratio	0.03

Table D.2: Rail parameters
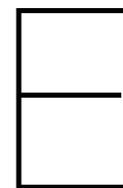
Attachment E

Zimmermann

With the aid of the Zimmermann Rail Support Model (1888) the numerical model created in the MBS software can be validated. According to Esveld (2001) the Zimmermann model is sufficient to understand the general behaviour of track structures. The basic concept of the Zimmermann model assumes a beam continuously supported by an elastic foundation with coefficient k and loaded by a wheel load Q (figure E.1).
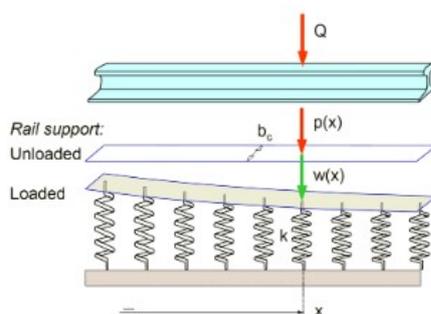

Figure E.1: A rail on an elastic foundation as stated by Zimmermann (TU Delft, 2020a)

An advantage of the Zimmermann model, relative to the Winkler model for example, is that the solution can be analytically derived. An infinite beam in length with bending stiffness EI and spring foundation has a differential equation that can be solved (Esveld, 2001).
After setting up boundary conditions, the answer to this problem can be found in the solution of a maximum displacement $w(x)$. or the bending moment $M(x)$.

$$w(x) = \frac{QL^3}{8EI} * \eta(x) = \frac{Q}{2kL} * \eta(x) \tag{E.1}$$

$$M(x) = \frac{QL}{4} * \mu(x) \tag{E.2}$$

With L being the characteristic length and $\mu(x)$ and $\eta(x)$ its corresponding shape functions.

These latter functions determine the form of the elastic displacement of the differential equation. In other words, from these functions it is possible to extract a certain wavelength that can be used to identify important frequencies.

$$L = \sqrt[4]{\frac{4EI}{k}} = \sqrt[4]{\frac{4EIa}{k_d}} \tag{E.3}$$

$$\eta(x) = e^{\frac{-x}{L}}[cos\frac{x}{L} + sin\frac{x}{L}] \; x \geq 0 \tag{E.4}$$

$$\mu(x) = e^{\frac{-x}{L}}[cos\frac{x}{L} - sin\frac{x}{L}] \; x \geq 0 \tag{E.5}$$

Whereas a is the sleeper spacing (600 mm) and k_d the spring constant.

For the equations stated above, the wheel load has to be derived as well. Instead of a static load, wheel loads are changing over time due to the track responses (e.g. track/wheel irregularities, track structure anomalies, et cetera). To make a first assumption of this load, instead of using advanced numerical models, the Dynamic Amplification Factor (DAF) can be used. This factor can multiply a static response to get the dynamic response, a quasi-static load. This method is called the Eisenmann empirical method (Esveld, 2001).

$$\text{Dynamic Response } = DAF * \text{ Static or Mean Response} \tag{E.6}$$

The DAF can be calculated as following:

$$DAF = 1 + t\varphi \text{ for } V \; < \; 60 \; km/h \tag{E.7}$$

$$DAF = 1 + t\varphi(1 + \frac{V - 60}{140}) \; \text{ for } 60 \; \leq \; V \; \leq \; 120 \; km/h \tag{E.8}$$

With the variable φ as track quality and t as a multiplication factor of the standard deviation based upon the confidence interval.

$$t = \begin{cases} 1 \text{ for } 68.3\% \; probality \\ 2 \text{ for } 95.4\% \\ 3 \text{ for } 99.7\% \end{cases} \tag{E.9}$$

$$\varphi = \begin{cases} 0.1 \text{ for very good condition} \\ 0.2 \text{ for good condition} \\ 0.3 \text{ for bad condition} \end{cases} \tag{E.10}$$

In this case, a t of 3 and φ of 0.1 has been taken. The velocity is taken as 25 m/s^2, which is the maximum velocity the ABA-measurement has been obtained at. According to information of ProRail (ProRail, 2019), the maximum axle loads at most of the railway track in the Netherlands is fixed at 22.5 tons. However, taking the Manchester Passenger Wagon into consideration,

the mass will be reduced to 11.1 tons. From equation E.6 and E.8 the following value could be found for a wheel load Q.

$$DAF = 1 + 3 * 0.1 * (1 + \frac{90 - 60}{140}) = 1.36 \tag{E.11}$$

$$Q_{wheel} = 1.36 * \frac{11.1 * 9.81}{2} = 74.42kN \tag{E.12}$$

Together with a characteristic length, the displacement can be plotted considering one single bogie. Using multiple bogies will not change the outcome as the value of the shape functions converge to zero with an increase of distance (x).

F
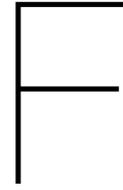
Attachment F

Method 1: flextrack analysis

Due to the size of the results and discussion of both the moving track analysis and flextrack analysis, the first models of methods 1 and method 2 are moved to the attachment. Here, the following models are presented:

Method 1

- Differential stiffness model - model 1

Method 2

- Differential stiffness moving track - model 1

- Differential settlement moving track - model 2

- Differential stiffness flextrack - model 1 (located at Method 1)

- Differential settlement flextrack - model 2

- Transition zone flextrack - model 3

Models method 1

Differential stiffness model - model 1

With the normal track model made, the first irregularity is introduced, the differential stiffness. The differential stiffness is simulated by increasing the base bushing (stiffness of the ballast). Only the parameters of the base are adjusted, the rail parameters stay the same. This model is made twice. One to simulate the embankment-bridge transition zone and one for the bridge-embankment transition zone. To make sure no vibrations from the vehicle interfere with the differential stiffness of the bridge, the length of the track is increased (as discussed in chapter 4). Both tracks are shown in figure F.1. With in red the section that acts as the bridge (higher stiffness), and in silver the open track. For the BE-zone, the bridge length is increased and for the EB-zone the embankment track is increased. Figure F.2 shows the results of the EB track model. Here, the wheel-rail contact, vertical acceleration, scalogram and GWPS of the acceleration are plotted. For both results sets, the data is filtered at the frequency related to the velocity (45 Hz). With the bridge section starting at 180 meters, the peak in force and acceleration is clear visible. The scalogram shows a frequency concentration at this location as well. For the GWPS the same conclusion from chapter 3 can be taken, higher frequencies in the lower frequency region of interest exist. Although the magnitude of the frequencies is small it is clear that the frequencies do occur. The frequencies for differential stiffness only at the EB zone are around 8 - 20 Hz. For the BE zone, the frequencies are lower and around 5 - 12 Hz. For the BE track model, shown in figure F.3, the same conclusions can be taken. A clear differential stiffness peak where the bridge stops (150 meters) and a higher frequency concentration according to the scalogram and GWPS. For both tracks also a stronger sleeper spacing frequency exist (around 40 Hz) for the open track.
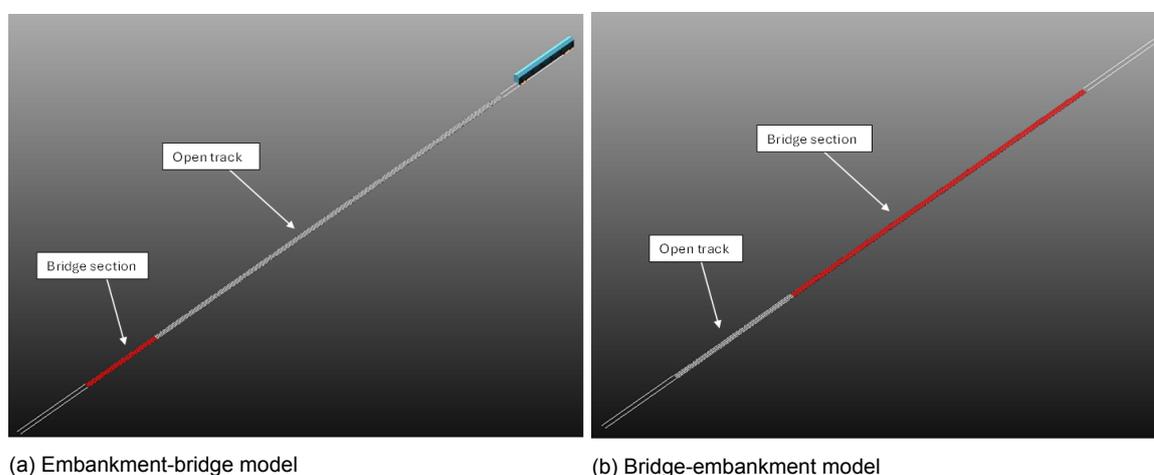

(a) Embankment-bridge model

(b) Bridge-embankment model

Figure F.1: Bridge models. In red the bridge is shown with a higher ballast stiffness

Models method 2

Differential stiffness moving track - model 1

For the moving track analysis the parameters of the track will be implemented in the Matlab file. As a result for both transition zones, a settlement of a little under 1 mm will occur at the transition from open track to rigid and vice versa. This settlement will be reached within 3

(a) Vertical wheel-rail contact forces

(b) Vertical acceleration, filtered

(c) Scalogram of the acceleration results. The red line marks the bridge beginning
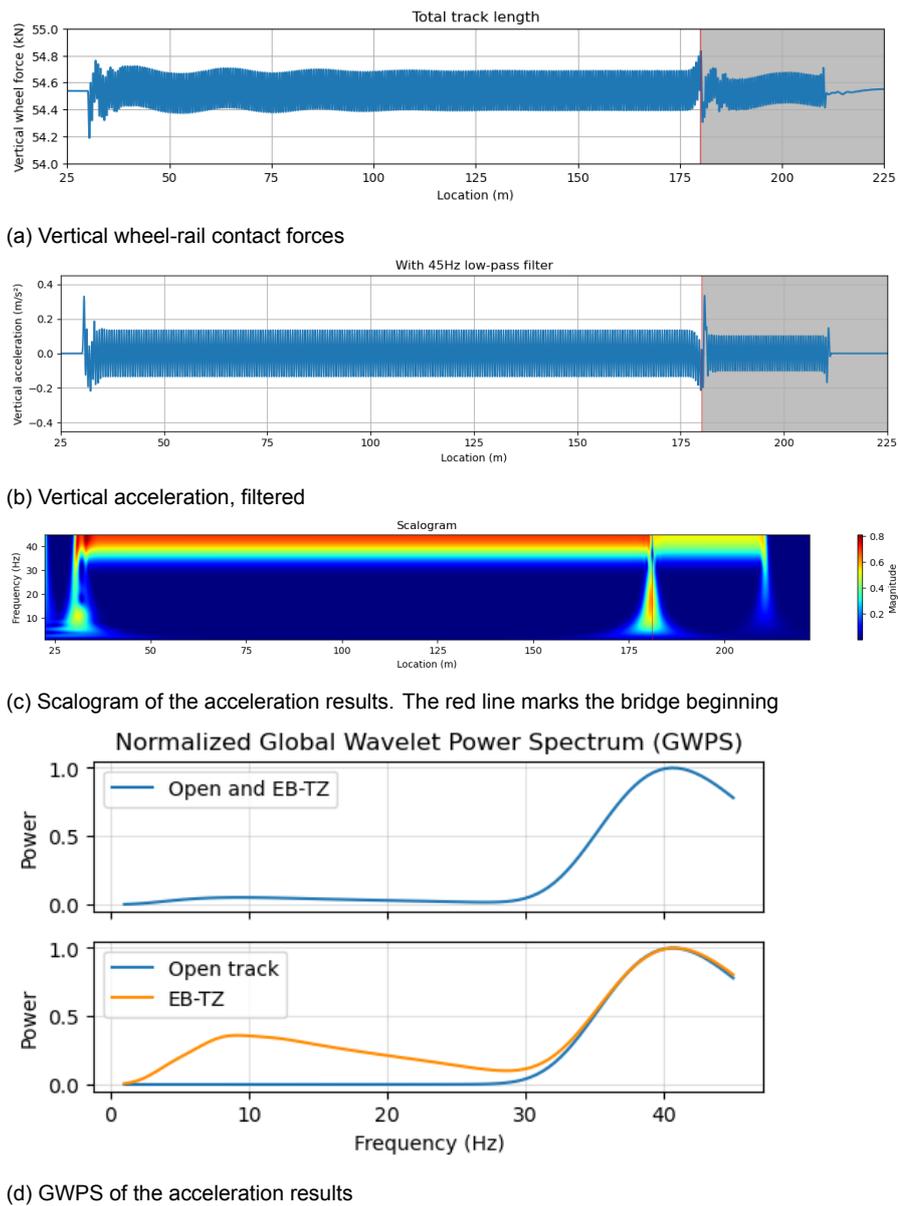

(d) GWPS of the acceleration results

Figure F.2: Results from the differential stiffness EB model. In gray the rigid bridge section is plotted

meters before and after the bridge section. Figure F.4 shows the settlement curve used for the moving track. The results from both transition zones are plotted in figure F.5 and F.6. For both transition zones the peak in force is similar and occurring within 3 meters from the start/end of the bridge. As for the acceleration results, the data keeps in between -1.5 and 1.5 m/s^2 which is higher than when using flextrack. The scalogram shows low frequency responses due to the implementation of the higher settlements. The frequency responses are concentrated around 30 Hz at the location where the settlement curve is present. These frequencies are higher than for the flextrack analysis (figures F.2 and F.3) which show lower frequencies. This is a direct result from the fact that the moving track analysis only takes the vehicle dynamics into account and not the railway track properties.
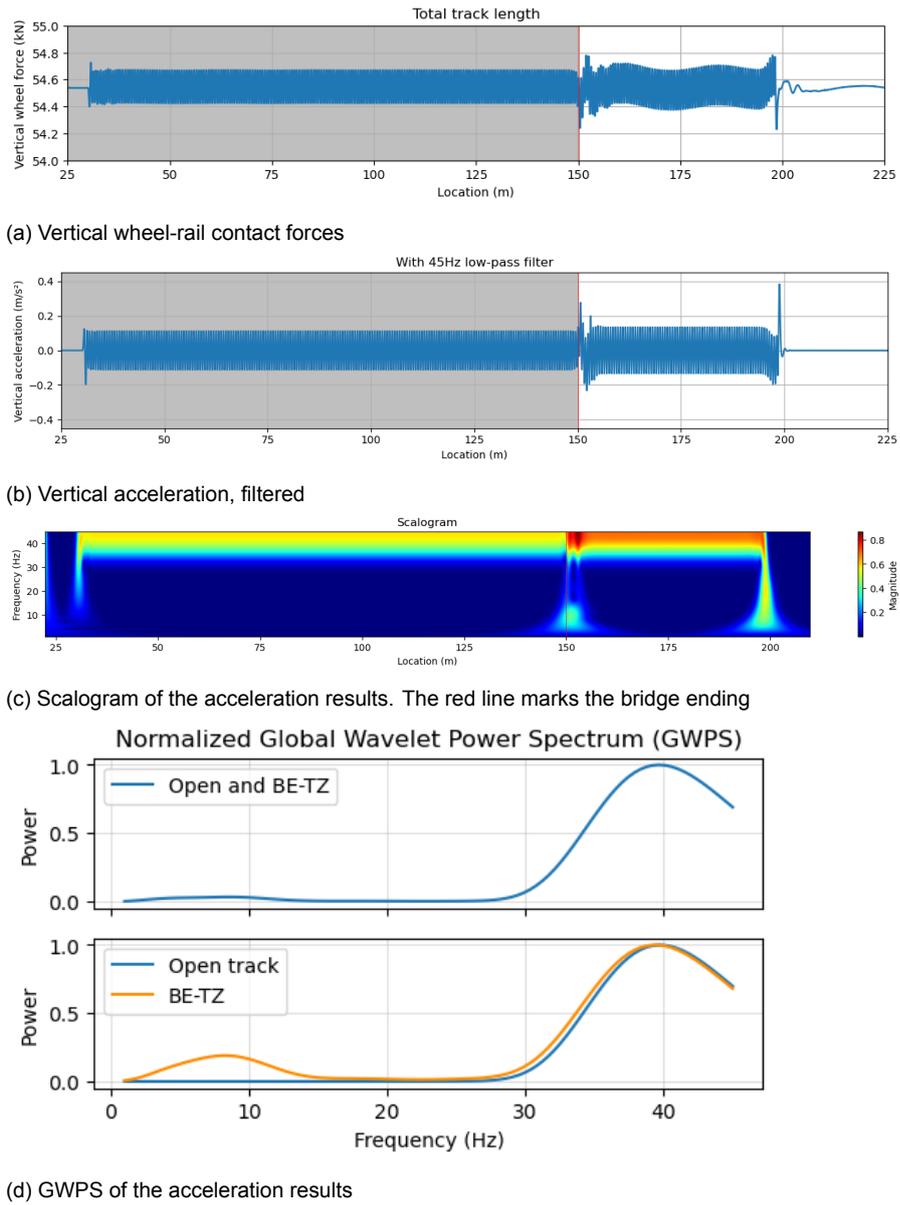
(a) Vertical wheel-rail contact forces

(b) Vertical acceleration, filtered

(c) Scalogram of the acceleration results. The red line marks the bridge ending

(d) GWPS of the acceleration results

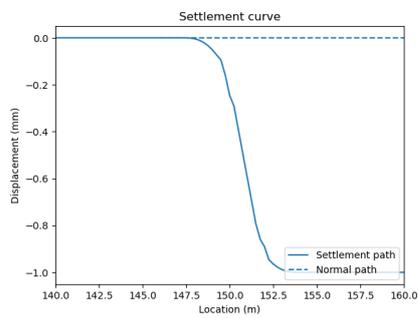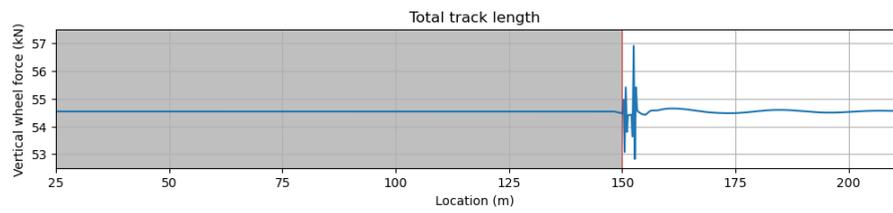Figure F.3: Results from the differential stiffness BE model. In gray the rigid bridge section is plotted
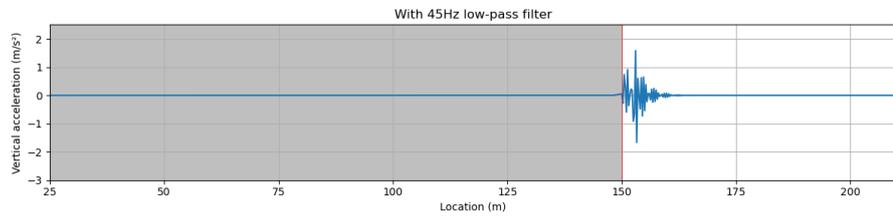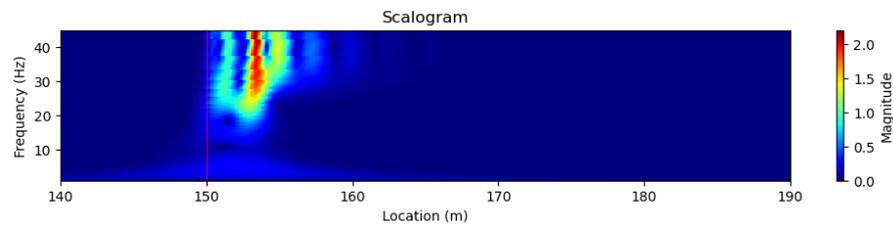

Figure F.4: Introduced settlement curve starting at 150 meters (BE transition zone)

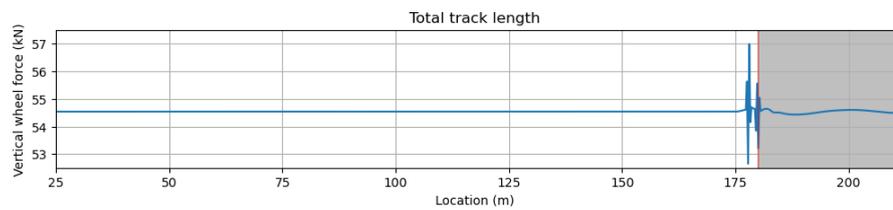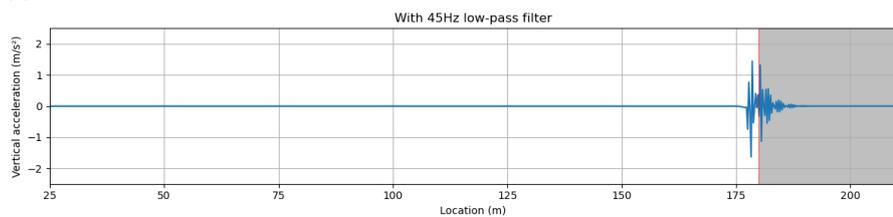(a) Vertical wheel-rail contact forces

(b) Vertical acceleration

(c) Scalogram of the acceleration results. The red line marks the bridge ending
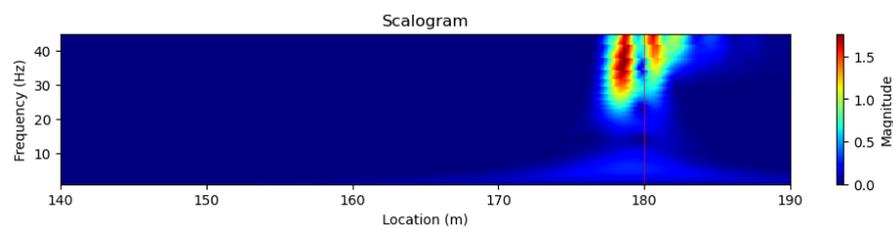
Figure F.5: Results from the BE model 1 using moving track. In gray the rigid bridge section is plotted

(a) Vertical wheel-rail contact forces

(b) Vertical acceleration

(c) Scalogram of the acceleration results. The red line marks the bridge beginning

Figure F.6: Results from the EB model 1 using moving track. In gray the rigid bridge section is plotted

Differential settlement moving track - model 2
Again, using the moving track, the differential settlement is modelled. The results are expected to be very similar to the differential stiffness results because the only difference between these two models is the value of the maximum settlement and the shape of settlement curve. Figures F.7, F.8 and F.9 show the settlement curve and simulation results. The settlement curve shows a displacement of 4 mm during a transition of around 7.5 meters. Due to this longer transition the amplitudes occurring at the force diagrams are a little lower than the situation where only the differential stiffness change was implemented. The wave propagation however, the sinusoidal wave following the peak is as expected longer. Especially the BE transition shows this wave as the EB transition only has a small peak roughly 7 meters before the bridge starts. As for the vertical acceleration, for both EB as BE transition zones these values are around -1 and 1 m/s^2 (again lower than before). The scalogram does show low frequency responses due to the implementation of the higher settlements. The differential settlement change is more concentrated compared to model 1.
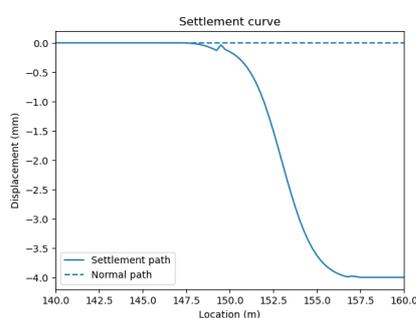

Figure F.7: Introduced settlement curve starting at 150 meters (BE transition zone)

With the identification of the high force locations as the goal of model 2, figure F.10 shows the amplification factors of the vertical wheel force in terms of damping to signal ratio's. The figure shows higher amplification factors and a longer wave propagation for the BE transition than for the EB zone. According to the research of Wang (2018), higher forces are expected at the EB transition due to the fast elevation of the rails. When the train leaves the bridge, depending on the speed, the wheels drop and bounces further, explaining the longer length for the BE zone. From the EB figure it looks like this higher force occurs on the bridge (where a peak of 1.025 is reached) and not at the transition zone. For the EB model, a length of 7 meters is taken as the length of the transition zone where higher forces occur. For the BE model a length of 9 meters is taken (where the line starts to run smooth). For both of them the highest forces occur within the first 2 meters of the bridge.

Differential settlement flextrack - model 2
Now that the moving track models are presented and discussed, the flextrack models will be made. As mentioned, the parameters to change here are the stiffness values of the base bushings. These represent the stiffness values of the ballast and/or ground. The differential stiffness model has already been discussed in section 4.2.1, therefore the differential settlement of model 2 will be introduced. From the Matlab file a differential settlement of 4 mm will occur using a foundation coefficient of 22.5E10$^6 N/m^2$. With the aid of formula 4.3 a stiffness of 1.35E10$^7 N/m$ is calculated for the base bushing. Figures F.11 and F.12 show the obtained graphs for the wheel-rail contact force and the vertical acceleration.
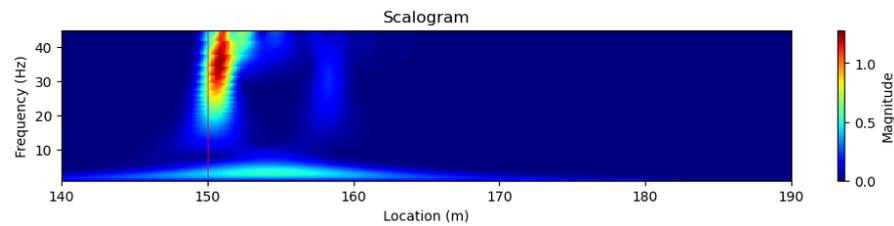
After implementing the differential settlement, the force and acceleration show the presence
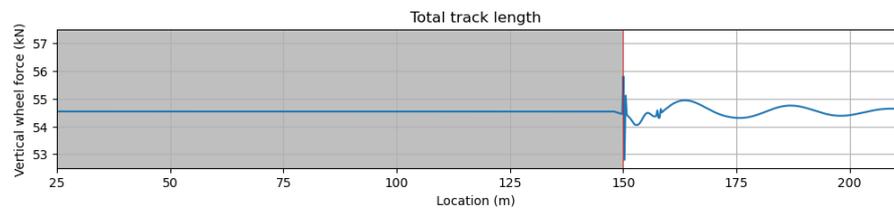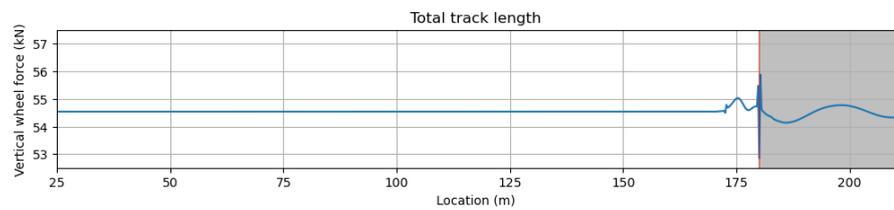
(a) Vertical wheel-rail contact forces
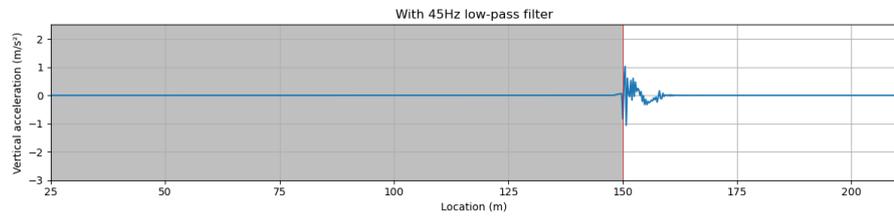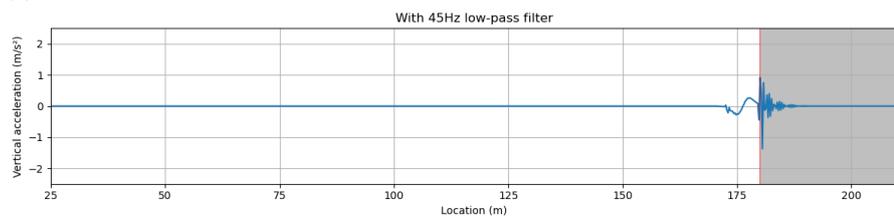

(b) Vertical acceleration

(c) Scalogram of the acceleration results. The red line marks the bridge ending
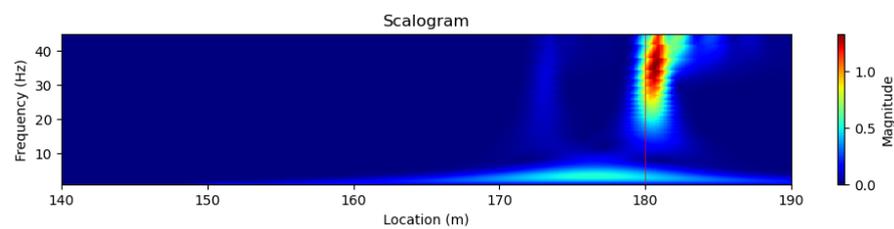
Figure F.8: Results from the BE model 2 using moving track. In gray the rigid bridge section is plotted

(a) Vertical wheel-rail contact forces

(b) Vertical acceleration

(c) Scalogram of the acceleration results. The red line marks the bridge beginning

Figure F.9: Results from the EB model 2 using moving track. In gray the rigid bridge section is plotted
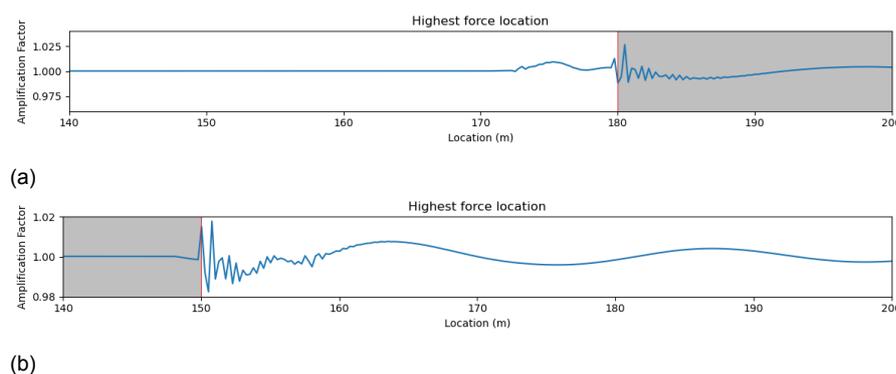
(a)

(b)

Figure F.10: Damping to signal ratio of the EB (top) and BE (bottom) models

of the lower stiffness. For the BE model, the force shows a clear transition from 0 to 4 mm settlement. The lower peak after the bridge at 150 meters suggests a bouncing movement from the bogie on the track. For the EB model a higher peak is shown, suggesting an increase in force. As for the vertical acceleration, in both models the differential settlement is clearly visible with peak between -0.25 and 0.75 m/s^2. Compared to model 1 of the flextrack analysis, the sleeper spacing is less significant present at the scalogram than before. This is not only a result from the lower base bushing used in model 2 but also the higher magnitude of the frequencies at the differential settlement locations (where the bridge starts and ends). Both settlements at either sides are clearly visible in the scalogram in terms of frequency. Again, the lower frequencies are in the region of interest for the condition assessment of the transition zone. The GWPS for the EB and BE confirm this. For the BE zone, the occurring frequencies are ranging from 4 - 11 Hz. The EB zone frequencies on the other hand are slightly higher and range from 6 - 25 Hz.

As the main goal of model 2 is the identification of the high force locations at the transition zones, figure F.13 shows the damping to signal ratio of both the EB and BE models. Again, the higher forces for the EB transition zone occur direct before the bridge, the first 2 meters (sleeper -1, -2, -3 before the bridge). For the BE transition zone, the higher forces are located at 152 - 154 meters (sleeper +3, +4, +5 from the bridge), slightly further away than where the bridge ends. Furthermore, the results are in line with the expectations that higher forces occur at the EB transition zone and a longer length of the transition at the BE zone (Wang, 2018).

Transition zone flextrack - model 3

Now that the high force locations are identified in the latter model (model 2), these sleepers can be adjusted with a lower stiffness to simulate a weak sleeper behavior (degradation phase). Figure F.14 shows a close up of the transition zones in both models made for the EB and BE analyses (the hanging sleepers are not activated until model 4). In red the bridge section is highlighted, in silver the open track (where the stiffness corresponding to 4 mm settlement is maintained), and in yellow the weaker sleepers. These latter mentioned sleepers have been given a stiffness corresponding to a settlement of around 5 mm. Slightly more than the surrounding track.

With model 3 a transition zone using MBS software is simulated. Both differential stiffness as settlement is introduced together with weaker sleepers. Comparing the results from figures F.15 and F.16 with the results from model 2, not so much difference can be seen. The force and acceleration values are almost the same for both EB and BE transition zones. The scalogram however, does show some differences. For the BE model, greater frequency concentrations are visible at the first meters after the bridge (150+ meters). These frequencies

(a) Vertical wheel-rail contact forces

(b) Vertical acceleration

(c) Scalogram of the acceleration results. The red line marks the bridge ending
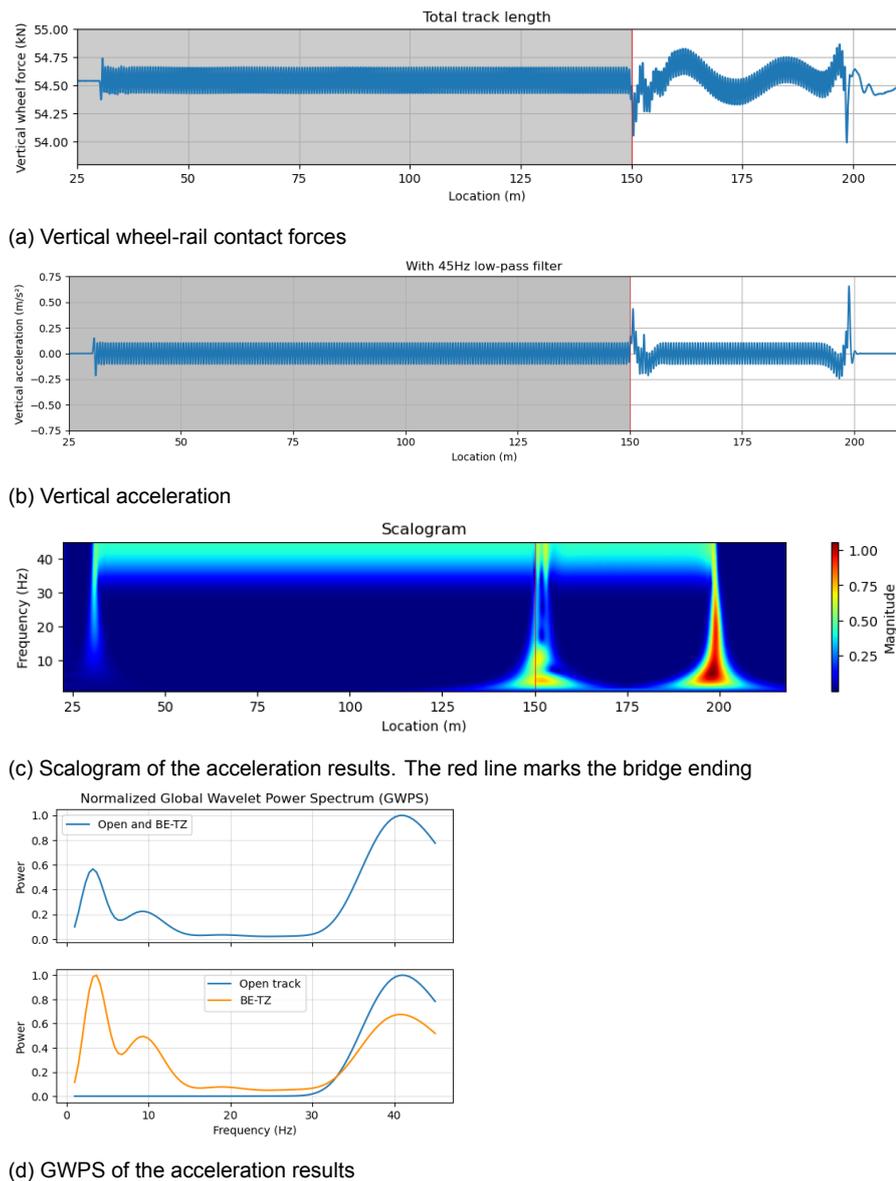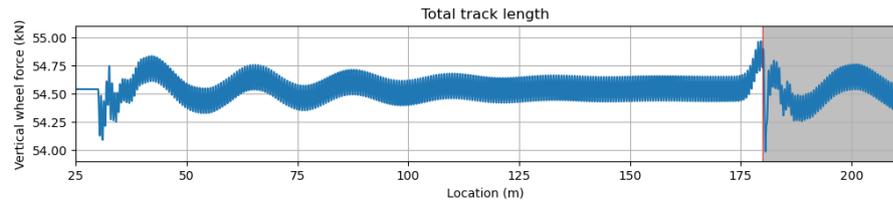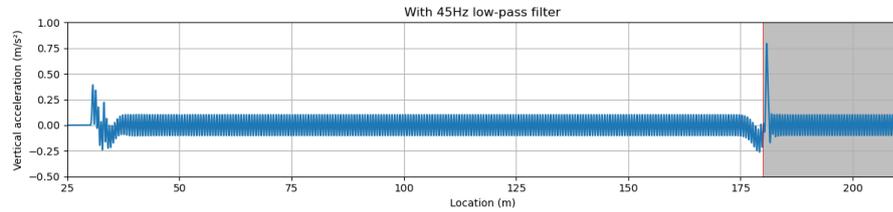

(d) GWPS of the acceleration results

Figure F.11: Results from the BE model 2 using flextrack. In gray the rigid bridge section is plotted

can be assigned to the lower stiffness sleepers that were introduced. For the EB model, this change is barely visible in the scalogram. Just as model 2, a clear frequency concentration is present at the EB transition from around 5 to 30 Hz. It could be possible that the stiffness value assigned to the property file of the weaker sleepers differs too little compared to the stiffness value of the surrounding sleepers. In chapter 6 this is tested further. Another possibility is that the effect of the lowering stiffness at certain sleepers should be done to more sleepers than just three to see a changes in the results. As for the GWPS, both the EB as BE zones do not differ from model 2. They show the same main frequencies.

(a) Vertical wheel-rail contact forces
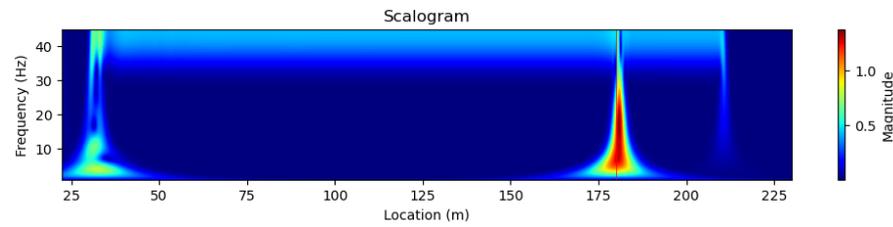
(b) Vertical acceleration

(c) Scalogram of the acceleration results. The red line marks the bridge beginning

(d) GWPS of the acceleration results

Figure F.12: Results from the EB model 2 using flextrack. In gray the rigid bridge section is plotted

(a)

(b)

Figure F.13: Damping to signal ratio of the EB (top) and BE (bottom) models
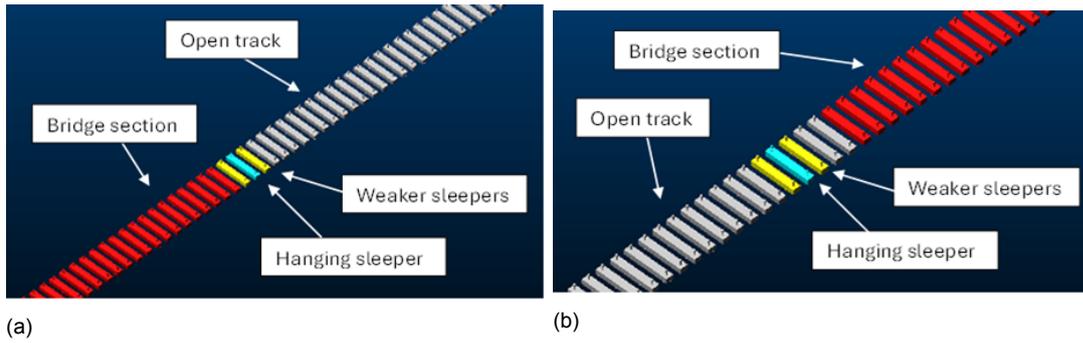
Figure F.14: Models of the (a) EB and (b) BE transition zones
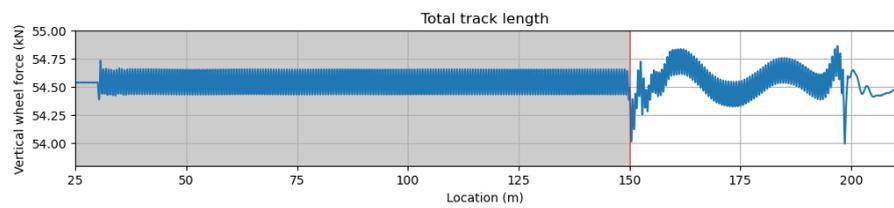
(a) Vertical wheel-rail contact forces
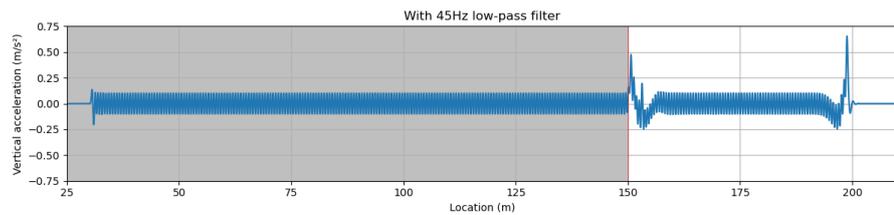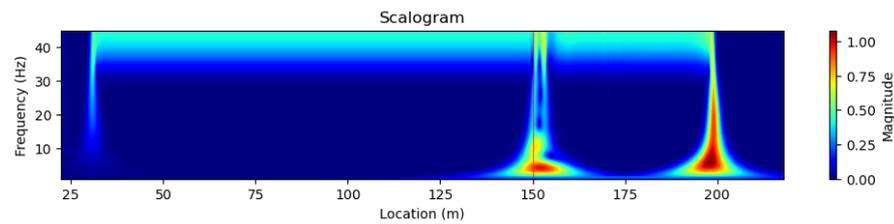
(b) Vertical acceleration

(c) Scalogram of the acceleration results. The red line marks the bridge ending
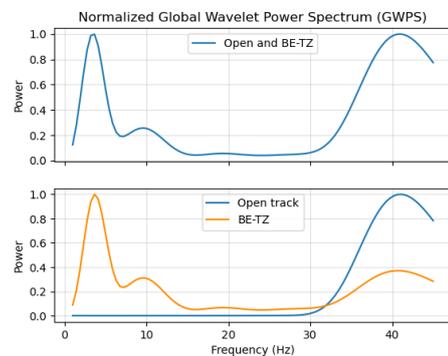
(d) GWPS of the acceleration results

Figure F.15: Results from the BE model 3 using flextrack. In gray the rigid bridge section is plotted
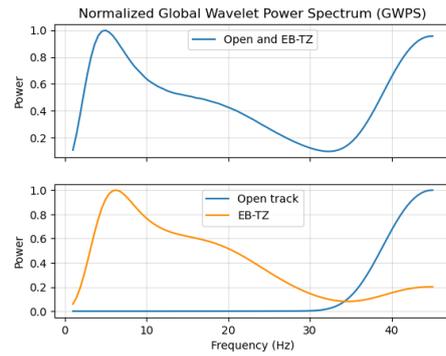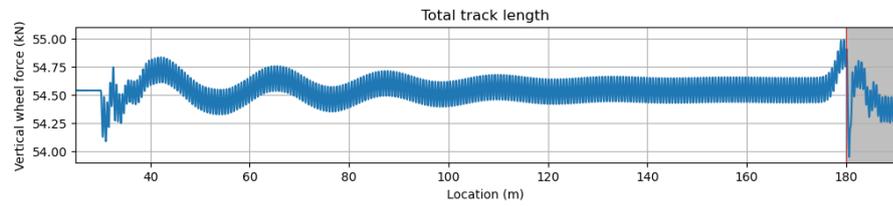
(a) Vertical wheel-rail contact forces
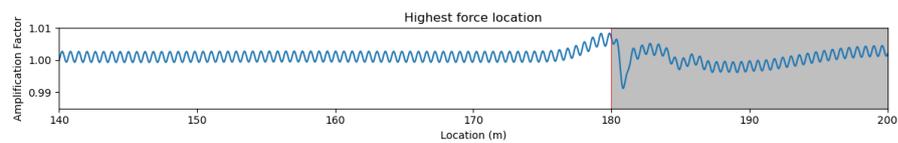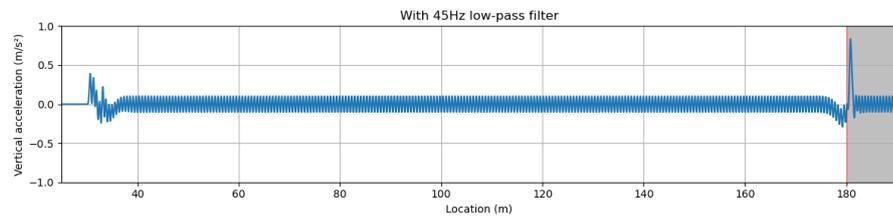

(b) Vertical acceleration
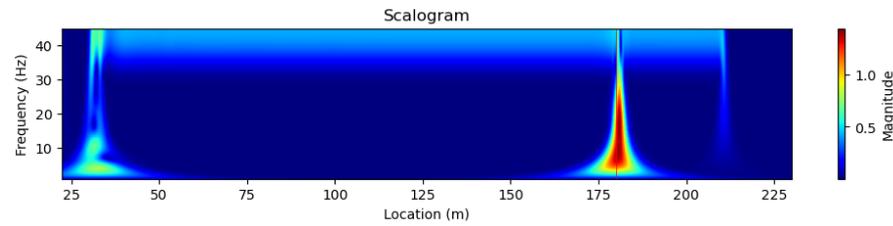
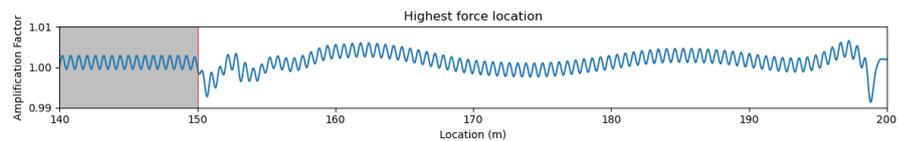(c) Scalogram of the acceleration results. The red line marks the bridge beginning
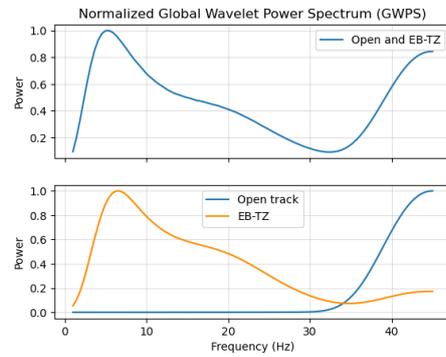
(d) GWPS of the acceleration results

Figure F.16: Results from the EB model 3 using flextrack. In gray the rigid bridge section is plotted

Bibliography

Alves Ribeiro, C., Paixão, A., Fortunato, E., & Calçada, R. (2015). Under sleeper pads in transition zones at railway underpasses: numerical modelling and experimental validation. *Structure and Infrastructure Engineering*, *11*(11), 1432–1449. https://doi.org/10.1080/15732479.2014.970203

Banimahd, M., Woodward, P. K., Kennedy, J., & Medero, G. M. (2012). Behaviour of train–track interaction in stiffness transitions. *Proceedings of the Institution of Civil Engineers - Transport*, *165*(3), 205–214. https://doi.org/10.1680/tran.10.00030

Basirat, R., et al. (2017). 2D Numerical Modeling of Differential Settlement in Transition Zone Induced by Train Load [Accessed: 2024-03-14].

Bezin, Y., Iwnicki, S. D., Cavalletti, M., de Vries, E., Shahzad, F., & Evans, G. (2009). An investigation of sleeper voids using a flexible track model integrated with railway multi-body dynamics. *Proceedings of the Institution of Mechanical Engineers, Part F: Journal of Rail and Rapid Transit*, *223*(6), 597–607. https://doi.org/10.1243/09544097JRRT276

Biggs, J., et al. (2020). How satellite InSAR has grown from opportunistic science to routine monitoring over the last decade [Accessed: 2023-05-12].

Bowness, D., Lock, A. C., Powrie, W., Priest, J. A., & Richards, D. J. (2007). Monitoring the dynamic displacements of railway track. *Proceedings of the Institution of Mechanical Engineers, Part F: Journal of Rail and Rapid Transit*, *221*(1), 13–22. https://doi.org/10.1243/0954409JRRT51

Carrigan, T. D., & Talbot, J. P. (2023). A new method to derive rail roughness from axle-box vibration accounting for track stiffness variations and wheel-to-wheel coupling. *Mechanical Systems and Signal Processing*, *192*, 110232. https://doi.org/10.1016/j.ymssp.2023.110232

Castillo-Mingorance, J. M., Sol-Sánchez, M., Moreno-Navarro, F., & Rubio-Gámez, M. C. (2020). A Critical Review of Sensors for the Continuous Monitoring of Smart and Sustainable Railway Infrastructures. *Sustainability*, *12*(22), 9428. https://doi.org/10.3390/su12229428

Chumyen, P., Connolly, D., Woodward, P., & Markine, V. (2022). The effect of soil improvement and auxiliary rails at railway track transition zones. *Soil Dynamics and Earthquake Engineering*, *155*, 107200. https://doi.org/10.1016/j.soildyn.2022.107200

Coelho, B. (2010). *Dynamics of railway transition zones in soft soils* (Doctoral dissertation). University of Technology Delft. Delft.

Coelho, B., Hölscher, P., & Barends, F. (2011). Enhancement of double integration procedure through spectral subtraction. *Soil Dynamics and Earthquake Engineering*, *31*(4), 716–722. https://doi.org/10.1016/j.soildyn.2010.12.013

Coelho, B., Hölscher, P., Priest, J., Powrie, W., & Barends, F. (2010). An assessment of transition zone performance. *Proceedings of the Institution of Mechanical Engineers, Part F: Journal of Rail and Rapid Transit*, *1*(-1), 1–11. https://doi.org/10.1243/09544097jrrt389

Cooley, J. W., & Tukey, J. W. (1965). An algorithm for the machine calculation of complex Fourier series. *Mathematics of Computation*, *19*(90), 297–301. https://doi.org/10.1090/S0025-5718-1965-0178586-1

Dahlberg, T. (2010). Railway Track Stiffness Variations – Consequences and Countermeasures. *International Journal of Civil Engineering*, *8*(1).

D'Amico, F., Gagliardi, V., Bianchini Ciampoli, L., & Tosti, F. (2020). Integration of InSAR and GPR techniques for monitoring transition areas in railway bridges. *NDT & E International*, *115*, 102291. https://doi.org/10.1016/j.ndteint.2020.102291

Dekking, F., Kraaikamp, C., Lopuhaä, H., & Meester, L. (2005). *A modern introduction to probability and statistics: Understanding why and how* (Second edition). Springer-Verlag.

Dimitrovová, Z., & Varandas, J. (2009). Critical velocity of a load moving on a beam with a sudden change of foundation stiffness: Applications to high-speed trains. *Computers & Structures*, *87*(19-20), 1224–1232. https://doi.org/10.1016/j.compstruc.2008.12.005

Electronics. (n.d.). Butterworth Filter Design [Accessed: 2023-08-04]. https://www.electronics-tutorials.ws/filter/filter_8.html

Esveld, C. (2001). *Modern railway track* (Second edition). MRT Productions.

Falamarzi, A., Moridpour, S., & Nazem, M. (2019). A Review on Existing Sensors and Devices for Inspecting Railway Infrastructure. *Jurnal Kejuruteraan*, *31*(1), 1–10. https://doi.org/10.17576/jkukm-2019-31(1)-01

Fortunato, E., Paixão, A., & Calçada, R. (2013). Railway Track Transition Zones: Design, Construction, Monitoring and Numerical Modelling. *International Journal of Railway Technology*, *2*(4), 33–58. https://doi.org/10.4203/ijrt.2.4.3

Gallego Giner, I., & López Pita, A. (2009). Numerical simulation of embankment—structure transition design. *Proceedings of the Institution of Mechanical Engineers, Part F: Journal of Rail and Rapid Transit*, *223*(4), 331–343. https://doi.org/10.1243/09544097JRRT234

Greenblatt, R., Pflieger, M., & Ossadtchi, A. (2012). Connectivity measures applied to human brain electrophysiological data. *Journal of Neuroscience Methods*, *207*(1), 1–16. https://doi.org/10.1016/j.jneumeth.2012.02.025

Hering, E., Schönfelder, G., Basler, S., Biehl, K.-E., Burkhardt, T., Engel, T., Feinäugle, A., Fericean, S., Forkl, A., Giebeler, C., Hahn, B., Halder, E., Herfort, C., Hubrich, S., Reichenbach, J., Röbel, M., & Sester, S. (2022). Geometric Quantities. *Sensors in science and technology* (pp. 147–372). Springer Fachmedien Wiesbaden. https://doi.org/10.1007/978-3-658-34920-2{_}3

Hlawatsch, F., & Boudreaux-Bartels, G. (1992). Linear and quadratic time-frequency signal representations. *IEEE Signal Processing Magazine*, *9*(2), 21–67. https://doi.org/10.1109/79.127284

Hunt, H. E. M. (1997). Settlement of railway track near bridge abutments. (Third paper in young railway engineer of the year (1996) award). *Proceedings of the Institution of Civil Engineers - Transport*, *123*(1), 68–73. https://doi.org/10.1680/itran.1997.29182

Iskander, M. (2018). Geotechnical Underground Sensing and Monitoring. *Underground sensing: Monitoring and hazard detection for environment and infrastructure* (pp. 141–202). Elsevier Inc. https://doi.org/10.1016/B978-0-12-803139-1.00003-5

Kong, Q., Siauw, T., & Bayen, A. (2020). *Python programming and numerical methods: A guide for engineers and scientists.* (Second edition). Academic press.

Kong, Q., et al. (2020). Python Programming And Numerical Methods: A Guide For Engineers And Scientists. Discrete Fourier Transform (DFT) [Accessed: 2023-08-12]. https://pythonnumericalmethods.berkeley.edu/notebooks/chapter24.02-Discrete-Fourier-Transform.html

Kouroussis, G., Caucheteur, C., Kinet, D., Alexandrou, G., Verlinden, O., & Moeyaert, V. (2015). Review of Trackside Monitoring Solutions: From Strain Gages to Optical Fibre Sensors. *Sensors*, *15*(8), 20115–20139. https://doi.org/10.3390/s150820115

Le Pen, L., Watson, G., Powrie, W., Yeo, G., Weston, P., & Roberts, C. (2014). The behaviour of railway level crossings: Insights through field monitoring. *Transportation Geotechnics*, *1*(4), 201–213. https://doi.org/10.1016/j.trgeo.2014.05.002

Le Pen, L., et al. (2018). Behaviour of under sleeper pads at switches and crossings – Field measurements [Accessed: 2023-05-03].

Lei, X., & Mao, L. (2004). Dynamic response analyses of vehicle and track coupled system on track transition of conventional high speed railway. *Journal of Sound and Vibration*, *271*(3-5), 1133–1146. https://doi.org/10.1016/S0022-460X(03)00570-4

Li, D., Asce, M., & Davis, D. (2005). Transition of Railroad Bridge Approaches. *Journal of Geotechnical and Geoenvironmental Engineering*, *131*(11), 1392–1398. https://doi.org/10.1061/ASCE1090-02412005131:111392

Li, Z. G., & Wu, T. X. (2008). Vehicle/Track Impact Due to Passing the Transition between a Floating Slab and Ballasted Track. *Noise and vibration mitigation for rail transportation systems* (pp. 94–100). Springer Berlin Heidelberg. https://doi.org/10.1007/978-3-540-74893-9{_}13

Li, Z., Molodova, M., Nunez, A., & Dollevoet, R. (2015). Improvements in axle box acceleration measurements for the detection of light squats in railway infrastructure. *IEEE Transactions on Industrial Electronics*, *62*(7), 4385–4397. https://doi.org/10.1109/TIE.2015.2389761

Liu, X., Liu, C., Wu, W., Liu, J., Sun, S., & Wei, Y. (2023). Transient dynamics of a full wheel rail set passing a weld irregularity at high speed. *Engineering Failure Analysis*, *148*, 107203. https://doi.org/10.1016/j.engfailanal.2023.107203

Liu, X., Markine, V., Wang, H., & Shevtsov, I. (2018). Experimental tools for railway crossing condition monitoring (crossing condition monitoring tools). *Measurement*, *129*, 424–435. https://doi.org/10.1016/j.measurement.2018.07.062

Lundqvist, A., & Dahlberg, T. (2005). Load impact on railway track due to unsupported sleepers. *Proceedings of the Institution of Mechanical Engineers, Part F: Journal of Rail and Rapid Transit*, *219*(2), 67–77. https://doi.org/10.1243/095440905X8790

MathWorks. (2019). Short-time Fourier transform [Accessed: 2023-07-05]. https://nl.mathworks.com/help/signal/ref/stft.html?searchHighlight=short%20time%20fourier%20transform&s_tid=srchtitle_support_results_2_short%2520time%2520fourier%2520transform

Miao, S., Gao, L., Tong, F., Zhong, Y., Ma, C., & Chen, Z. (2023). Ballastless track mortar layer void detection by high-order statistical analysis of axle box acceleration. *Measurement*, *211*, 112681. https://doi.org/10.1016/j.measurement.2023.112681

Molodova, M., Li, Z., Nunez, A., & Dollevoet, R. (2014). Automatic detection of squats in railway infrastructure. *IEEE Transactions on Intelligent Transportation Systems*, *15*(5), 1980–1990. https://doi.org/10.1109/TITS.2014.2307955

Molodova, M., Li, Z., Núñez, A., & Dollevoet, R. (2014). Validation of a finite element model for axle box acceleration at squats in the high frequency range. *Computers & Structures*, *141*, 84–93. https://doi.org/10.1016/j.compstruc.2014.05.005

Molodova, M., Li, Z., Núñez, A., & Dollevoet, R. (2015). Parametric study of axle box acceleration at squats. *Proceedings of the Institution of Mechanical Engineers, Part F: Journal of Rail and Rapid Transit*, *229*(8), 841–851. https://doi.org/10.1177/0954409714523583

Molodova, M., Oregui, M., Núñez, A., Li, Z., & Dollevoet, R. (2016). Health condition monitoring of insulated joints based on axle box acceleration measurements. *Engineering Structures*, *123*, 225–235. https://doi.org/10.1016/j.engstruct.2016.05.018

Molodova, M., Li, Z., & Dollevoet, R. (2011). Axle box acceleration: Measurement and simulation for detection of short track defects. *Wear*, *271*(1-2), 349–356. https://doi.org/10.1016/j.wear.2010.10.003

Mori, H., Tsunashima, H., Kojima, T., Matsumoto, A., & Mizuma Takeshi. (2010). Condition Monitoring of Railway Track Using In-service Vehicle. *Journal of Mechanical Systems for Transportation and Logistics*, *3*(1), 154–165. https://doi.org/10.1299/jmtl.3.154

Namura, A., & Suzuki, T. (2007). Evaluation of Countermeasures against Differential Settlement at Track Transitions. *Quarterly Report of RTRI*, *48*(3), 176–182. https://doi.org/10.2219/rtriqr.48.176

NEN. (2019). NEN-EN 13848-1, Railtoepassingen - Bovenbouw - Geometrische kwaliteit van het spoor - Deel 1: Beschrijving van de spoorgeometrie [Accessed: 2023-07-08]. www.connect.nen.nl

Ngamkhanong, C., Ming, Q. Y., Li, T., & Kaewunruen, S. (2020). Dynamic train-track interactions over railway track stiffness transition zones using baseplate fastening systems. *Engineering Failure Analysis*, *118*, 104866. https://doi.org/10.1016/j.engfailanal.2020.104866

Nicks, J. E. (2009). *The Bump at the End of the Railway Bridge* (Doctoral dissertation). Texas A&M University. Texas.

Nunez, A. ; Hendriks, A. ; Moraal, J. ; Ramirez Fonseca, J., Dollevoet, I. ; & Li, R. ; (2018). Rail Condition Monitoring using Axle Box Acceleration Measurements: Defect detection in the Netherlands and Romania. *Proceedings of the 2018 World Transport Convention*.

Omega. (n.d.). Strain Gauges [Accessed: 2023-04-012]. https://www.omega.com/en-us/resources/strain-gages

OmegaEngineering. (2020). What is an Accelerometer and How Does it Work? [Accessed: 2023-01-02]. https://www.youtube.com/watch?v=q4_VZte-8wg

Oregui, M., Li, S., Núñez, A., Li, Z., Carroll, R., & Dollevoet, R. (2017). Monitoring bolt tightness of rail joints using axle box acceleration measurements. *Structural Control and Health Monitoring*, *24*(2), e1848. https://doi.org/10.1002/stc.1848

Paixão, A., Alves Ribeiro, C., Pinto, N., Fortunato, E., & Calçada, R. (2015). On the use of under sleeper pads in transition zones at railway underpasses: experimental field

testing. *Structure and Infrastructure Engineering*, *11*(2), 112–128. https://doi.org/10.1080/15732479.2013.850730

Paixão, A., Fortunato, E., & Calçada, R. (2014). Transition zones to railway bridges: Track measurements and numerical modelling. *Engineering Structures*, *80*, 435–443. https://doi.org/10.1016/j.engstruct.2014.09.024

Paixão, A., Fortunato, E., & Calçada, R. (2015). Design and construction of backfills for railway track transition zones. *Proceedings of the Institution of Mechanical Engineers, Part F: Journal of Rail and Rapid Transit*, *229*(1), 58–70. https://doi.org/10.1177/0954409713499016

Paixão, A., Fortunato, E., & Calçada, R. (2016). A numerical study on the influence of backfill settlements in the train/track interaction at transition zones to railway bridges. *Proceedings of the Institution of Mechanical Engineers, Part F: Journal of Rail and Rapid Transit*, *230*(3), 866–878. https://doi.org/10.1177/0954409715573289

Paixão, A., Varandas, J. N., Fortunato, E., & Calçada, R. (2018). Numerical simulations to improve the use of under sleeper pads at transition zones to railway bridges. *Engineering Structures*, *164*, 169–182. https://doi.org/10.1016/j.engstruct.2018.03.005

Paixão, A., et al. (2014). Transition zones to railway bridges: Track measurements and numerical modelling [Accessed: 2023-05-06].

Paixão, A., et al. (2015). On the use of under sleeper pads in transition zones at railway underpasses: experimental field testing [Accessed: 2023-05-03].

Paixãoa, A., et al. (2018). Numerical simulations to improve the use of under sleeper pads at transition zones to railway bridges [Accessed: 2023-05-14].

Pieringer, A., & Kropp, W. (2022). Model-based estimation of rail roughness from axle box acceleration. *Applied Acoustics*, *193*, 108760. https://doi.org/10.1016/j.apacoust.2022.108760

Pinto, N., Ribeiro, C. A., Gabriel, J., & Calçada, R. (2015). Dynamic monitoring of railway track displacement using an optical system. *Proceedings of the Institution of Mechanical Engineers, Part F: Journal of Rail and Rapid Transit*, *229*(3), 280–290. https://doi.org/10.1177/0954409713509980

ProRail. (2019). Aanvulling 1 op de Netverklaring 2020 [Accessed: 2023-06-04]. https://www.prorail.nl/siteassets/homepage/samenwerken/vervoerders/documenten/2020-netverklaring-aanvulling-1.pdf

ProRail. (2023). ProRail Basisbheerkaart (BKK) [Accessed: 2023-07-10]. https://maps.prorail.nl/portal/apps/webappviewer/index.html?id=b27bc5d895da4d1b8d7fb5503a223a9e

Ramos, A., Gomes Correia, A., Calçada, R., & Connolly, D. P. (2022). Ballastless railway track transition zones: An embankment to tunnel analysis. *Transportation Geotechnics*, *33*. https://doi.org/10.1016/j.trgeo.2022.100728

RealPars. (2022). Basics of the Linear Variable Differential Transformer (LVDT) [Accessed: 2023-01-02]. https://www.youtube.com/watch?v=o_hEmYip248

Rodríguez, A., Sañudo, R., Miranda, M., Gómez, A., & Benavente, J. (2021). Smartphones and tablets applications in railways, ride comfort and track quality. Transition zones analysis. *Measurement*, *182*, 109644. https://doi.org/10.1016/j.measurement.2021.109644

Salvador, P., Naranjo, V., Insa, R., & Teixeira, P. (2016). Axlebox accelerations: Their acquisition and time–frequency characterisation for railway track monitoring purposes. *Measurement*, *82*, 301–312. https://doi.org/10.1016/j.measurement.2016.01.012

Sañudo, R., Dell'Olio, L., Casado, J. A., Carrascal, I. A., & Diego, S. (2016). Track transitions in railways: A review. *Construction and Building Materials*, *112*, 140–157. https://doi.org/10.1016/j.conbuildmat.2016.02.084

Shahraki, M., Warnakulasooriya, C., & Witt, K. J. (2015). Numerical study of transition zone between ballasted and ballastless railway track. *Transportation Geotechnics*, *3*, 58–67. https://doi.org/10.1016/j.trgeo.2015.05.001

Shan, Y., Albers, B., & Savidis, S. A. (2013). Influence of different transition zones on the dynamic response of track–subgrade systems. *Computers and Geotechnics*, *48*, 21–28. https://doi.org/10.1016/j.compgeo.2012.09.006

Shen, C., Wei, Z., Burgelman, N., Dollevoet, R., & Li, Z. (2016). Effects of wheelset flexibility on the simulation of vehicle-track interaction at crossings. *The dynamics of vehicles on roads and tracks* (pp. 1549–1558). CRC Press. https://doi.org/10.1201/b21185-165

Shi, C., & Chen, Z. (2021). Coupled DEM/FDM to evaluate track transition stiffness under different countermeasures. *Construction and Building Materials*, *266*, 121167. https://doi.org/10.1016/j.conbuildmat.2020.121167

Shi, J., Burrow, M. P. N., Chan, A. H., & Wang, Y. J. (2013). Measurements and simulation of the dynamic responses of a bridge–embankment transition zone below a heavy haul railway line. *Proceedings of the Institution of Mechanical Engineers, Part F: Journal of Rail and Rapid Transit*, *227*(3), 254–268. https://doi.org/10.1177/0954409712460979

Stark, T. D., & Wilk, S. T. (2016). Root cause of differential movement at bridge transition zones. *Proceedings of the Institution of Mechanical Engineers, Part F: Journal of Rail and Rapid Transit*, *230*(4), 1257–1269. https://doi.org/10.1177/0954409715589620

Torrence, C., & Compo, G. P. (1998). A Practical Guide to Wavelet Analysis. *Bulletin of the American Meteorological Society*, *79*(1), 61–78. https://doi.org/10.1175/1520-0477(1998)079<0061:APGTWA>2.0.CO;2

Trackopedia. (n.d.). Wayside Train Monitoring System (WTMS) [Accessed: 2023-05-14]. https://www.trackopedia.com/en/encyclopedia/infrastructure/wayside-train-monitoring-system-wtms

TU Delft. (2014). ABA measurement system [Accessed: 2023-06-05]. https://www.tudelft.nl/en/ceg/about-faculty/departments/engineering-structures/sections-labs/railway-engineering/research/aba-measurement-system

TU Delft. (2020a). Course Structural Design of Railway Track [Accessed: 2023-05-05]. www.brightspace.tudelft.nl

TU Delft. (2020b). Elements of Railway Engineering [Accessed: 2023-05-15]. www.brightspace.tudelft.nl

Unsiwilai, S., Wang, L., Nunez, A., & Li, Z. (2023). *Measurement Multiple-Axle Box Acceleration Measurements at Railway Transition Zones Highlights (for review) Multiple-Axle Box Acceleration Measurements at Railway Transition Zones* (tech. rep.).

Varandas, J. N., Hölscher, P., & Silva, M. A. (2011). Dynamic behaviour of railway tracks on transitions zones. *Computers & Structures*, *89*(13-14), 1468–1479. https://doi.org/10.1016/j.compstruc.2011.02.013

VI-Grade. (2016). VI-Rail FlexTrack Toolkit [Accessed: 2023-10-07]. http://www.accsimia-software.com/wp-content/uploads/2016/03/VI-Rail-Datasheet-V16.pdf

VI-Grade. (2022). *Vi-rail 2022.1 documentation*. VI-grade GmbH.

Vukušičová, D. (2017). Analysis of dynamic effects acting on railway crossings [Accessed: 2023-05-04].

Wang, H., Markine, V. L., & Dollevoet, R. ; (2016). Improvement of train-track interaction in transition zones via reduction of ballast damage. *Proceedings of the 24th international symposium on dynamics of vehicles on roads and tracks, IAVSD 2015*, 1–13.

Wang, H. (2018). *Measurement, Assessment, Analysis and Improvement of Transition Zones in Railway Track* (Doctoral dissertation). University of Technology Delft. Delft. https://doi.org/10.4233/uuid:73830b2c-deb1-4da9-b19c-5e848c5cfa4d

Wang, H., Chang, L., & Markine, V. (2018). Structural Health Monitoring of Railway Transition Zones Using Satellite Radar Data. *Sensors*, *18*(2), 413. https://doi.org/10.3390/s18020413

Wang, H., & Markine, V. (2018a). Corrective countermeasure for track transition zones in railways: Adjustable fastener. *Engineering Structures*, *169*, 1–14. https://doi.org/10.1016/j.engstruct.2018.05.004

Wang, H., & Markine, V. (2018b). Methodology for the comprehensive analysis of railway transition zones. *Computers and Geotechnics*, *99*, 64–79. https://doi.org/10.1016/j.compgeo.2018.03.001

Wang, H., Markine, V., & Liu, X. (2018). Experimental analysis of railway track settlement in transition zones. *Proceedings of the Institution of Mechanical Engineers, Part F: Journal of Rail and Rapid Transit*, *232*(6), 1774–1789. https://doi.org/10.1177/0954409717748789

Wang, H., Silvast, M., Markine, V., & Wiljanen, B. (2017). Analysis of the Dynamic Wheel Loads in Railway Transition Zones Considering the Moisture Condition of the Ballast and Subballast. *Applied Sciences*, *7*(12), 1208. https://doi.org/10.3390/app7121208

Wang, H., et al. (2017). Analysis of the Dynamic Wheel Loads in Railway Transition Zones Considering the Moisture Condition of the Ballast and Subballast [Accessed: 2023-05-12].

Wang, H., & Markine, V. (2018). Methodology for the comprehensive analysis of railway transition zones [Accessed: 2023-05-13].

Wei, Z., Núñez, A., Li, Z., & Dollevoet, R. (2017). Evaluating Degradation at Railway Crossings Using Axle Box Acceleration Measurements. *Sensors*, *17*(10), 2236. https://doi.org/10.3390/s17102236

Wei, Z., Shen, C., Li, Z., & Dollevoet, R. (2017). Wheel–Rail Impact at Crossings: Relating Dynamic Frictional Contact to Degradation. *Journal of Computational and Nonlinear Dynamics*, *12*(4). https://doi.org/10.1115/1.4035823

Yoder, N. C., & Adams, D. E. (2014). Commonly used sensors for civil infrastructures and their associated algorithms. *Sensor technologies for civil infrastructures* (pp. 57–85). Elsevier Inc. https://doi.org/10.1533/9780857099136.57

Zakeri, J. A., & Ghorbani, V. (2011). Investigation on dynamic behavior of railway track in transition zone. *Journal of Mechanical Science and Technology*, *25*(2), 287–292. https://doi.org/10.1007/s12206-010-1202-x